Stress Distribution around Coal Seam Gas Wells, Application to Coal Failure Onset Prediction

Mohammadreza Zare Reisabadi

B.Sc. (Hons), M.Sc.

A thesis submitted for the degree of

Doctor of Philosophy (PhD)

Australian School of Petroleum and Energy Resources

Faculty of Engineering, Computer & Mathematical Sciences

The University of Adelaide, Australia

March 2021

Contents

Abstract

Coal Seam Gas (CSG) reservoirs have grown quickly as an important part of unconventional gas resources. CSG reservoirs are considered unconventional resources because of their unique characteristics. The gas production mechanism and performance in CSG are significantly different from conventional resources. Depressurizing by water production is a pre-requisite to reduce the pressure in cleat system to a critical desorption pressure for commercial gas production. Later, during gas production, the coal matrix shrinks. This shrinkage impacts the stress distribution around the producing wells and within the coal seam layer. CSG reservoirs typically have low rock strength. The differential stress around the wellbore might exceed the coal mechanical strength and result in rock failure.

Coal failure brings several detrimental consequences which places gas production on the margin of economic efficiency. Created fines resulting from the coal failure may move towards the well by fluid flow and causes the plugging of downhole pumps. Moreover, the created coal particles may plug the cleat system and cause permeability reduction. In addition to downhole issues, solid particles can create erosion in surface facilities causing significant economic losses. Despite the detrimental effects of coal failure, limited research has been conducted into the stress modelling and the prediction of the onset of failure. Also, the details of how matrix shrinkage affects coal failure still have remained uncertain. Besides, coal permeability is significantly stress-dependent and it changes dynamically throughout the life of the reservoir. Furthermore, in the previous studies, less attention has been paid to the impact of desorption radius and its expansion on the stress distribution and permeability changes.

The main aim of this study is to develop comprehensive models to properly understand the effect of matrix shrinkage on stress distribution near the wellbore, the complexity of coal failure in CSG wells, and to investigate the effect of wellbore trajectory and in situ stress regimes on coal failure. A mathematical model is also developed to estimate the stress

distribution within the reservoir and evaluate the permeability during production from CSG reservoirs.

The thesis chapters are divided in three parts. In the first part, a new workflow is presented to evaluate stress distribution around CSG wells and predicts coal failure by coupling the effects of pressure depletion, matrix shrinkage, and wellbore simultaneously. The model calculates Maximum Coal Free Drawdown Pressure (MCFDP) by considering the effects of all contributing parameters and the Mogi-Coulomb failure criterion. Data from a vertical well in the San Juan Basin in the USA is used to evaluate the validity of the developed model. Coal failure is investigated in different in situ stress regimes. The results show that there is a high possibility of stress regime change from reverse and strike-slip regime to normal stress regime during depletion. Therefore, the optimum production trajectory is not static and it will change during production.

In the second part, the mathematical model for stress distribution near the wellbore is improved by considering the varying pore pressure. The model is utilized to analyse coal failure in Moranbah Coal Measures, in Bowen Basin, Australia. The results reveal that the stress path value in CSG reservoirs, is not constant during production and it can even be more than one due to the matrix shrinkage. It is shown that the stress differential may increase or decrease, depending on shrinkage/swelling magnitude and wellbore trajectory.

Part three of this study presents a mathematical model to analytically evaluate the dynamic stress distribution within the reservoir and accordingly permeability by coupling the geomechanics, sorption, and fluid flow in the cleat system. The results indicate that previous models, in which either uniform desorption or no desorption was assumed, cannot reflect the correct stress distribution in coalbed and accordingly overestimate or underestimate permeability, respectively. This is attributed to neglecting the varying desorption radius. The proposed model gives a more realistic evaluation of permeability as it only considers the effect of matrix shrinkage in the desorption area.

Declaration

I certify that this work contains no material which has been accepted for the award of any other degree or diploma in my name, in any university or other tertiary institution and, to the best of my knowledge and belief, contains no material previously published or written by another person, except where due reference has been made in the text. In addition, I certify that no part of this work will, in the future, be used in a submission in my name, for any other degree or diploma in any university or other tertiary institution without the prior approval of the University of Adelaide and where applicable, any partner institution responsible for the joint-award of this degree.

I acknowledge that the copyright of published works contained within this thesis resides with the copyright holder(s) of those works.

I also give permission for the digital version of my thesis to be made available on the web, via the University's digital research repository, the Library Search and also through web search engines, unless permission has been granted by the University to restrict access for a period of time.

I acknowledge the support I have received for my research through the provision of the Adelaide Scholarship International and Australian Government Research Training Program Scholarship.

Mohammadreza Zare Reisabadi 25/03/2021

Acknowledgments

Reaching this stage of finishing my PhD was not possible without the help and support of the kind people around me. I would like to take the opportunity to express my gratitude to only some of whom it is possible to give a particular mention here.

First and foremost, I would like to extend my deepest gratitude to my parents, Mohtaram and Gholamhosein. I have felt your love, support, and presence every single day despite the physical distance between us. I would also like to thank my siblings who through my study career had always encouraged me to follow my heart and inquisitive mind. You have always provided unwavering love and support, I owe you a lot.

This thesis would not have been possible without the help, support, and patience of my principal supervisor, Assoc. Professor Manouchehr Haghighi. He made me feel welcome and trusted in my curiosity to explore my intriguing domain of research. Thank you for motivating me to grow into an independent researcher and supporting me all along the way Manny.

I am grateful to my co-supervisors Dr. Abbas Khaksar and Dr. Alireza Salmachi for their constructive pieces of advice, motivating discussions, and supportive words.

A very special thanks to Dr. Sayyafzadeh for his contribution in developing the analytical model, motivating me, being patient, sharing his knowledge with me, and giving me technical assistance.

I am very grateful to have the opportunity to meet amazing people who made this journey so easier and much more fun. Very special thanks to my close friend Dr. Gabriel Malgaresi for always being there for me. Thanks for helping me out with deriving the equations, thank you for listening to my complaints, and thanks for being a friend on any occasion. Thank you for being a great friend. I would also like to thank my colleagues at the Australian School of Petroleum and Energy Resources, Abdullah, Abolfaz, Cuong, Grace, Marat, Mike, Mojtaba, Monica, Nassim, Roozbeh, Saurabh, Shahdad, Shuyan, Tammy, Tuan, and Yazan.

I am also grateful for the supports and assistance provided by the staff and administrative people of the Australian School of Petroleum and Energy Resources who patiently supported me during this journey.

Lastly, I would like to acknowledge the support I have received for my research through the provision of the Adelaide Scholarship International.

Thesis by Publication

Zare Reisabadi M, Haghighi M, Salmachi A, Sayyafzadeh M, Khaksar A. Analytical modelling of coal failure in coal seam gas reservoirs in different stress regimes. International Journal of Rock Mechanics and Mining Sciences. 2020; 128:104259.

Zare Reisabadi M, Haghighi M, Sayyafzadeh M, Khaksar A. Effect of matrix shrinkage on wellbore stresses in coal seam gas: An example from Bowen Basin, east Australia. Journal of Natural Gas Science and Engineering. 2020; 77:103280.

Zare Reisabadi M, Haghighi M, Khaksar A. Stress Changes and Coal Failure Analysis in Coal Seam Gas Wells Accounting for Matrix Shrinkage: An Example from Bowen Basin, East Australia. SPE/AAPG/SEG Asia Pacific Unconventional Resources Technology Conference. Brisbane, Australia: Unconventional Resources Technology Conference; 2019. p. 11.

Zare Reisabadi M, Haghighi M, Sayyafzadeh M, Khaksar A. Stress distribution and permeability modelling in coalbed methane reservoirs by considering desorption radius expansion. Fuel. 2021; 289:119951.

Mohammadreza Zare Reisabadi, Mojtaba Rajabi, Arian Velayati, Yasser Pourmazaheri, Manouchehr Haghighi. 1D Mechanical Earth Model in a Carbonate Reservoir of the Abadan Plain, Southwestern Iran: Implications for Wellbore Stability. AAPG Asia Pacific Region GTW, Pore Pressure & Geomechanics: From Exploration to Abandonment. Perth, Australia, June 6-7, 2018.

1 Contextual Statement

1.1 Research background

While conventional energy resources continue to decline, the energy demand is increasing significantly. To satisfy the growing energy demand, unconventional gas resources have become increasingly important. During the past decades, Coal Seam Gas (CSG) or Coal Bed Methane (CBM) reservoirs have grown quickly as an important part of unconventional gas resources. The development of CSG has commercially been established in countries such as U.S., China, Canada, India, and Australia. Particularly in eastern Australia, CSG is the main part of the gas industry, as of 2018, 98% of the natural gas being produced in Queensland is coal seam gas. Australia began exporting gas produced from these coal seams, as Liquefied Natural Gas (LNG), to Asian markets in January 2015, and 80% of the gas being produced in Queensland is being exported as LNG. The total investment in CSG and LNG development to 2017 was approximately $70 billion (GA and BREE, 2012; Liu et al., 2020; Towler et al., 2019). Bowen and Surat basins in Queensland are large reserves of coal and 97% of produced CSG of Australia is coming from these two basins and the remainder from New South Wales.

Optimum production from CSG reservoirs is a challenging task as their rock properties are highly geomechanical-sensitive. CSG reservoirs are considered unconventional gas resources because methane is normally adsorbed on the coal matrix while the coal cleat system is saturated with water. Dewatering is initially carried out to deplete the reservoir pressure and this causes the progressive desorption of gas. Gas desorption from the coal matrix causes matrix shrinkage which affects material behaviour and leads to a specific stress path and permeability evolution during production. This makes the CSG unique in terms of production and stress distribution around the well. As the CSG are naturally fractured rocks and typically they have low rock strength compared to conventional reservoir rocks, by pressure depletion and matrix shrinkage, the stress concentration around the well might exceed the coal

mechanical strength and results in coal failure and coal particle production (Gentzis, 2009; Lu and Connell, 2016; Palmer et al., 2005). Coal failure causes serious issues during gas production from CSG. Created coal fines may move towards the well by fluid flow or deposit at the bottom of the well, and plug the downhole pumps (Moore et al., 2011). In this case, frequent workovers are required to clean out the coal particles to ensure proper gas production. There are wide reported issues while drilling and production from CSG around the world, particularly in depleted deviated and horizontal wells. Moreover, in some cases, a sudden drop in coal reservoir permeability was observed, which was coincided with coal fines production after several years of production (Espinoza et al., 2015; Moore et al., 2011; Okotie and Moore, 2011). The created coal particles plug the cleat system and cause permeability reduction (Bai et al., 2017; Wei et al., 2015). For support of high volumes of gas demand for the LNG and domestic markets in Australia, there was intense drilling activity, peaking at over 350 wells per quarter and it continued at 136 wells in the January to March 2018 quarter (Towler et al., 2019). Some of the recently drilled horizontal wells in the Moranbah Coal Measures, Bowen Basin, and Surat Basin have experienced unexpected solid production during production from coal layers (Alboub et al., 2013; Mazumder et al., 2012; Puspitasari et al., 2014).

Palmer et al. (2005) investigated the coal failure mechanism and its consequences. They used a conventional sanding onset model to predict coal failure but did not consider the shrinkage effect and its induced stress path on coal failure. Liu and Harpalani (2014) carried out a qualitative analysis of coal failure by illustrating Mohr's circle and considered gas depletion. They noticed that methane desorption had a significant effect on in situ stress state and as a result, shear failure takes place earlier than a conventional reservoir where there is no shrinkage effect. Recently, Espinoza et al. (2015) and Connell et al. (2016) developed an analytical model to consider the effect of desorption on coal failure. However, the effect of the wellbore trajectory on stress redistribution around the wellbore was not considered.

In stress-sensitive unconventional reservoirs such as CSG, permeability changes dynamically throughout the life of the reservoir, depending on the stress distribution around the well and within the reservoir. Dewatering and accordingly depressurizing during production result in the expansion of the desorption area outward. The significance of desorption area has been presented in the literature and analytical models have been developed to evaluate desorption area expansion during production from CSG reservoirs (Sun et al., 2017; Xu et al., 2013). Previously developed permeability models have neglected the effect of desorption radius, and therefore the stress distribution as a result of the matrix shrinkage and depletion is explained by the same equation from the wellbore to the reservoir boundary, regardless of water-gas ratio. There exists a large number of experimental and theoretical studies that have evaluated the coal permeability by including the effective stress and matrix shrinkage effect (Connell et al., 2016; Liu and Harpalani, 2013; Liu et al., 2020; Mitra et al., 2012; Palmer, 2009; Saurabh and Harpalani, 2018; Wu et al., 2010). In these models, the effective stress is not estimated as a function of distance from the wellbore, and therefore the permeability only changes by time not by the distance from the wellbore. Shi and Durucan (2004) presented a model to evaluate the effective horizontal stress changes and permeability estimation in the field scale. This study indicates the possibility of 10 times permeability enhancement around a CSG producing well due to matrix shrinkage and reservoir depletion. However, the desorption radius and its expansion were not considered in this study. Moreover, the fluid flow was described by the same equation of pressure (P) approach for the entire area between the wellbore and reservoir boundary rather than the pressure squared (P^2) approach for gas flow in the desorption area.

Although a few studies have been conducted to model coal failure in recent years, the role of matrix shrinkage on the stress distribution around the wellbore and coal failure has not been fully understood. Moreover, the effect of wellbore trajectory and different stress regimes

on coal failure has not been investigated. Besides, in terms of coal permeability evolution during production, there is a lack of knowledge about the role of desorption radius and its expansion effect on permeability within the reservoir. Therefore, a comprehensive stress model, a coal failure analysis, and permeability modelling are necessary for CSG reservoirs.

1.2 Research objectives

Significant CSG productivity declines have been observed due to coal failure-associated issues. The main aim of this study is to develop comprehensive models to properly understand the effect of matrix shrinkage on stress distribution, complexity of coal failure in CSG wells, and to estimate permeability evolution during production from CSG reservoirs. Specifically, mathematical models will be established by considering the influences of geomechanics, fluid flow, and wellbore effects. To facilitate this goal, the following research objectives will be addressed:

a) Developing the analytical model for stress distribution around CSG wells;
b) Presenting a new workflow to predict coal failure by coupling the effects of pressure depletion, matrix shrinkage, and wellbore simultaneously.
c) Validating the developed analytical model by real field data application from San Juan Basin, USA;
d) Investigating the effect of in situ stress regimes on coal failure;
e) Coal failure analysis in Bowen Basin, Australia;
f) Investigating the effect of wellbore trajectory on coal failure;
g) Developing a mathematical stress-permeability model to describe the permeability changes during production from CSG reservoirs.
h) Investigating the effect of desorption radius expansion on stress and permeability evolution.

1.3 Structure of thesis

This is a PhD thesis by publication. Five papers are included in the thesis, of which three papers have been published in peer-reviewed journals and two were presented at conferences. The PhD student is the first author in all of the papers. Table 1 summarizes all the publications included in this thesis.

The thesis body is formed by six chapters. *Chapter one* has the contextual statement, the research background, research objectives, structure of the thesis, and how the papers fulfil the aim of the thesis. The main contextual statement in chapter one is to describe the goal of the PhD study. The *second chapter* provides a literature review of CSG reservoir fundamentals and coal failure situation, involving mathematical models, experimental investigations, and field observations. Observed coal failure challenges in different CSG reservoirs around the world are studied. Experimental and theoretical works on stress path, wellbore stress distribution, and permeability evaluation are reviewed and the gaps in the current literature in stress and permeability modelling in CSG are highlighted. The effect of matrix shrinkage and desorption radius on stress distribution and gas production in CSG is studied. *Chapter three* presents the derivation of the mathematical model and validation for stress distribution near the CSG wells. Based on the presented stress model, the analytical coal failure model is derived and validated by real field observation. This chapter also provides the effect of different stress regimes on coal failure. *Chapter four* includes the improved mathematical model for stress distribution by considering the varying pore pressure and its application for coal failure analysis in a case study from Bowen Basin, Australia. The effect of matrix shrinkage on coal failure in different wellbore trajectories is presented in this chapter. This chapter presents two papers including one journal paper and one peer-reviewed conference paper. The conference paper was written at the early stage of the model development and, therefore, the paper in section 4.1 (journal paper) is more comprehensive and thorough of this particular study. The order of the papers in the

chapter is based on the quantity of work done in each paper. *Chapter five* includes the derivation of a mathematical model for stress and permeability evolution during CSG reservoir production. As the permeability is not limited to the area around the wellbore, this chapter focuses on the stress-permeability model for two distinct areas around the wellbore and within the reservoirs. The effect of desorption radius and its expansion by production is considered for permeability modelling. *Chapter six* summarizes the main results and findings of this research.

Table 1. Publications list

Chapter	Title	Paper	Status
Chapter 3	Analytical modelling of coal failure in coal seam gas reservoirs in different stress regimes	1	Published
Chapter 4	Effect of matrix shrinkage on wellbore stresses in coal seam gas: An example from Bowen Basin, east Australia	2	Published
	Stress Changes and Coal Failure Analysis in Coal Seam Gas Wells Accounting for Matrix Shrinkage: An Example from Bowen Basin, East Australia	3	Published
Chapter 5	Stress distribution and permeability modelling in coalbed methane reservoirs by considering desorption radius expansion	4	Published
Appendix	1D mechanical earth model in a carbonate reservoir of the Abadan plain: implications for wellbore stability	5	Published

1.4 How publications are related to the thesis

In the paper "Analytical modelling of coal failure in coal seam gas reservoirs in different stress regimes" the first four objectives of the thesis (section 1.2) are addressed. A mathematical model is derived to evaluate the stress distribution around the wellbore by coupling the effect of depletion, matrix shrinkage, and the wellbore. An analytical model is developed to calculate the Critical Coal Free Bottom-hole Pressure (CCFBP) and Maximum Coal Free Drawdown Pressure (MCFDP). The model is validated by field data in the San Juan

Basin. Moreover, the developed model is utilized to investigate the effect of different in situ stress regimes, and pressure depletion on coal failure. The results of this paper indicate that pressure depletion and matrix shrinkage have a significant effect on coal failure in all stress regimes. In the case of strike-slip and reverse stress regimes, pressure depletion and matrix shrinkage may cause the change of stress regime and therefore, the optimum wellbore trajectory can change significantly during the life of the reservoir. Additionally, it is found that in the normal stress regime the depletion and matrix shrinkage reduces the MCFDP of horizontal wellbores more than the vertical wells. However, in the reverse stress regime, depletion and shrinkage cause more reduction of MCFDP in vertical wellbores compared to horizontal wells. It should be noticed because the rock failure starts near the wellbore, the presented model in this paper focuses only on the stress distribution around the wellbore where there is matrix shrinkage effect and it does not consider the stress distribution within the reservoirs.

The developed mathematical model in paper one for stress distribution around the wellbore is improved in the next two papers (section 4.1 and section 4.2). In the developed model in paper one, only the values of wellbore pressure and reservoir pressure were considered, and the pore pressure profile versus distance from the wellbore was not considered. In the second paper entitled "Effect of matrix shrinkage on wellbore stresses in coal seam gas: An example from Bowen Basin, east Australia", an analytical model is developed for stress distribution around CSG wells by considering the varying pressure profile versus distance from the wellbore. Paper three "Stress Changes and Coal Failure Analysis in Coal Seam Gas Wells Accounting for Matrix Shrinkage: An Example from Bowen Basin, East Australia" also presents the improved model application in Bowen Basin. This paper was written at the early stage of the model development and, therefore, the journal paper in section 4.1 is more comprehensive and thorough of this particular study. The order of the papers in chapter 4 is

based on the quantity of work done in each paper. The developed model in these two papers is applied to investigate the stress distribution around both vertical and horizontal wells in Moranbah Coal Measures, in the Bowen Basin eastern Australia. The developed model is used to analyse the observed coal failure in the Bowen Basin. The results reveal that the stress path value in CSG reservoirs, is not constant during production and it can even be more than one due to the matrix shrinkage. The shrinkage effect can significantly alter the effective horizontal stresses which accordingly can cause a considerable change to the near-wellbore stress distribution. For the CSG wells in Bowen Basin, the matrix shrinkage decreases stress differential on the wellbore wall in vertical wells and consequently, reduces the coal failure potentials. However, in highly deviated and horizontal wells, the matrix shrinkage causes an extra increase of the tangential stress and reduction of radial stress on the wellbore wall (i.e., greater stress differentials on the wellbore wall). This increases the coal failure risks with depletion. Therefore, this paper fulfils the objective of coal failure analysis in Bowen Basin and investigating the effect of well trajectory on failure (objectives e and f, section 1.2).

The derived analytical stress solution in the previous paper is applicable for coal failure as they focus on stress distribution near the wellbore. However, these models are not applicable for permeability evaluation as they do not consider the desorption radius effect and its expansion by production; the desorption area and non-desorption area were not differentiated. Therefore, in paper four, "Stress distribution and permeability modelling in coalbed methane reservoirs by considering desorption radius expansion", a more complicated mathematical model is derived. The developed model evaluates the dynamic stress distribution and accordingly permeability by coupling the geomechanics, sorption, and fluid flow in the cleat system. In this approach, the coalbed is divided into two regions: desorption area and non-desorption area. The desorption area represents the region with a low water–gas ratio, where the pressure squared (P2) approach is applied for flow modelling. The non-desorption area

represents the region with a high water-gas ratio with almost no desorption effect, where Darcy's equation (P approach) is used for flow modelling. The results indicate that previous models, in which either uniform desorption or no desorption was assumed, cannot reflect the correct stress distribution in coalbed and accordingly overestimate or underestimate permeability, respectively. This is attributed to neglecting the varying desorption radius. The results demonstrate that this has a significant effect on stress distribution. The proposed model gives a more realistic evaluation of stress distribution and permeability as it only considers the effect of matrix shrinkage in the desorption area. Therefore, this paper fulfils the objective of the realistic permeability model in CSG and investigates the effect of desorption radius expansion on permeability (g and h part of section 1.2.).

The paper in the appendix titled "1D mechanical earth model in a carbonate reservoir of the Abadan plain: implications for wellbore stability", presents the workflow and case study for constructing the mechanical earth model. 1D mechanical earth model of studied well is required for rock failure analysis or solid production.

1.5 Reference

Alboub, M. et al., 2013. Calibrated Mechanical Earth Models Answer Questions on Hydraulic Fracture Containment and Wellbore Stability in Some of the CSG Wells in the Bowen Basin, SPE Unconventional Resources Conference and Exhibition-Asia Pacific. Society of Petroleum Engineers, Brisbane, Australia.

Bai, T. et al., 2017. Dimensional analysis and prediction of coal fines generation under two-phase flow conditions. Fuel, 194: 460-479.

Connell, L.D. et al., 2016. Laboratory characterisation of coal matrix shrinkage, cleat compressibility and the geomechanical properties determining reservoir permeability. Fuel, 165: 499-512.

Espinoza, D.N., Pereira, J.M., Vandamme, M., Dangla, P. and Vidal-Gilbert, S., 2015. Desorption-induced shear failure of coal bed seams during gas depletion. International Journal of Coal Geology, 137: 142-151.

GA and BREE, 2012. Australian gas resource assessment, Department of Resources, Energy and Tourism, Geoscience Australia and Bureau of Resources and Energy Economics, Canberra.

Gentzis, T., 2009. Review of Mannville Coal Geomechanical Properties: Application to Coalbed Methane Drilling in the Central Alberta Plains, Canada. Energy Sources, Part A: Recovery, Utilization, and Environmental Effects, 32(4): 355-369.

Liu, S. and Harpalani, S., 2013. Permeability prediction of coalbed methane reservoirs during primary depletion. International Journal of Coal Geology, 113: 1-10.

Liu, S. and Harpalani, S., 2014. Evaluation of in situ stress changes with gas depletion of coalbed methane reservoirs. Journal of Geophysical Research: Solid Earth, 119(8): 6263-6276.

Liu, T. et al., 2020. Stress response during in-situ gas depletion and its impact on permeability and stability of CBM reservoir. Fuel, 266: 117083.

Lu, M. and Connell, L., 2016. Coal failure during primary and enhanced coalbed methane production — Theory and approximate analyses. International Journal of Coal Geology, 154-155: 275-285.

Mazumder, S., Scott, M. and Jiang, J., 2012. Permeability increase in Bowen Basin coal as a result of matrix shrinkage during primary depletion. International Journal of Coal Geology, 96-97: 109-119.

Mitra, A., Harpalani, S. and Liu, S., 2012. Laboratory measurement and modeling of coal permeability with continued methane production: Part 1 – Laboratory results. Fuel, 94: 110-116.

Moore, R.L., Loftin, D.F. and Palmer, I.D., 2011. History Matching and Permeability Increases of Mature Coalbed Methane Wells in San Juan Basin, SPE Asia Pacific Oil and Gas Conference and Exhibition. Society of Petroleum Engineers, Jakarta, Indonesia.

Okotie, V.U. and Moore, R.L., 2011. Well-Production Challenges and Solutions in a Mature, Very-Low-Pressure Coalbed-Methane Reservoir.

Palmer, I., 2009. Permeability changes in coal: Analytical modeling. International Journal of Coal Geology, 77(1): 119-126.

Palmer, I.D., Moschovidis, Z.A. and Cameron, J.R., 2005. Coal Failure and Consequences for Coalbed Methane Wells, SPE Annual Technical Conference and Exhibition. Society of Petroleum Engineers, Dallas, Texas.

Puspitasari, R., Gan, T., Pallikathekathil, Z.J. and Luft, J., 2014. Wellbore Stability Modelling for Horizontal and Multi-Branch Lateral Wells in CBM: Practical Solution to Better Understand the Uncertainty in Rock Strength and Coal Heterogeneity, SPE Asia Pacific Oil & Gas Conference and Exhibition. Society of Petroleum Engineers, Adelaide, Australia.

Saurabh, S. and Harpalani, S., 2018. Stress path with depletion in coalbed methane reservoirs and stress based permeability modeling. International Journal of Coal Geology, 185: 12-22.

Shi, J.Q. and Durucan, S., 2004. Drawdown Induced Changes in Permeability of Coalbeds: A New Interpretation of the Reservoir Response to Primary Recovery. Transport in Porous Media, 56(1): 1-16.

Sun, Z. et al., 2017. A semi-analytical model for drainage and desorption area expansion during coal-bed methane production. Fuel, 204: 214-226.

Towler, B., Firouzi, M. and Wilkinson, R., 2019. Australia's gas resources and its new approaches. Journal of Natural Gas Science and Engineering, 72: 102970.

Wei, C., Zou, M., Sun, Y., Cai, Z. and Qi, Y., 2015. Experimental and applied analyses of particle migration in fractures of coalbed methane reservoirs. Journal of Natural Gas Science and Engineering, 23: 399-406.

Wu, Y., Liu, J., Elsworth, D., Miao, X. and Mao, X., 2010. Development of anisotropic permeability during coalbed methane production. Journal of Natural Gas Science and Engineering, 2(4): 197-210.

Xu, B. et al., 2013. An analytical model for desorption area in coal-bed methane production wells. Fuel, 106: 766-772.

2 Literature Review

2.1 Coal seam gas reservoir

Coal seam gas is a naturally fractured reservoir that consists of two sets of fractures called cleats (Figure 1). The dominant fracture system is face cleats and the secondary fracture system is butt cleats. Face cleats are well-developed, long, and continuous fractures that are nearly parallel fissures. Butt cleats are less well-developed, short and discontinuous fractures perpendicular to the face cleats which usually terminate at the intersection with them. Cleats are the primary flow conduits in a coal seam and contain most of the moveable water but little sorbed gas (Seidle, 2011).

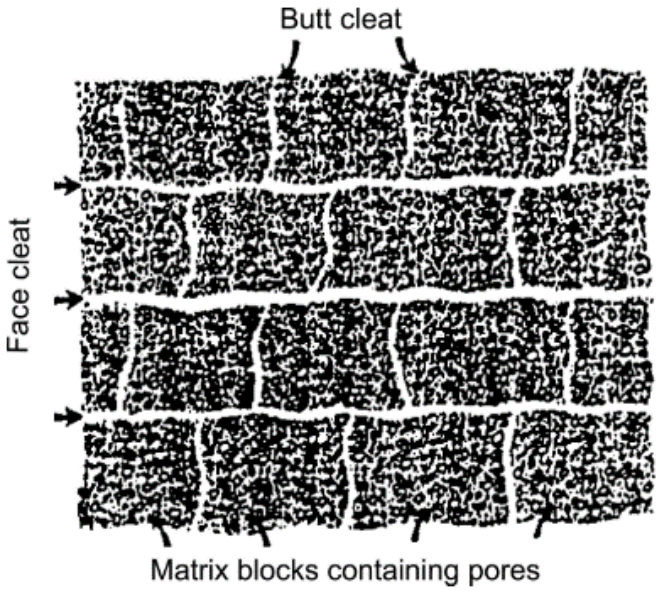

Figure 1. A schematic of fracture system in coal seam gas reservoirs(Shi and Durucan, 2005)

CSG reservoirs are considered unconventional gas resources as methane is not trapped by overlying seals and usually is adsorbed on the pore surface of the coal matrix. Physical adsorption is the primary gas storage mechanism and it accounts for about 98% of the gas in a CSG, depending on the pressure at which gas is adsorbed (Gray, 1987). The surface area of the coal on which the methane is adsorbed is very large (20–200 m2/g) and, if saturated, coalbed

methane reservoirs can have five times the volume of gas contained in a conventional sandstone gas reservoir of comparable size(Shi and Durucan, 2004). The adsorption capacity of coal has widely been studied in the literature and it can be described approximately with the Langmuir equation:

$$V = V_L \frac{P}{P_L + P} \quad (1)$$

Where VL and PL are Langmuir volume and Langmuir pressure of adsorption respectively. P is pressure and V is absorption volume.

As most coal seam gas reservoirs are completely water-saturated, dewatering is the first production stage in these reservoirs. By producing water from the reservoir, depressurizing is carried out as a common method for the commercial production of gas from CSG reservoirs. The reservoir pressure depletion causes progressively desorbing of the adsorbed gas from the coal matrix which comes up with matrix shrinkage (Day et al., 2008; Fan and Liu, 2018).

2.2 Matrix swelling/shrinkage in CSG

Coal exhibits a unique behaviour which is called matrix swelling/shrinkage. In sorptive gas, coal matrix swells due to the adsorption of sorptive gas with pressures increasing and it shrinks due to desorption of sorptive gas with pressures decreasing. Sorption-induced coal matrix shrinkage has been widely studied in the literature and the matrix shrinkage was measured as a function of pressure in the laboratory. The adsorption-induce swelling and desorption-induce matrix shrinkage of coal results in an additional volumetric strain. Since there is an additional volumetric strain from matrix shrinkage, the poroelastic process, stress distribution, and permeability of CSG reservoirs are different from conventional oil and gas reservoirs (Liu and Harpalani, 2014).

During depletion of CSG reservoirs, matrix shrinkage results in opening up the cleats (Cui and Bustin, 2005; Cui et al., 2007; Gray, 1987; Pan and Connell, 2012; Saurabh and Harpalani, 2018; Shi and Durucan, 2004). Thus there are two competing effects on coal permeability; decreasing the pressure during production acts to increase the effective stress (same as conventional reservoirs) which is called the poromechanical effect and thus decreases the permeability due to cleat compression. However, the pressure reduction also results in desorption-induced matrix shrinkage and consequent increasing of coal cleat apertures and thus permeability (Connell et al., 2013). If the shrinkage is great enough, then it can counteract any decrease in permeability from dewatering (poromechanical effect) and cleat closure. Some researchers (Harpalani and Chen, 1995; Levine, 1996; Seidle and Huitt, 1995) measured the matrix shrinkage in the laboratory and related it to adsorption pressures with the Langmuir type equation as:

$$\varepsilon_s = \varepsilon_l \frac{p}{p + p_\varepsilon} \tag{2}$$

Where ε_s is volumetric matrix strain, ε_l is referred to the maximum volumetric strain that would be induced when the coal is fully saturated with gas, and p_ε is the gas pressure at which the matrix strain is half of its maximum value.

Several researchers have investigated coal matrix swelling/shrinkage due to methane and carbon dioxide adsorption/desorption. In most of the studies, the shrinkage/swelling coefficient was calculated based on changes in the volume with pressure (Table 2).

Table 2. Reported coal matrix shrinkage coefficient in the literature

Gas	Shrinkage coefficient, $psia^{-1}$	Reference
CO2	6.55E-05	Reucroft and Patel (1986)
Methane	8.618E-07	Gray (1987)
CO2	1.25 E-05	Gray (1987)
Methane	6.21E-06	Harpalani and Schraufnagel (1990)
Methane	1.59E-06	Harpalani and Chen (1995)
Methane	1.80E-03	Levine (1996)
Methane	7.38E-06	Mitra and Harpalani (2007)
CO2	2.67E-05	Mitra and Harpalani (2007)

2.3 Permeability evaluation in coal seam gas

Coal seam gas permeability is one of the main factors controlling gas production from CSG reservoirs. CSG reservoirs are naturally fractured and cleats are the main path of fluid flow. As a naturally fractured reservoir, CSG often exhibits a strong contrast between matrix and fracture permeability. Coal matrix permeability is on the order of microdarcies or nanodarcies, while coal cleat permeability range from 0.1 to 1,000 md. However, unlike conventional naturally fractured reservoirs, where matrix permeability often dominates reservoir performance, coal cleat permeability plays a significant role in the fluid movement in CSG reservoirs (Palmer, 2010; Seidle, 2011). The cleats are significantly sensitive to stress changes and they may undertake most of the deformation upon a stress change (Cui et al., 2007).

Depressurizing by water production is a pre-requisite to reduce the cleat pressure to a critical desorption pressure for commercial gas production from CSG reservoirs. During the dewatering phase and the CSG depletion, the decrease of the pore pressure leads to an increase of the effective stress (poromechanical effect). The increase of the effective stress causes the reduction of cleat width and negatively contributes to the permeability; a relationship supported by extensive laboratory and field studies (Seidle et al., 1992; Somerton et al., 1975; Sparks et al., 1995). On the other hand, the matrix shrinkage due to gas desorption plays an opposite role and increases cleat width, increasing permeability (Cui and Bustin, 2005; Cui et al., 2007; Gray, 1987; Pan and Connell, 2012; Saurabh and Harpalani, 2018; Shi and Durucan, 2004). The permeability rebound and enhancement during CSG production were identified in many studies. A strong permeability increase of 10 fold increase was identified over 300 psi of depletion in Bowen Basin, Australia (Gouth et al., 2014). Figure 2 shows the history matching of production data for a Fruitland coal, Fairway CBM well. It indicates a 10 fold increase of the gas effective permeability from 932 psi to approximately 100 psi (Clarkson et al., 2007; Clarkson et al., 2008a; Clarkson et al., 2008b).

Hence, a complication with coal permeability is that it can vary significantly during gas production in response to decreases in pore pressure and gas desorption-induced coal matrix shrinkage (Gray, 1987; Liu et al., 2020; Pan and Connell, 2012).

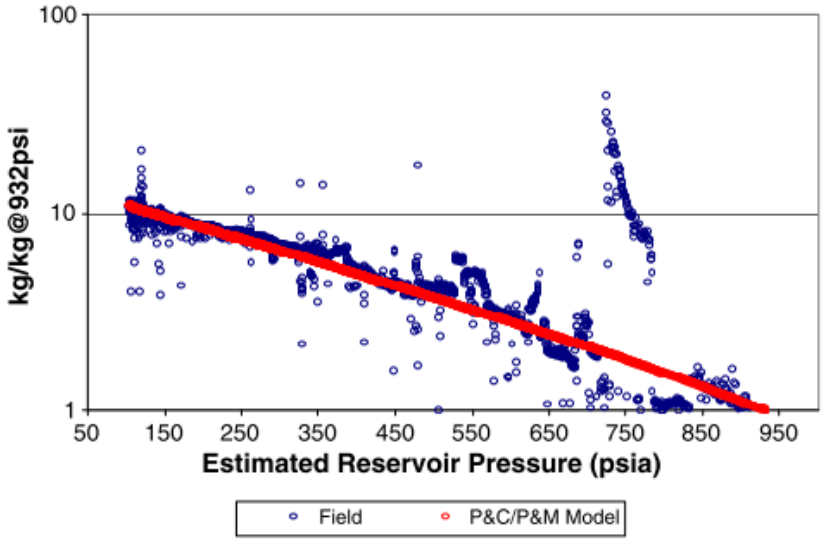

Figure 2. Gas permeability evaluation in Fairway CBM(Pan and Connell, 2012)

The developed permeability models for conventional reservoirs are not applicable to CSG as they do not consider the coal swelling/shrinkage effect on permeability. In the literature, many models have been presented to describe coal permeability by including the impact of effective stress and coal swelling/shrinkage. These models including Gray (1987), Seidle et al. (1992), Seidle and Huitt (1995), Ian Palmer (1998), Shi and Durucan (2004), Shi and Durucan (2005), Palmer (2009), Mitra et al. (2012), Espinoza et al. (2014), Connell et al. (2016), (Shi et al., 2019), and Liu et al. (2020).

Among these models, the permeability models presented by Ian Palmer (1998), and Shi and Durucan (2004) are the two most popular and have seen the extensive practical application. These models consider the uniaxial strain condiction and constant vertical stress assumption which is widely accepted during depletion of CSG (Espinoza et al., 2015; Geertsma, 1957; Liu and Harpalani, 2014; Olson et al., 2009). The uniaxial strain means zero lateral strain and associated inconstant horizontal stresses (Figure 3). They also assume matchstick like geometry for the coal matrix and cleat system (Figure 4).

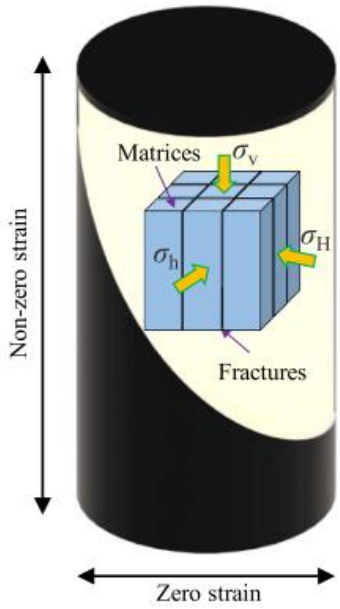

Figure 3. Uniaxial strain condition in CSG reservoirs (Liu et al., 2020)

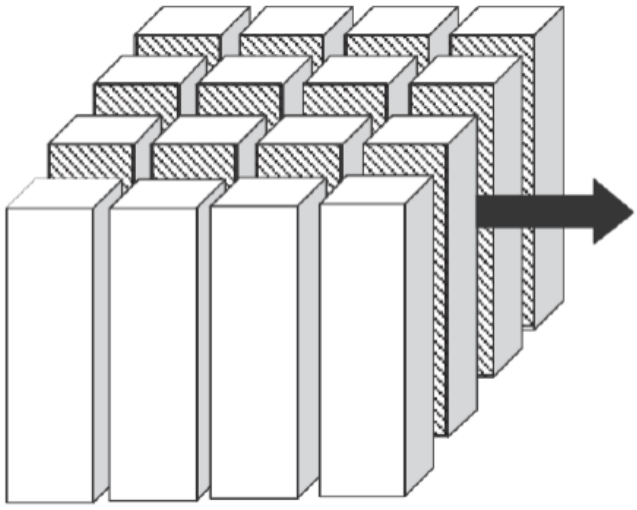

Figure 4. Matchstick geometry showing flow through cleats in CSG reservoirs (Harpalani and Chen, 1995)

Ian Palmer (1998) relate the coal permeability to the porosity and then describe the change in porosity with respect to the pressure decrease and matrix shrinkage:

$$\frac{k}{k_0} = \left(\frac{\varphi}{\varphi_0} \right)^3 \tag{3}$$

$$\varphi = \varphi_0 + c_m\left(p - p_0\right) + \left[\frac{K}{M} - 1\right]\left(\varepsilon_s - \varepsilon_{s0}\right) \tag{4}$$

$$c_m = \frac{1}{M} - \left[\frac{K}{M} + f - 1\right]c_r \tag{5}$$

$$M = \frac{E\left(1-\nu\right)}{\left(1+\nu\right)\left(1-2\nu\right)} \tag{6}$$

$$K = \frac{E}{3\left(1-2\nu\right)} \tag{7}$$

φ	Porosity at pressure p
φ_0	Initial porosity
k	Permeability at pressure p
k_0	Initial permeability
ε_s	Volumetric matrix strain at pressure p
K	Bulk modulus
M	Constrained axial modulus
f	Fraction from 0 to 1
c_r	Grain compressibility
E	Young's modulus
ν	Poisson's ratio

Shi and Durucan (2004) model relates the coal permeability to the effective horizontal stress instead of porosity:

$$\frac{k}{k_0} = \exp\left(-3c_f \Delta\sigma_h\right) \tag{8}$$

$$\Delta\sigma_h = \frac{-\nu}{1-\nu}\left(p - p_0\right) + \frac{E}{3\left(1-\nu\right)}\varepsilon_l\left(\frac{p}{p+p_\varepsilon} - \frac{p_0}{p_0+p_\varepsilon}\right) \tag{9}$$

k	Permeability at pressure p
k_0	Initial permeability
c_f	Cleat volume compressibility
p	Pressure
p_0	Initial pressure
ε_l	Maximum matrix shrinkage strain
p_ε	Langmuir pressure
E	Young's modulus
ν	Poisson's ratio

2.4 Coal failure issues during CSG production

As the CSG are naturally fractured rocks and typically they have low rock strength compared to conventional reservoir rocks, by pressure depletion and matrix shrinkage, the stress concentration around the well might exceed the coal mechanical strength and results in coal failure and coal particle production (Lu and Connell, 2016; Palmer et al., 2005; Seidle, 2011). Coal failure may cause serious issues during gas production from CSG (Gentzis, 2009; Lu and Connell, 2016). The created coal may move towards the well by fluid flow or deposit at the bottom of the well, and plug the downhole pumps (Moore et al., 2011). Figure 5 shows

the produced coal particles in a visualized surface container on the left photo and coal fines in a plugged pump on the right. In this case, frequent workovers are required to clean out the coal particles to ensure proper gas production. There are wide reported issues while drilling and production from CSG, particularly in depleted deviated and horizontal wells.

Figure 5. Produced/Plugged coal fines (Okotie and Moore, 2011).

It has been reported that 40 percent of drilled horizontal CSG wells in the Qinshui basin in China have serious instability problems during drilling and production (Yang et al., 2014). Some of the recently drilled horizontal and multi-lateral wells in Bowen Basin, Australia have experienced unintended fines and solid production after drilling and during production from coal layers (Puspitasari et al., 2014). Rajora et al. (2019) reported that the majority of artificial lift failures (75%) in Surat Basin, Australia were due to solids production into the wellbore. In the San Juan basin, USA, massive coal fine production was observed at the late production stage when the reservoir pressure was decreased to a specific value of around 300 psi. It was noticed that the matrix shrinkage and desorption-induced horizontal stress change were the driven forces of this geomechanical failure (Espinoza et al., 2015; Fan and Liu, 2018; Moore et al., 2011). Moreover in Arkoma basin, Oklahoma where the horizontal wells are commonly drilled in CBM, several borehole failure and coal fine production were experienced in depleted coal (Palmer et al., 2005).

In recent years, many researchers noticed that after an exponential increase in permeability (because of desorption-induce shrinkage), in some cases there is a sudden drop in coal reservoir permeability (Figure 6), which is coincided with coal fines production after several years of production (Espinoza et al., 2015; Moore et al., 2011; Okotie and Moore, 2011). It was concluded that the sudden decrease in permeability and accompanied coal fines production were results of coal failure caused by matrix shrinkage and stress change within the reservoir. The created coal particles plug the cleat system and cause permeability reduction (Bai et al., 2017; Wei et al., 2015). Therefore, maintaining the wellbore stable during drilling and preventing coal failure during production, particularly in depleted CSG reservoirs, is one of the most challenging problems in CSG. Palmer et al. (2005) investigated the coal failure mechanism and its consequences. They used a conventional sanding onset model to predict coal failure but did not consider the shrinkage effect and its induced stress path on coal failure. Liu and Harpalani (2014) carried out a qualitative analysis of coal failure by illustrating Mohr's circle and considered gas depletion. They noticed that methane desorption had a significant effect on in situ stress state and as a result, shear failure takes place earlier than a conventional reservoir where there is no shrinkage effect. Recently, Espinoza et al. (2015) and Connell et al. (2016) developed an analytical model to consider the effect of desorption on coal failure. However, the effect of the wellbore trajectory on stress redistribution around the wellbore was not considered. Although a few studies have been conducted in recent years, the roles of matrix shrinkage on the stress distribution around the wellbore and coal failure, the effective stress path, the effect of wellbore trajectory, and the change of permeability have not been fully understood.

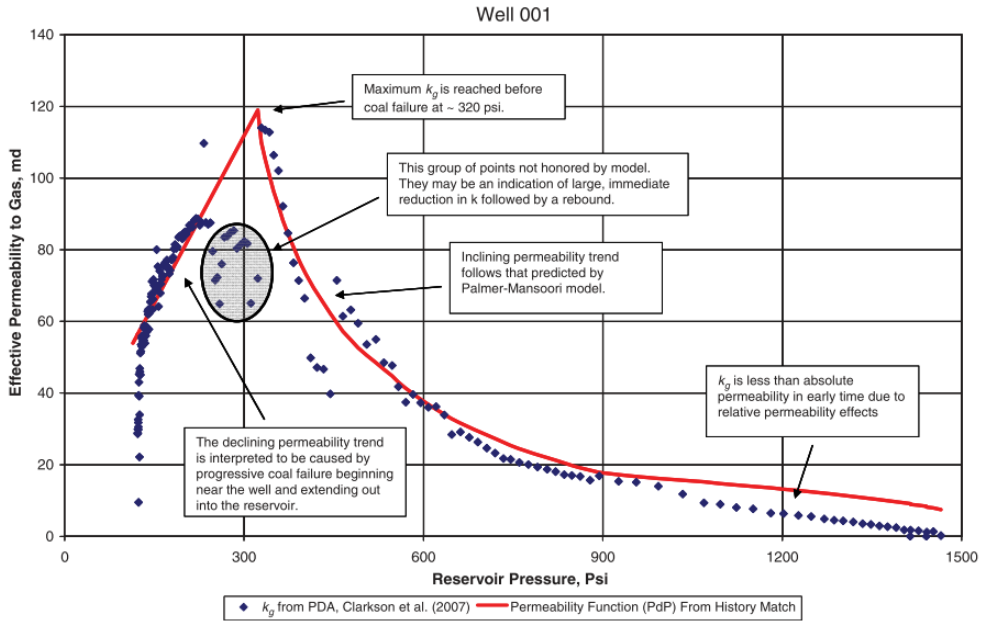

Figure 6. Permeability changes during production (Okotie and Moore, 2011)

2.5 Reservoir depletion and stress path

2.5.1 Stress path in conventional reservoirs

It has been well known that by fluid withdrawal from the reservoir, the reservoir pressure gradually decreases and it results in the changing of in situ stresses. The uniaxial strain condition is widely accepted during depletion in laterally extensive reservoirs, which means the constant vertical stress, zero lateral strain, and associated inconstant horizontal stresses (Espinoza et al., 2015; Geertsma, 1957; Liu and Harpalani, 2014; Olson et al., 2009). The stress variations are quantified by reservoir stress path which is defined as the changes in total horizontal stresses per unit change of pore pressure during production from the reservoir as following:

$$\frac{\Delta S}{\Delta P} = K = \alpha \frac{1-2v}{1-v} \tag{10}$$

$$\sigma_h = S_h - \alpha P_o \tag{11}$$

$$\frac{\Delta\sigma_h}{\Delta P} = -\alpha\frac{\nu}{1-\nu} \tag{12}$$

Where the S is total stress and σ indicates effective stress. Sh is the total minimum horizontal stress, σ_h is the effective minimum horizontal stress, Po is initial pore pressure, P is current pore pressure, α is Biot's coefficient, and ν is Poisson's ratio.

These equations reveal that the reservoir depletion is expected to be accompanied by reduction of total horizontal stresses and hereby, increase of effective horizontal stress which has been confirmed by field observations in conventional reservoirs (Addis, 1997b; Teufel et al., 1991; Zoback and Zinke, 2002). By the increase of the effective stress during pressure depletion, the reservoir permeability will decrease. Figure 7 shows the observed changes of total horizontal stress by pore pressure depletion in Ekofisk and Valhall field in the North Sea respectively. As the Poisson's ratio of the rock is less than 0.5, the stress path in different points of the reservoir is less than one for different conventional reservoirs. This is consistent with the measured data in different reservoirs around the world in Table 3.

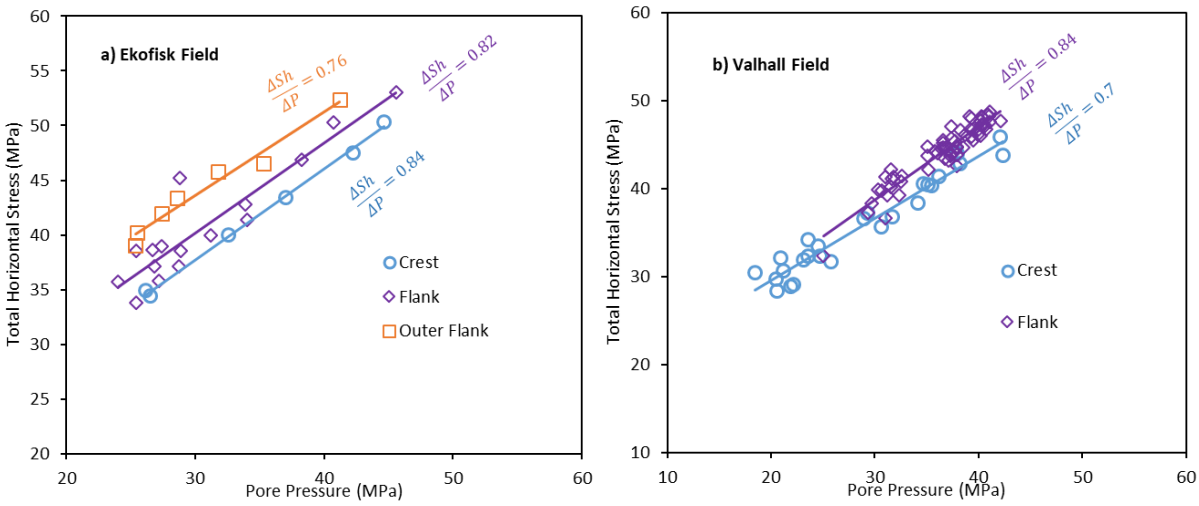

Figure 7. Total horizontal stress path with depletion in conventional reservoirs. Data points in (a) from (Teufel et al., 1991) and data points in (b) from (Zoback and Zinke, 2002).

Table 3. Stress Path measurement within different conventional reservoirs after (Addis, 1997a)

Field	**Measured Stress Path**
Ekofisk, central North sea	0.8
Magnus, UK sector of North Sea	0.68
Venture, Colorado	0.56
Vicksburg Fm., South Texas	0.53
Waskom, East Texas	0.57
Wytch Farm, England	0.55
Valhall, central North sea	0.8
Gulf Coast, Texas	0.46
Lake Maracaibo, Venezuela	0.56
Brunei, Brunei	0.49

One may plot the effective in situ stress profile during depletion in conventional reservoirs by considering uniaxial strain condition and constant vertical stress. As the total vertical stress is constant, therefore the change in effective vertical stress by depletion is given by $\Delta\sigma_V$=- $\alpha\Delta P > 0$, and for the effective horizontal stress it would be $\Delta\sigma_h = -\alpha\frac{\vartheta}{1-\vartheta}\Delta P > 0$. However, as Figure 8 indicates the increasing rate of effective vertical stress (red line) is more than effective horizontal stress (green line) which results in the increase of deviatoric stress with production. The blue line represents the effective horizontal stress without considering the depletion effect. Figure 8 shows that by continuous depletion, a significant stress anisotropy may occur at the late time of production. As Figure 8.b indicates this stress anisotropy becomes larger by time and it may lead the rock failure around the wellbore. This failure is the cause of

fine production in conventional reservoirs and has widely been studied in the literature for sand production (Behnoud far et al., 2016; Kaffash and Zare-Reisabadi, 2013; Zhang et al., 2016).

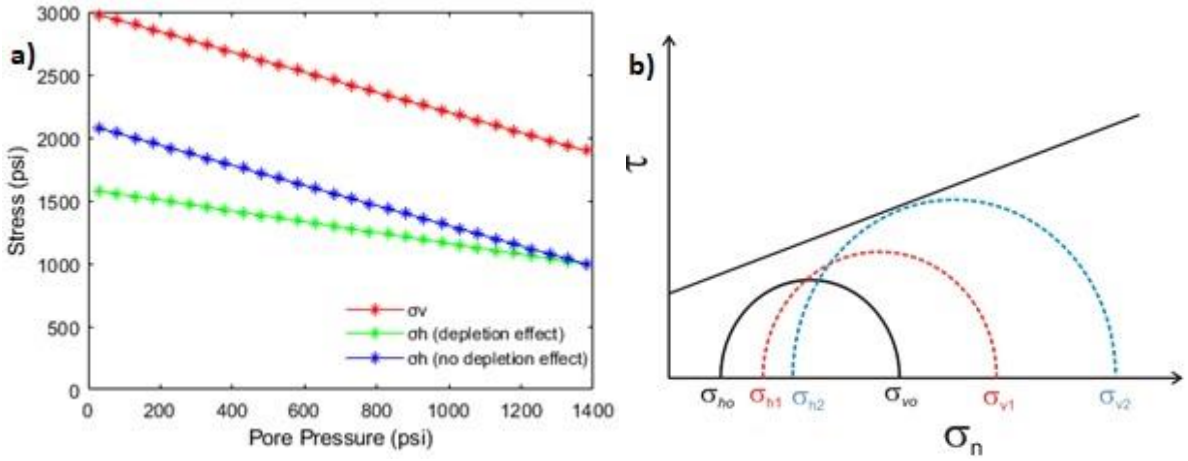

Figure 8. The effective stress profile during depletion a) the vertical and horizontal stress change during depletion b) rock failure in reservoir scale during production

2.5.2 Stress path in CSG Reservoirs

Depressurizing and depletion is a common method is carried out for the commercial production of gas from CSG reservoirs. The uniaxial strain condition is widely accepted during depletion of CSG, which means the constant vertical stress, zero lateral strain, and associated inconstant horizontal stresses (Espinoza et al., 2015; Geertsma, 1957; Liu and Harpalani, 2014; Olson et al., 2009). Based on uniaxial strain condition and as the same as conventional reservoirs, the effective stress will increase. Conversely, the methane desorption from the coal is associated with matrix shrinkage and hereby the effective horizontal stress will reduce (Day et al., 2008; Feng et al., 2018; Shi and Durucan, 2004). These two opposing effects make the CSG unique in the aspect of stress path during depletion.

Recently some researchers have investigated the stress path profile during depletion in CSG reservoirs. Many experimental studies reveal that the stress path in CSG reservoirs is more than 1 (Espinoza et al., 2015; Liu and Harpalani, 2014; Mitra et al., 2012; Saurabh and

Harpalani, 2018; Saurabh et al., 2016). The conventional value of the stress path for any combination of Poisson's ratio and Biot's constant would be less than 1.Therefore, it was noticed that the theoretical conventional stress path (values in Table 3) cannot describe the stress profile of CSG reservoirs during depletion. Shi and Durucan (2004) utilized the elastic theory of stress and strain relation and analogy between thermal contraction and matrix shrinkage to develop effective stress change during depletion:

$$\sigma_{ij} = \frac{E}{1+\nu}\left(\varepsilon_{ij} + \frac{\nu}{1-2\nu}\varepsilon_b\delta_{ij}\right) + \frac{E}{3(1-\nu)}\varepsilon_s\delta_{ij} \tag{13}$$

Where E is Modulus of elasticity, ε_{ij} is poromechanical strain, δ_{ij} is the Kronecker delta, ε_b is volumetric strain and ε_s is the volumetric matrix shrinkage strain.

By considering uniaxial strain condition and fitting the matrix shrinkage strain to the Langmuir type curves the horizontal effective stress is as following:

$$\Delta\sigma_h = \frac{-\nu}{1-\nu}\Delta P + \frac{E}{3(1-\nu)}\varepsilon_l\left(\frac{P}{P+P_\varepsilon} - \frac{P_0}{P_0+P_\varepsilon}\right) \tag{14}$$

Where ε_l and P_ε are Langmuir-type matrix shrinkage parameters.

The first term on the right-hand side of the equation is poromechanical effect which is the same as conventional reservoirs and the second term is shrinkage effect with is just observed in unconventional reservoirs consist adsorbed gas. Shi and Durucan (2004) didn't consider the effect of poroelasticity and Biot's constant in their model. Cui and Bustin (2005) found through experimental tests that matrix shrinkage volumetric strain is proportional to the volume of adsorbed gas (Figure 9). They also determined the adsorbed gas volume based on Langmuir isotherm equation:

$$\varepsilon_v = \varepsilon_g V_g \tag{15}$$

$$V_g = \frac{V_L P}{P + P_L} \tag{16}$$

Where V_g is the volume of adsorbate is gas, and ε_v is the sorption-induced volumetric strain, ε_g is the coefficient of sorption induced volumetric strain and V_L and P_L are the Langmuir constants.

By considering the equations 13, 15, and 16 one may determine the effective horizontal stress as follows:

$$\Delta\sigma_h = \frac{-\nu}{1-\nu}\Delta P + \frac{E}{3(1-\nu)}\varepsilon_g V_L\left(\frac{P}{P+P_L} - \frac{P_0}{P_0+P_L}\right) \tag{17}$$

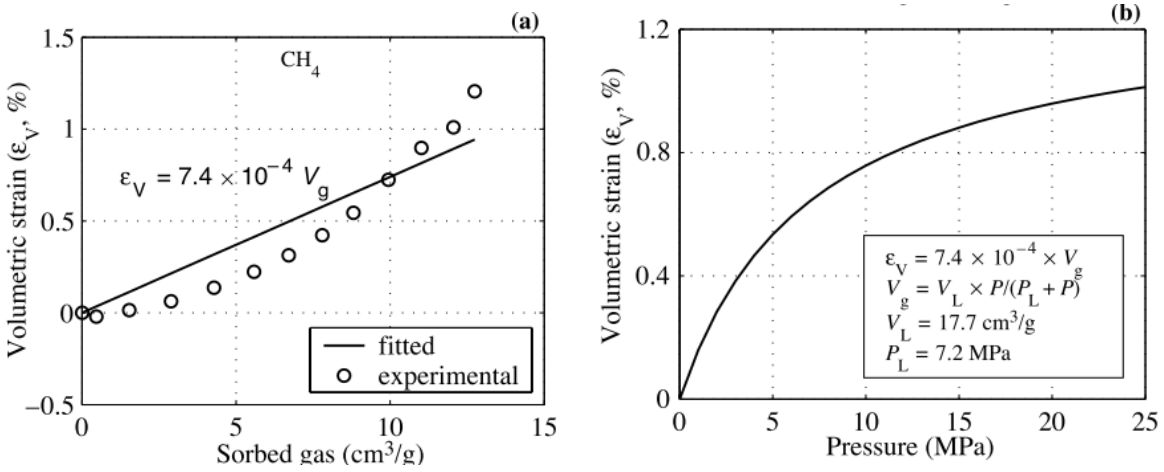

Figure 9. The experimental volumetric strain (a) and the predicted volumetric strain induced by CH4 adsorption, Piceance basin, Canada (b) (Cui and Bustin, 2005).

Mitra et al. (2012) did the first laboratory test on the coal samples under the uniaxial strain condition to investigate the stress path and its accompanied permeability change. They used coal samples from San Juan Basin and they observed the stress path of around 1.57 for coal. Liu and Harpalani (2014) carried out experimental tests on coal samples to measure the horizontal stress changes under reservoir depletion. The samples were saturated with helium as non-adsorptive gas, methane, and CO2. Figure 10 indicates in the case of helium saturated core, where there is no dispersion, the stress path was less than 1 (same as conventional

reservoirs). However, in the case of methane and CO2 as adsorptive gases, there are additional strains from coal shrinkage, and the gradient of the straight line is greater than unity (Figure 11). It indicates that there is a greater loss in horizontal stress compare to the corresponding reduction in pore pressure. Figure 11 shows the rate of horizontal stress loss with CO2 is larger than methane.

Saturated with helium, $S_{\mathrm{h}} = 0.8P + 3.1$ (18)

Saturated with methane, $S_{\mathrm{h}} = 1.2P + 0.8$ (19)

Saturated with CO2, $S_{\mathrm{h}} = 1.3P + 1$ (20)

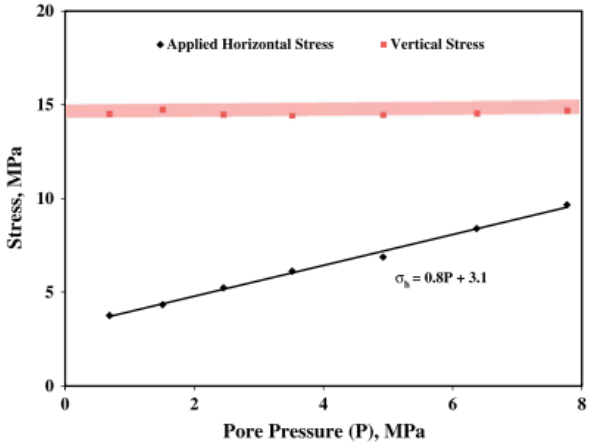

Figure 10. Horizontal and vertical stresses change with helium depletion (Liu and Harpalani, 2014).

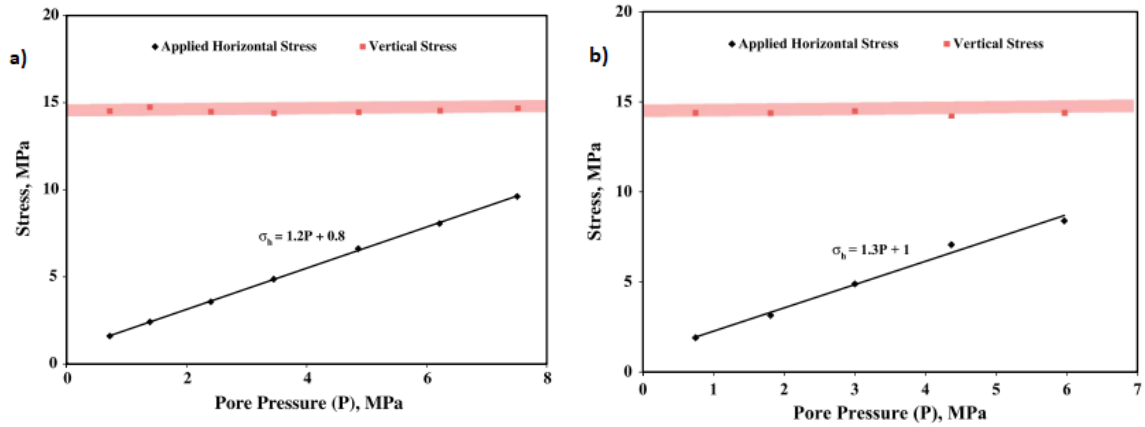

Figure 11. Horizontal and vertical stresses change with a) methane depletion, b) CO2 depletion (Liu and Harpalani, 2014).

Espinoza et al. (2015) carried out a laboratory test to investigate the effective stress reduction induced by desorption. They also developed a double porosity poroelastic model to estimate the horizontal stress changes:

$$\Delta S_h = b\frac{1-2v}{1-v}\Delta P_c + (1-b)\left(\frac{1-2v}{1-v}\right)\frac{ds^a}{dp_m}\Delta P_m \quad (21)$$

Where b is Biot's coefficient, Pc is pressure in the cleats, Pm is the equilibrium pressure in the coal matrix and s^a is the adsorption stress.

Saurabh et al. (2016) also performed the same test on coal samples and they also find the following stress path for helium and methane saturated samples:

Saturated with helium, $S_{\mathrm{h}} = 0.54P + 0.8$ (22)

Saturated with methane, $S_{\mathrm{h}} = 1.17P + 0.8$ (23)

Then they utilized equation 21 and develop a Biot-like coefficient to determine effective horizontal stress reduction by considering depletion and desorption effect:

$$\Delta\sigma_h = b\frac{-v}{1-v}\Delta P + (1-b)\left(\frac{1-2v}{1-v}\right)(-1.7P + 22)\Delta P \quad (24)$$

Table 4 summarized the developed models for stress path in CSG reservoirs.

Table 4. Stress path modelling in CSG reservoirs

Authors	Correlations	Comment
Shi & Durucan, (2004)	$S_{ij} = \frac{E}{1+v}(\varepsilon_{ij} + \frac{v}{1-2v}\varepsilon_b\delta_{ij}) + \alpha P\delta_{ij} + \frac{E}{3(1-v)}\varepsilon_s\delta_{ij}$ $\varepsilon_s = \frac{\varepsilon_l P}{P+P_\varepsilon}$ $\Delta\sigma_{\mathrm{h}} = \frac{-v}{1-v}\Delta P + \frac{E}{3(1-v)}\varepsilon_l(\frac{P}{P+P_\varepsilon} - \frac{P_o}{P_o+P_\varepsilon})$	Uniaxial Strain Condition, α=1
Cui and Bustin (2005)	$\varepsilon_v = \varepsilon_g V_g \ , \ V_g = \frac{V_l P}{P+P_L}$ $\Delta\sigma_{\mathrm{h}} = \frac{-v}{1-v}\Delta P + \frac{E}{3(1-v)}\varepsilon_g V_l(\frac{P}{P+P_l} - \frac{P_o}{P_o+P_l})$	Uniaxial Strain, Piceance Basin, α=1
Mitra et al., (2012)	$S_{\mathrm{h}} = 1.57P$	Uniaxial Strain, San Juan basin
Liu and Harpalani (2014)	$S_{\mathrm{h}} = 0.8P + 3.1, \quad S_{\mathrm{h}} = 1.2P + 0.8 \quad S_{\mathrm{h}} = 1.3P + 1$	Uniaxial Strain, San Juan basin
Epizona et al., (2014)	$\Delta S_{\mathrm{h}} = \alpha\frac{1-2v}{1-v}\Delta \mathrm{P}_c$ +(1-α) $\frac{1-2v}{1-v}\frac{ds^a}{dp_m}\Delta \mathrm{P}_m$	Uniaxial Strain, Double porosity
Saurabh et al., (2016)	$S_{\mathrm{h}} = 0.54P + 0.8, \quad S_{\mathrm{h}} = 1.17P + 0.8$	Uniaxial Strain, San Juan basin
Saurabh et al., (2016)	$\Delta\sigma_{\mathrm{h}} = \alpha\frac{-v}{1-v}\Delta P$ + (1-α) $(\frac{1-2v}{1-v})$(-1.7P+22) ΔP	Uniaxial Strain, San Juan basin

Figure 12.a shows the changes in effective horizontal stress caused by poromechanical and shrinkage effect during depletion by using equation 14. The poromechanical effect results in positive changes of effective horizontal stress whereas the matrix shrinkage effect cause

reduction of effective horizontal stress. These two terms are competing with each other. The state of effective stress dynamically varies with depletion and its evolution is a complex process, depending on the rock mechanical and how sorptive is the coal. The effective in situ stress profile versus reservoir pressure has been depicted in Figure 12.b as an example. The vertical effective stress changes differently from the trend of horizontal stress by depletion. In comparison with conventional reservoirs (Figure 8), CSG shows different stress profiles during production, and as Figure 12.b indicates the effective horizontal stress will decrease rather than increase. It means that because of as matrix shrinkage effect in CSG reservoirs, the stress anisotropy will increase by production which makes the shear failure more susceptible compare to the conventional case.

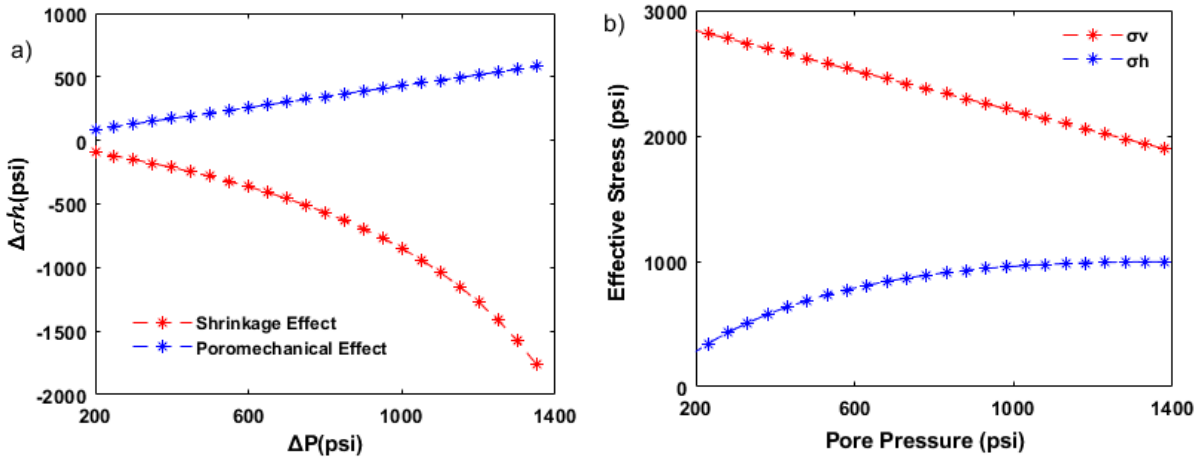

Figure 12. a) The shrinkage and poromechanical effect, b) The effective in situ stresses profile

Liu and Harpalani (2014) discussed the quantitative coal failure situation through Mohr-Coulomb circles in CSG reservoirs (Figure 13). The initial state of stress in a CSG reservoir has shown in Figure 13.a where there is a normal stress regime. Figure 13.b shows a conventional reservoir without any sorption effect. In this case, both vertical and horizontal stresses will increase and the Mohr's circle moves toward the right. For a reservoir with a low sorption effect, the effective horizontal does not change significantly, while the vertical stress will increase and the Mohr's circle will move to the right (Figure 13.c). If a reservoir exhibits

a medium sorption effect associated with depletion, Mohr's circle remains at the same position as the initial condition but its radius is increased and gets closer to the failure line (Figure 13.d). Figure 13.e illustrates a reservoir with a strong sorption effect. It reveals that during depletion, the effective horizontal stress is decreasing, whilst the effective vertical stress is increasing. Therefore, Mohr's circle moves to the left while its radius is increasing by gas production and it results in coal failure.

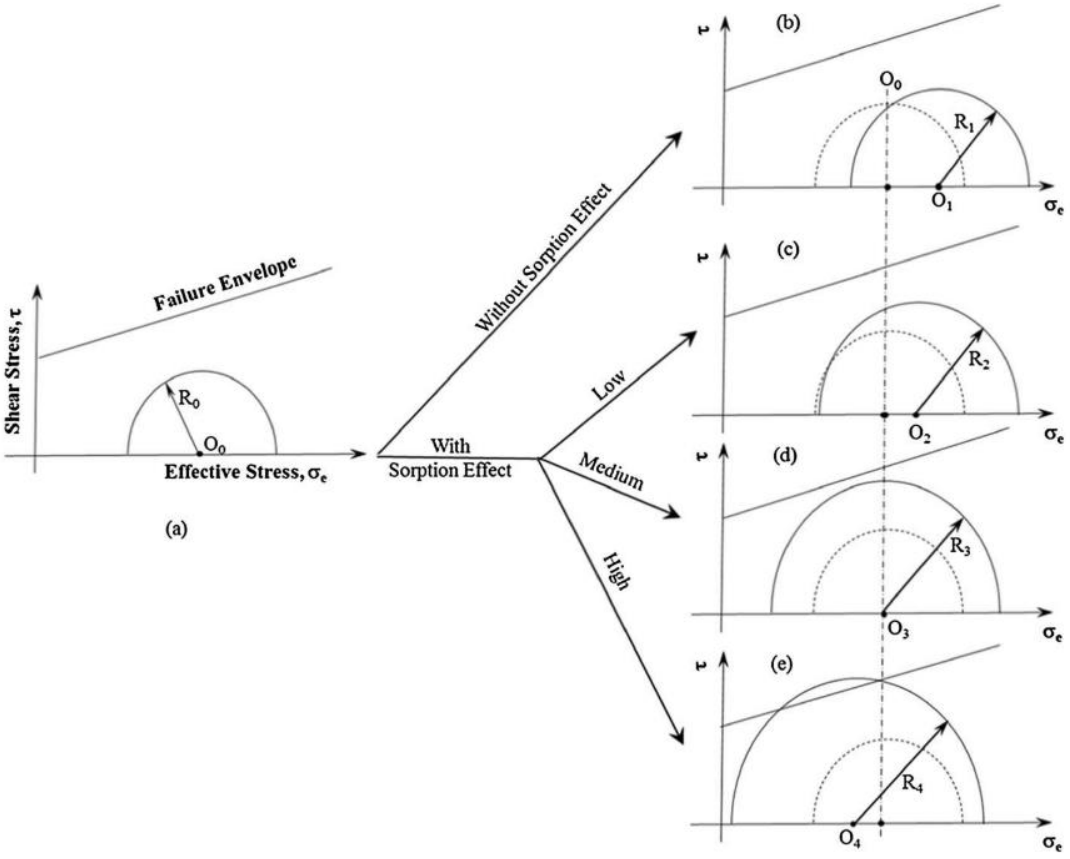

Figure 13. Coal failure situation by Mohr circle diagrams for state of stress evolution with pressure depletion (Liu and Harpalani, 2014)

2.6 CSG production and desorption radius expansion

Throughout the production life of a CSG reservoir, three following stages commonly take place: First is the dewatering stage; the next stage is the stable production stage, and finally there is the decline stage (Figure 14).

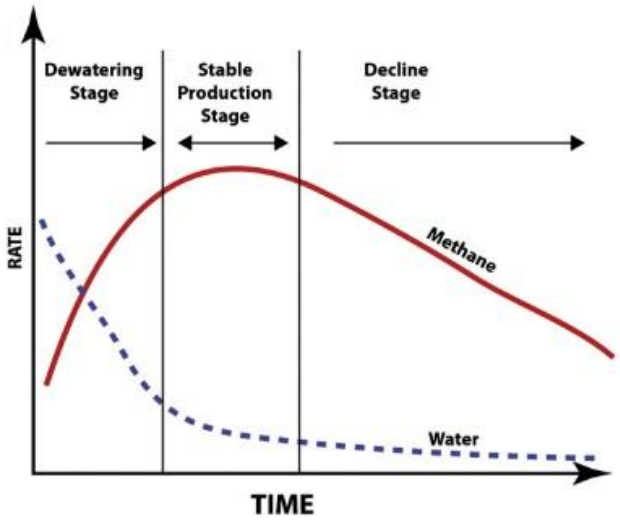

Figure 14. Schematic of water and gas production in a CSG reservoir(Moore, 2012)

During the dewatering stage, since the Bottom-Hole Pressure (BHP) is higher than the critical desorption pressure, no gas has been desorbed. Therefore, the water is the only flowing fluid and there is no matrix shrinkage. After a period of production, when the BHP drops below the critical desorption pressure, the gas desorption starts, and relative permeability to gas will start to increase causing WGR to be reduced from very high to a low value. This transition period is relatively short which has little influence on the pressure profile, and it can be neglected as discussed by Sun et al. (2017). However, continuing the production during the stable and decline stage (which are characterized by low WGR) results in the expansion of desorption radius from the wellbore towards the reservoir boundary (Figure 15). Recently, a few analytical models were developed to predict the expansion of desorption area during production (Sun et al., 2017; Xu et al., 2013). They divided the reservoir domain into two

different regions, i.e., desorption area and non-desorption area to estimate desorption area expansion during CSG production.

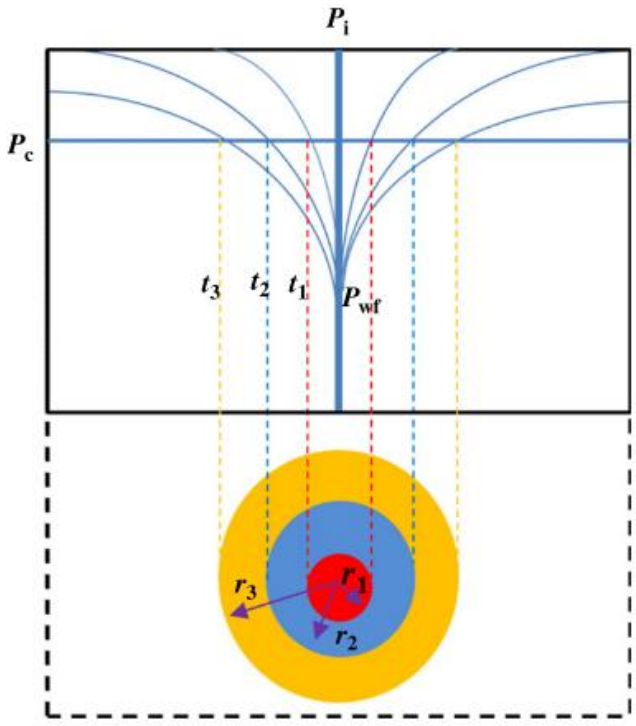

Figure 15. Desorption area expansion during production from a CSG well (Xu et al., 2013).

Our literature review revealed that the desorption radius concept has not been considered in the previously developed models for coal permeability estimation. There exists a large number of experimental and theoretical studies that have evaluated the coal permeability by including the effective stress and matrix shrinkage effect (Connell et al., 2016; Liu and Harpalani, 2013; Liu et al., 2020; Palmer, 2009; Saurabh and Harpalani, 2018; Wu et al., 2010). In these models, the effective stress is not estimated as a function of distance from the wellbore, and therefore the permeability only changes by time not by the distance from the wellbore. Cui et al. (2007) developed an analytical model for stress distribution around a vertical CSG well by considering the impacts of adsorption-induced swelling and applying different boundary conditions. Their study indicates the possibility of 10 times permeability enhancement around a CSG producing well due to matrix shrinkage and reservoir depletion. However, they did not

consider the desorption radius and pressure squared approach for gas flow in the cleat. Additionally, in the previous permeability models, the fluid flow was described by the same equation of pressure (P) approach for the entire area between the wellbore and reservoir boundary rather than the pressure squared (P2) approach for gas flow in the desorption area.

2.7 References

Addis, M.A., 1997a. Reservoir depletion and its effect on wellbore stability evaluation. International Journal of Rock Mechanics and Mining Sciences, 34(3): 4.e1-4.e17.

Addis, M.A., 1997b. The Stress-Depletion Response Of Reservoirs, SPE Annual Technical Conference and Exhibition. Society of Petroleum Engineers, San Antonio, Texas, pp. 11.

Bai, T. et al., 2017. Dimensional analysis and prediction of coal fines generation under two-phase flow conditions. Fuel, 194: 460-479.

Behnoud far, P., Hassani, A.H., Al-Ajmi, A.M. and Heydari, H., 2016. A novel model for wellbore stability analysis during reservoir depletion. Journal of Natural Gas Science and Engineering, 35: 935-943.

Clarkson, C.R., Bustin, R.M. and Seidle, J.P., 2007. Production-Data Analysis of Single-Phase (Gas) Coalbed-Methane Wells. SPE-96018-PA, 10(03): 312-331.

Clarkson, C.R., Jordan, C.L., Gierhart, R.R. and Seidle, J.P., 2008a. Production Data Analysis of Coalbed-Methane Wells. SPE-96018-PA, 11(02): 311-325.

Clarkson, C.R., Pan, Z., Palmer, I.D. and Harpalani, S., 2008b. Predicting Sorption-Induced Strain and Permeability Increase With Depletion for CBM Reservoirs.

Connell, L.D. et al., 2013. Characterisation of Bowen Basin Coal Shrinkage and Geomechanical Properties and Their Influence on Reservoir Permeability, SPE Asia Pacific Oil and Gas Conference and Exhibition. Society of Petroleum Engineers, Jakarta, Indonesia.

Connell, L.D. et al., 2016. Laboratory characterisation of coal matrix shrinkage, cleat compressibility and the geomechanical properties determining reservoir permeability. Fuel, 165: 499-512.

Cui, X. and Bustin, R.M., 2005. Volumetric strain associated with methane desorption and its impact on coalbed gas production from deep coal seams. AAPG Bulletin, 89(9): 1181-1202.

Cui, X., Bustin, R.M. and Chikatamarla, L., 2007. Adsorption-induced coal swelling and stress: Implications for methane production and acid gas sequestration into coal seams. Journal of Geophysical Research: Solid Earth, 112(B10).

Day, S., Fry, R. and Sakurovs, R., 2008. Swelling of Australian coals in supercritical CO2. International Journal of Coal Geology, 74(1): 41-52.

Espinoza, D.N., Pereira, J.M., Vandamme, M., Dangla, P. and Vidal-Gilbert, S., 2015. Desorption-induced shear failure of coal bed seams during gas depletion. International Journal of Coal Geology, 137: 142-151.

Espinoza, D.N., Vandamme, M., Pereira, J.M., Dangla, P. and Vidal-Gilbert, S., 2014. Measurement and modeling of adsorptive–poromechanical properties of bituminous coal cores exposed to CO2: Adsorption, swelling strains, swelling stresses and impact on fracture permeability. International Journal of Coal Geology, 134-135: 80-95.

Fan, L. and Liu, S., 2018. Numerical prediction of in situ horizontal stress evolution in coalbed methane reservoirs by considering both poroelastic and sorption induced strain effects. International Journal of Rock Mechanics and Mining Sciences, 104: 156-164.

Feng, R., Harpalani, S. and Saurabh, S., 2018. Experimental investigation of in situ stress relaxation on deformation behavior and permeability variation of coalbed methane reservoirs during primary depletion. Journal of Natural Gas Science and Engineering, 53: 1-11.

Geertsma, J., 1957. The Effect of Fluid Pressure Decline on Volumetric Changes of Porous Rocks. Society of Petroleum Engineers, pp. 10.

Gentzis, T., 2009. Review of Mannville Coal Geomechanical Properties: Application to Coalbed Methane Drilling in the Central Alberta Plains, Canada. Energy Sources, Part A: Recovery, Utilization, and Environmental Effects, 32(4): 355-369.

Gouth, F., Belushko, I. and Herwin, H., 2014. Dynamic Behavior of a Multi-Layered Coal Seams Gas Reservoir in the Bowen Basin.

Gray, I., 1987. Reservoir Engineering in Coal Seams: Part 1-The Physical Process of Gas Storage and Movement in Coal Seams. SPE Reservoir Engineering, 2(01): 28-34.

Harpalani, S. and Chen, G., 1995. Estimation of changes in fracture porosity of coal with gas emission. Fuel, 74(10): 1491-1498.

Harpalani, S. and Schraufnagel, R.A., 1990. Shrinkage of coal matrix with release of gas and its impact on permeability of coal. Fuel, 69(5): 551-556.
Ian Palmer, J.M., 1998. How Permeability Depends on Stress and Pore Pressure in Coalbeds: A New Model.
Kaffash, A. and Zare-Reisabadi, M.R., 2013. Borehole stability evaluation in overbalanced and underbalanced drilling: based on 3D failure criteria. Geosystem Engineering, 16(2): 175-182.
Levine, J.R., 1996. Model study of the influence of matrix shrinkage on absolute permeability of coal bed reservoirs. Geological Society, London, Special Publications, 109(1): 197.
Liu, S. and Harpalani, S., 2013. Permeability prediction of coalbed methane reservoirs during primary depletion. International Journal of Coal Geology, 113: 1-10.
Liu, S. and Harpalani, S., 2014. Evaluation of in situ stress changes with gas depletion of coalbed methane reservoirs. Journal of Geophysical Research: Solid Earth, 119(8): 6263-6276.
Liu, T. et al., 2020. Stress response during in-situ gas depletion and its impact on permeability and stability of CBM reservoir. Fuel, 266: 117083.
Lu, M. and Connell, L., 2016. Coal failure during primary and enhanced coalbed methane production — Theory and approximate analyses. International Journal of Coal Geology, 154-155: 275-285.
Mitra, A. and Harpalani, S., 2007. Modeling Incremental Swelling of Coal Matrix with CO2 Injection in Coalbed Methane Reservoirs, Eastern Regional Meeting. Society of Petroleum Engineers, Lexington, Kentucky USA, pp. 8.
Mitra, A., Harpalani, S. and Liu, S., 2012. Laboratory measurement and modeling of coal permeability with continued methane production: Part 1 – Laboratory results. Fuel, 94: 110-116.
Moore, R.L., Loftin, D.F. and Palmer, I.D., 2011. History Matching and Permeability Increases of Mature Coalbed Methane Wells in San Juan Basin, SPE Asia Pacific Oil and Gas Conference and Exhibition. Society of Petroleum Engineers, Jakarta, Indonesia.
Moore, T.A., 2012. Coalbed methane: A review. International Journal of Coal Geology, 101: 36-81.
Okotie, V.U. and Moore, R.L., 2011. Well-Production Challenges and Solutions in a Mature, Very-Low-Pressure Coalbed-Methane Reservoir.
Olson, J.E., Laubach, S.E. and Lander, R.H., 2009. Natural fracture characterization in tight gas sandstones: Integrating mechanics and diagenesis. AAPG Bulletin, 93(11): 1535-1549.
Palmer, I., 2009. Permeability changes in coal: Analytical modeling. International Journal of Coal Geology, 77(1): 119-126.
Palmer, I., 2010. Coalbed methane completions: A world view. International Journal of Coal Geology, 82(3): 184-195.
Palmer, I.D., Moschovidis, Z.A. and Cameron, J.R., 2005. Coal Failure and Consequences for Coalbed Methane Wells, SPE Annual Technical Conference and Exhibition. Society of Petroleum Engineers, Dallas, Texas.
Pan, Z. and Connell, L.D., 2012. Modelling permeability for coal reservoirs: A review of analytical models and testing data. International Journal of Coal Geology, 92: 1-44.
Puspitasari, R., Gan, T., Pallikathekathil, Z.J. and Luft, J., 2014. Wellbore Stability Modelling for Horizontal and Multi-Branch Lateral Wells in CBM: Practical Solution to Better Understand the Uncertainty in Rock Strength and Coal Heterogeneity, SPE Asia Pacific Oil & Gas Conference and Exhibition. Society of Petroleum Engineers, Adelaide, Australia.
Rajora, A. et al., 2019. Deviated Pad Wells in Surat: Journey So Far, SPE/AAPG/SEG Asia Pacific Unconventional Resources Technology Conference. Unconventional Resources Technology Conference, Brisbane, Australia, pp. 14.
Reucroft, P.J. and Patel, H., 1986. Gas-induced swelling in coal. Fuel, 65(6): 816-820.
Saurabh, S. and Harpalani, S., 2018. Stress path with depletion in coalbed methane reservoirs and stress based permeability modeling. International Journal of Coal Geology, 185: 12-22.
Saurabh, S., Harpalani, S. and Singh, V.K., 2016. Implications of stress re-distribution and rock failure with continued gas depletion in coalbed methane reservoirs. International Journal of Coal Geology, 162: 183-192.
Seidle, J., 2011. Fundamentals of Coalbed Methane Reservoir Engineering. PennWell Corporation.

Seidle, J.P., Jeansonne, M.W. and Erickson, D.J., 1992. Application of Matchstick Geometry To Stress Dependent Permeability in Coals, SPE Rocky Mountain Regional Meeting. Society of Petroleum Engineers, Casper, Wyoming, pp. 12.

Seidle, J.R. and Huitt, L.G., 1995. Experimental Measurement of Coal Matrix Shrinkage Due to Gas Desorption and Implications for Cleat Permeability Increases.

Shi, J.-Q. and Durucan, S., 2005. A Model for Changes in Coalbed Permeability During Primary and Enhanced Methane Recovery.

Shi, J. et al., 2019. An accurate method for permeability evaluation of undersaturated coalbed methane reservoirs using early dewatering data. International Journal of Coal Geology, 202: 147-160.

Shi, J.Q. and Durucan, S., 2004. Drawdown Induced Changes in Permeability of Coalbeds: A New Interpretation of the Reservoir Response to Primary Recovery. Transport in Porous Media, 56(1): 1-16.

Somerton, W.H., Söylemezoğlu, I.M. and Dudley, R.C., 1975. Effect of stress on permeability of coal. International Journal of Rock Mechanics and Mining Sciences & Geomechanics Abstracts, 12(5): 129-145.

Sparks, D.P., McLendon, T.H., Saulsberry, J.L. and Lambert, S.W., 1995. The Effects of Stress on Coalbed Reservoir Performance, Black Warrior Basin, U.S.A.

Sun, Z. et al., 2017. A semi-analytical model for drainage and desorption area expansion during coal-bed methane production. Fuel, 204: 214-226.

Teufel, L.W., Rhett, D.W. and Farrell, H.E., 1991. Effect of Reservoir Depletion And Pore Pressure Drawdown On In Situ Stress And Deformation In the Ekofisk Field, North Sea, The 32nd U.S. Symposium on Rock Mechanics (USRMS). American Rock Mechanics Association, Norman, Oklahoma, pp. 10.

Wei, C., Zou, M., Sun, Y., Cai, Z. and Qi, Y., 2015. Experimental and applied analyses of particle migration in fractures of coalbed methane reservoirs. Journal of Natural Gas Science and Engineering, 23: 399-406.

Wu, Y., Liu, J., Elsworth, D., Miao, X. and Mao, X., 2010. Development of anisotropic permeability during coalbed methane production. Journal of Natural Gas Science and Engineering, 2(4): 197-210.

Xu, B. et al., 2013. An analytical model for desorption area in coal-bed methane production wells. Fuel, 106: 766-772.

Yang, Y. et al., 2014. A new attempt of a CBM tree-like horizontal well: A pilot case of Well ZS 1P-5H in the Qinshui Basin. Natural Gas Industry B, 1(2): 205-209.

Zhang, R. et al., 2016. Critical drawdown pressure of sanding onset for offshore depleted and water cut gas reservoirs: Modeling and application. Journal of Natural Gas Science and Engineering, 34: 159-169.

Zoback, M.D. and Zinke, J.C., 2002. Production-induced Normal Faulting in the Valhall and Ekofisk Oil Fields. pure and applied geophysics, 159(1): 403-420

3 Analytical modelling of coal failure in coal seam gas reservoirs in different stress regimes

3.1 Analytical modelling of coal failure in coal seam gas reservoirs in different stress regimes

Zare Reisabadi M, Haghighi M, Salmachi A, Sayyafzadeh M, Khaksar A. International Journal of Rock Mechanics and Mining Sciences. 2020; 128:104259.

Statement of Authorship

Title of Paper	Analytical modelling of coal failure in coal seam gas reservoirs in different stress regimes
Publication Status	☑ Published ☐ Accepted for Publication ☐ Submitted for Publication ☐ Unpublished and Unsubmitted w ork w ritten in manuscript style:
Publication Details	Zare Reisabadi M, Haghighi M, Salmachi A, Sayyafzadeh M, Khaksar A. International Journal of Rock Mechanics and Mining Sciences. 2020; 128:104259.

Principal Author

Name of Principal Author (Candidate)	Mohammadreza Zare Reisabadi		
Contribution to the Paper	Literature review, Model development, Analysis of results, wiring the manuscript.		
Overall percentage (%)	70		
Certification:	This paper reports on original research I conducted during the period of my Higher Degree by Research candidature and is not subject to any obligations or contractual agreements with a third party that would constrain its inclusion in this thesis. I am the primary author of this paper.		
Signature		Date	09/03/2021

Co-Author Contributions

By signing the Statement of Authorship, each author certifies that:

i. the candidate's stated contribution to the publication is accurate (as detailed above);

ii. permission is granted for the candidate in include the publication in the thesis; and

iii. the sum of all co-author contributions is equal to 100% less the candidate's stated contribution.

Name of Co-Author	Manouchehr Haghighi		
Contribution to the Paper	Support in analysis of results, Reviewing the manuscript		
Signature		Date	9/3/21

Name of Co-Author	Alireza Salmachi		
Contribution to the Paper	Support in analysis of results, Reviewing the manuscript		
Signature		Date	12/03/2021

Name of Co-Author	Mohammad Sayyafzadeh		
Contribution to the Paper	Support in analysis of results, Reviewing the manuscript		
Signature		Date	9/3/2021

Name of Co-Author	Abbas Khaksar		
Contribution to the Paper	Support in analysis of results, Reviewing the manuscript		
Signature		Date	15/3/2021

International Journal of Rock Mechanics & Mining Sciences 128 (2020) 104259

Contents lists available at ScienceDirect

International Journal of Rock Mechanics and Mining Sciences

journal homepage: http://www.elsevier.com/locate/ijrmms

Analytical modelling of coal failure in coal seam gas reservoirs in different stress regimes

Mohammadreza Zare Reisabadi [a,*], Manouchehr Haghighi [a], Alireza Salmachi [a], Mohammad Sayyafzadeh [a], Abbas Khaksar [b]

[a] Australian School of Petroleum, The University of Adelaide, Australia
[b] Baker Hughes, a GE Company, Perth, Australia

ARTICLE INFO

Keywords:
Coal seam gas
Matrix shrinkage
Depletion
Coal failure
Stress path

ABSTRACT

Coal seam gas (CSG) reservoirs typically have low rock strength. During gas production, pressure depletion and matrix shrinkage may cause the differential stress around the wellbore to exceed the coal mechanical strength and result in rock failure. Coal failure has several detrimental consequences including coal fines production, permeability reduction, wellbore filling and damage to pumps and compressors. The matrix shrinkage causes a unique stress path in CSG reservoirs. However, the details of how matrix shrinkage affects coal failure still have remained uncertain. This paper presents a new workflow to evaluate stress distribution around CSG wells and predicts coal failure by coupling the effects of pressure depletion, matrix shrinkage and wellbore simultaneously. The model calculates Maximum Coal Free Drawdown Pressure (*MCFDP*) by considering the effects of all contributing parameters and Mogi-Coulomb failure criterion. Data from a vertical well in the San Juan Basin in USA were used to evaluate the validity of the developed model. The developed model was applied to evaluate coal failure under three different stress regimes. The results indicate that pressure depletion and matrix shrinkage have a significant effect on coal failure in all stress regimes. In the case of a normal stress regime, it is found that vertical wellbores are the most stable during the life of a reservoir. However, in the case of strike-slip and reverse stress regimes, pressure depletion and matrix shrinkage could cause the change of stress regime and therefore, the optimum wellbore trajectory could change. Additionally, it is found that in the normal stress regime the depletion and matrix shrinkage reduces the *MCFDP* of horizontal wellbores more than the vertical wells. However, in the reverse stress regime, depletion and shrinkage cause more reduction of *MCFDP* in vertical wellbores compared to horizontal wells.

1. Introduction

During past decades, CSG or Coal Bed Methane (CBM) have increasingly become an important part of natural gas resource. The world CSG resource constitutes around 2980 to 9260 Tcf.[1,2] Moreover, by the exploration of more CSG around the world and development of new technologies that enable commercial production from CSG, an increase in production from these reservoirs is expected in the future.[3]

CSG reservoirs are considered as unconventional gas resources because methane is not trapped by overlying seals and is normally adsorbed on the coal matrix while the coal cleat system is saturated with water. Dewatering is initially carried out to deplete the reservoir pressure and this causes the progressive desorption of gas. Gas desorption from the coal matrix causes matrix shrinkage.[4,5] The matrix shrinkage will affect material behavior and leads to a specific stress path during production (section 2.2). This makes the CSG unique in terms of stress distribution around the well. Since the CSG reservoirs are naturally fractured and typically have low rock strength, pressure depletion, and matrix shrinkage can change the stress concentration around the wellbore so that it exceeds the coal mechanical strength and results in coal failure and coal particles production.

Coal failure may cause serious gas production issues from CSG reservoirs.[6,7] There are wide reported problems during drilling and production, particularly in deviated and horizontal CSG wells in pressure depleted condition. It has been reported that 40% of the horizontal CSG wells in the Qinshui Basin in China have serious instability problems during drilling and production.[8] Some of the recently drilled horizontal and multi-lateral wells in the Bowen Basin, Australia have experienced

* Corresponding author.
E-mail address: mohammadreza.zarereisabadi@adelaide.edu.au (M. Zare Reisabadi).

https://doi.org/10.1016/j.ijrmms.2020.104259
Received 8 August 2019; Received in revised form 11 February 2020; Accepted 11 February 2020
Available online 20 February 2020

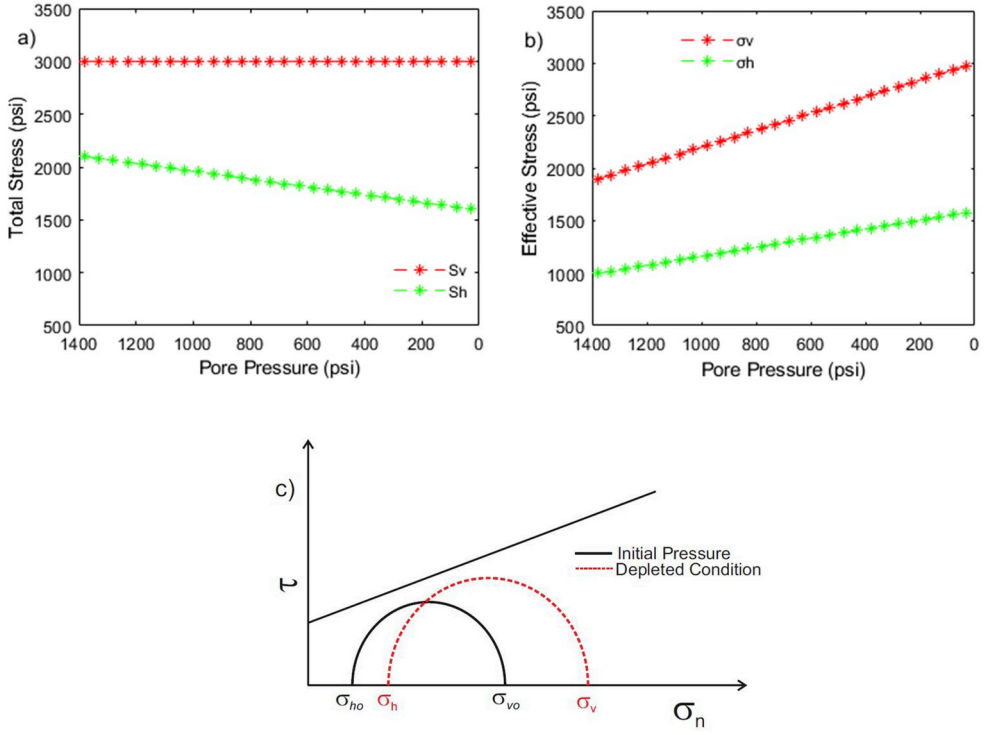

Fig. 1. a) The total vertical and horizontal stress changes during depletion b) The effective vertical and horizontal stress changes c) Schematic Failure envelope and change of Mohr Circles during production.

coal fines production during production.[9] In San Juan Basin, USA, massive coal fines production has also been observed during late production, when reservoir pressure had decreased to less than 300 psi from initial pressure of 1260 psi. Matrix shrinkage, desorption with pressure depletion induced horizontal stress changes are interpreted as the cause of geomechanical failure.[3,5,10] Moreover, several borehole failure and coal fines production events are experienced in depleted coal in the Arkoma Basin, Oklahoma.[11]

Recently, many researchers have shown that after a long-term exponential increase in permeability with depletion caused by desorption-induced shrinkage, a sudden decrease in coal reservoir permeability is observed and coincided with coal fines production.[3,10,12] Keshavarz, Badalyan[13] concluded that during depletion, coal permeability may decrease due to the cleat closure. Production of coal particles has adverse effects on downhole and surface facilities and artificial lift pumps. The failed coal can also plug the cleat system and cause permeability reduction.[14,15]

Palmer, Moschovidis[11] investigated the coal failure mechanism and its consequences. They used a conventional sanding onset model to predict coal failure but did not consider the shrinkage effect and its induced stress path on coal failure. Liu and Harpalani[16] carried out a qualitative analysis of coal failure by illustrating Mohr's circle and considered gas depletion. They noticed that methane desorption had a significant effect on in situ stress state and as a result, shear failure takes place earlier than a conventional reservoir where there is no shrinkage effect. Bai, Chen[17] and Bai, Chen[15] used numerical simulation to characterize coal failure and fines generation during dewatering and gas production. Recently, Espinoza, Pereira[3] and Lu and Connell[7] developed an analytical model to consider the effect of desorption on coal failure. However, the effect of the wellbore trajectory on stress redistribution around the wellbore was not considered. Saurabh, Harpalani[18] conducted laboratory experiments to measure coal matrix volumetric strain from desorption and modeled the lateral stress changes during experiments.

This paper presents an analytical model to evaluate the stress distribution around the wellbore by coupling the effect of depletion, matrix shrinkage, and the wellbore. An analytical model is also developed to calculate the Critical Coal Free Bottom-hole Pressure (CCFBP) and Maximum Coal Free Drawdown Pressure (*MCFDP*). The model is validated by field data in the San Juan Basin. Moreover, the developed model is utilized to investigate the effect of different well inclinations and azimuths, pressure depletion on coal failure in different situ stress regimes.

2. Stress path and workflow for coal failure

2.1. Stress path in conventional reservoirs

The uniaxial strain condition is commonly used as a simplified model during depletion from a laterally extensive reservoir, which means constant vertical stress, zero lateral strain and associated changes in horizontal stresses.[3,16,19,20] The horizontal stress variations are quantified by reservoir stress path which is defined as the changes in total horizontal stresses per unit change of pore pressure during production from a reservoir as follows:

$$\frac{\Delta S_h}{\Delta P} = K = \beta \frac{1-2v}{1-v} \tag{1}$$

$$\sigma_h = S_h - \beta P \tag{2}$$

$$\frac{\Delta \sigma_h}{\Delta P} = -\beta \frac{v}{1-v} \tag{3}$$

Where S_h is the total horizontal stress, σ_h is the effective horizontal stress, P is initial pore pressure, β is Biot's coefficient and ν is Poisson's ratio. Equations (1)–(3) show that the reservoir depletion is expected to be accompanied by reduction of total horizontal stresses and hereby, increase of effective horizontal stress which has been confirmed by field observations in many conventional reservoirs around the world.[21–23] The increase of the effective stress during pressure depletion also decreases the reservoir permeability. As the Poisson's ratio of the rock is

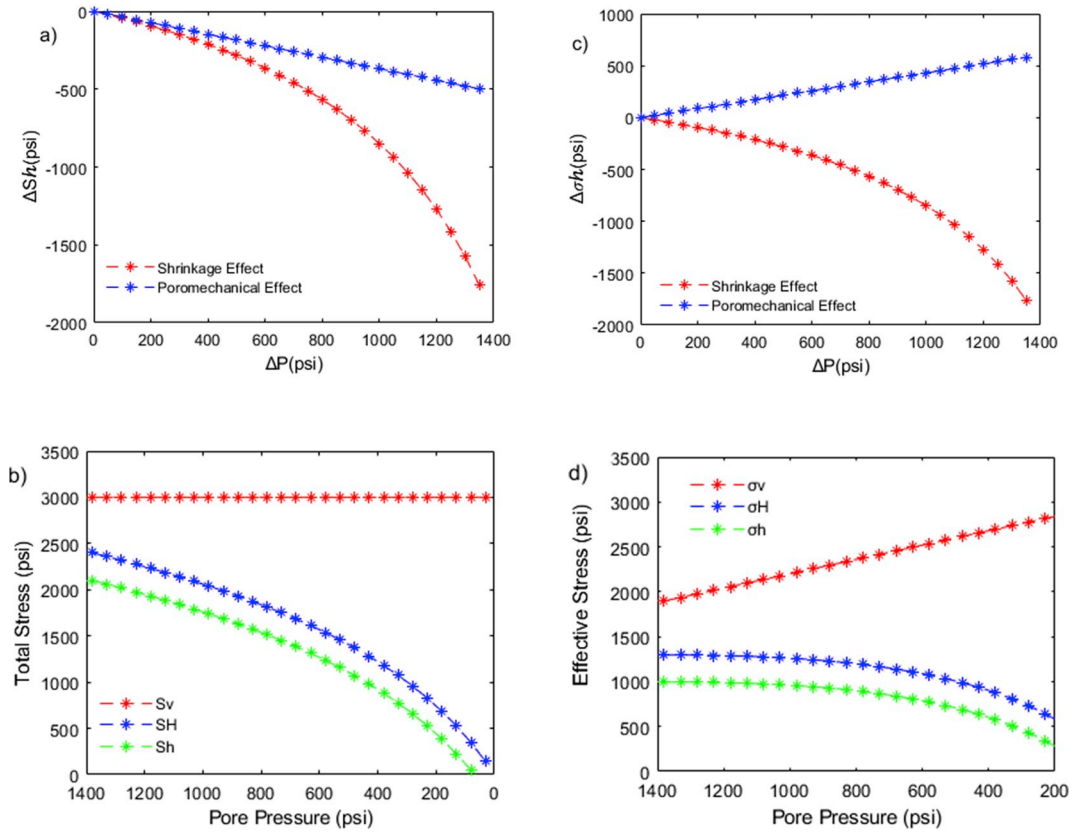

Fig. 2. a) Shrinkage and poromechanical terms of total stress change, b) Total in situ stresses profile during production, c) Shrinkage and poromechanical terms of effective stress change, d) Effective in situ stresses profile during production.

less than 0.5, therefore the stress path will be less than one for conventional reservoirs.

Based on uniaxial strain condition, the total vertical stress is constant and it results in the reduction of effective vertical stress by depletion: $\Delta\sigma_V = -\beta\Delta P > 0$. In the case of horizontal stress, the total stress will decrease and then the change of effective horizontal stress would be $\Delta\sigma_h = -\beta\frac{\nu}{1-\nu}\Delta P > 0$. The total stresses and effective stresses versus production have been shown in Fig. 1.a and Fig. 1.b respectively. It is clear from Fig. 1.a that total vertical stress is constant during depletion, whilst the total horizontal stress will decrease. Fig. 1.b indicates the changes in effective vertical stress are more than effective horizontal stress, which results in an increase of deviatoric stress with production. These stress changes by depletion cause the Mohr circle to move to the right, and the different changes of vertical and horizontal effective stresses make Mohr circle bigger during depletion (Fig. 1c). With further depletion, a significant stress anisotropy may occur which could lead to the failure around the wellbore and fine production. This has been widely studied in the literature for sand production.[24–27] The change of Mohr circle by production in unconventional reservoirs is different which will be discussed in the following section.

2.2. Stress path in CSG reservoirs

The pressure depletion during production from CSG reservoirs has two impacts on effective horizontal stress. First, based on uniaxial strain condition and similar to conventional reservoirs, the effective stress will increase. On the other hand, the methane desorption from the coal will be associated with matrix shrinkage and conversely, the effective horizontal stress will be reduced because of changes in total horizontal stress with shrinkage.[4,28,29] Many experimental studies revealed that the stress path in CSG reservoirs could be more than one.[3,16,18,30,31] Therefore, the commonly used theoretical stress path (equation (1)) cannot describe the stress profile of CSG reservoirs during depletion as the conventional value of stress path for any combination of Poisson's ratio and Biot's constant would be less than one.

Shi and Durucan[29] utilized the elastic theory of stress and strain relation and analogy between thermal contraction and matrix shrinkage to develop effective stress change during depletion:

$$\sigma_{ij} = \frac{E}{1+\nu}\left(\varepsilon_{ij} + \frac{\nu}{1-2\nu}\varepsilon_b\delta_{ij}\right) + \frac{E}{3(1-\nu)}\varepsilon_s\delta_{ij} \tag{4}$$

Where E is the modulus of elasticity, ε_{ij} is poromechanical strain, δ_{ij} is the Kronecker delta, ε_b is volumetric strain and ε_s is the volumetric matrix shrinkage strain. By considering uniaxial strain condition and fitting the matrix shrinkage strain to the Langmuir type curves the horizontal total stress and horizontal effective stress will be as follows:

$$\Delta S_h = \frac{1-2\nu}{1-\nu}\Delta P + \frac{E}{3(1-\nu)}\varepsilon_l\left(\frac{P}{P+P_\varepsilon} - \frac{P_o}{P_o+P_\varepsilon}\right) \tag{5}$$

$$\Delta\sigma_h = \frac{-\nu}{1-\nu}\Delta P + \frac{E}{3(1-\nu)}\varepsilon_l\left(\frac{P}{P+P_\varepsilon} - \frac{P_o}{P_o+P_\varepsilon}\right) \tag{6}$$

Where ε_l and P_ε are Langmuir-type matrix shrinkage parameters. P and P_o are current and initial reservoir pressure respectively. The first term in the right-hand side of the equation is poromechanical effect which is the same as conventional reservoirs and the second term is shrinkage effect with is only observed in unconventional reservoirs with adsorbed gas.

Cui and Bustin[32] found through experimental tests that matrix shrinkage volumetric strain is proportional to the volume of adsorbed gas. They also determined the adsorbed gas volume based on the Langmuir isotherm equation:

$$\varepsilon_v = \varepsilon_g V_g \quad \text{and} \quad V_g = \frac{V_l P}{P + P_L} \tag{7}$$

Where V_g is the volume of adsorbate (gas), and ε_v is sorption or desorption-induced volumetric strain, P is current reservoir pressure, ε_g is the coefficient of sorption induced volumetric strain and V_l and P_L are the Langmuir constants. By considering equations (4) and (7), and the uniaxial strain condition one may determine the effective horizontal stress as follows:

$$\Delta\sigma_h = \frac{-\nu}{1-\nu}\Delta P + \frac{E}{3(1-\nu)}\varepsilon_g V_l\left(\frac{P}{P+P_l} - \frac{P_o}{P_o+P_l}\right) \tag{8}$$

Mitra, Harpalani[30] did the first laboratory test on coal samples under uniaxial strain condition to investigate the stress path and its accompanied permeability change. They used some coal samples from the San Juan Basin. They determined a stress path of approximately 1.57 for their coal samples. Liu and Harpalani[16] carried out laboratory experiments on coal samples to measure the horizontal stress changes under reservoir depletion. The samples were saturated with helium as non-adsorptive gas, methane, and CO2. They noticed in the case of helium saturated core, the stress path was less than 1, but as methane and CO2 are adsorptive gas there is additional strain from coal shrinkage, and the resultant stress path were more than 1:

$$\text{Saturated with helium } S_h = 0.8P + 3.1 \tag{9}$$

$$\text{Saturated with methane } S_h = 1.2P + 0.8 \tag{10}$$

$$\text{Saturated with CO2 } S_h = 1.3P + 1 \tag{11}$$

Espinoza, Pereira[3] carried out laboratory tests to investigate the effective stress reduction induced by desorption. They also developed a double porosity poroelastic model to estimate the horizontal stress changes:

$$\Delta S_h = \beta\frac{1-2\nu}{1-\upsilon}\Delta P_c + (1-\beta)\left(\frac{1-2\nu}{1-\upsilon}\right)\frac{ds^a}{dp_m}\Delta P_m \tag{12}$$

Where β is Biot's coefficient, Pc is pressure in the cleats, Pm is the equilibrium pressure in the coal matrix and s^a is the adsorption stress. Saurabh, Harpalani[18] also performed similar tests on coal samples and they too found the following stress path for helium and methane saturated samples:

$$\text{Saturated with helium } S_h = 0.54P + 0.8 \tag{13}$$

$$\text{Saturated with methane } S_h = 1.17P + 0.8 \tag{14}$$

They utilized equation (12) to develop a Biot-like stress path coefficient to determine effective horizontal stress reduction by considering both the pressure depletion and desorption effects:

$$\frac{d\sigma_h}{dP} = \beta\left(\frac{-\nu}{1-\upsilon}\right) + (1-\beta)\left(\frac{1-2\nu}{1-\upsilon}\right)(-1.7P + 22) \tag{15}$$

Fig. 2.a shows changes in total horizontal stress caused by poromechanical and shrinkage effect by pore pressure depletion and methane desorption (Equation (5)). Both poromechanical and shrinkage effects are negative and that is why the stress path in CSG reservoirs is higher than conventional. The total horizontal stresses profile versus reservoir pressure are plotted in Fig. 2. b. Based on the uniaxial strain condition and same as conventional reservoirs case, that the total vertical stress will be unaffected by pressure depletion, whilst both principal horizontal stresses will reduce. Fig. 2. c shows the changes in effective horizontal stress caused by poromechanical and shrinkage effect by pore pressure depletion (Equation (6)). As Fig. 2. c indicates, the poromechanical effect results in positive changes of effective horizontal stress whereas the matrix shrinkage effect reduces the effective horizontal stress. The effective in situ stresses profile versus reservoir pressure have been depicted in Fig. 2. d. The effective vertical stress will increase during production whilst effective horizontal stresses will decrease. In comparison with conventional reservoirs (Fig. 1), CSG shows different stress profiles during production and the effective horizontal stress will decrease rather than increase. It means that as matrix shrinkage happens, the stress anisotropy will increase which makes the shear failure more susceptible than the conventional case. The effective horizontal stresses and the possible failure in the normal fault stress regime have been shown in Fig. 3. It reveals that unlike the conventional case where both effective stresses were increasing, depleting the CSG reservoirs will not move the Mohr circle to the right-hand side. It causes reduction of effective minimum horizontal stress and increase of effective vertical stress and hence there will be a larger Mohr circle which depending on the initial values of in situ stresses, the depletion levels, and the coal strength coal failure could occur.

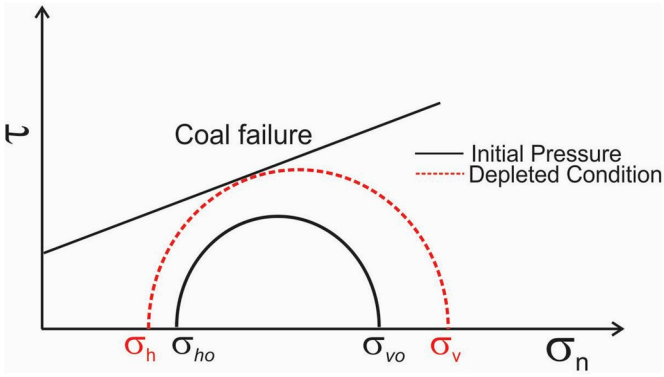

Fig. 3. Coal failure because of the reduction of minimum horizontal stress.

2.3. Analytical model and workflow

In order to couple the effect of pressure depletion, desorption and wellbore effect on coal failure during production from CSG reservoirs, the coal strength and principal stresses around the wellbore are evaluated by using a failure criterion. Linear poroelasticity model is utilized in a cylindrical geometry to model the stress distribution around the wellbore (detailed equations can be found in Zare-Reisabadi, Kaffash[33]). Based on this model the maximum stress concentration, and the resulting failure is on the wellbore wall. The stress distribution for a deviated wellbore is as following:

$$S_r = P_w$$

$$S_\theta = \sigma_x^o + \sigma_y^o - 2\left(\sigma_x^o - \sigma_y^o\right)cos2\theta - 4\tau_{xy}^o sin2\theta - P_w + \beta_0\left(P_w - P_f\right) \tag{16}$$

$$S_z = \sigma_v - \upsilon\left(2\left(\sigma_x^o - \sigma_y^o\right)cos\,2\theta - 4\tau_{xy}^o\,sin\,2\theta\right) + \beta_0\left(P_w - P_f\right)$$

$$\tau_{\theta z} = 2\left(\tau_{yz}^o\,cos\,\theta - \tau_{xz}^o\,sin\,\theta\right)$$

$$\tau_{r\theta} = 0$$

$$\tau_{rz} = 0$$

$$\beta_0 = \frac{1-2v}{1-v}.\beta$$

Where S_r is radial stress, S_θ is tangential stress, S_z is axial stress, P_w is bottom-hole pressure, P_f is current reservoir pressure, θ is the angular position around the wellbore.

And

$$\sigma_x^o = \left(S_H cos^2\alpha + S_h sin^2\alpha\right)cos^2 i + S_v sin^2 i,$$

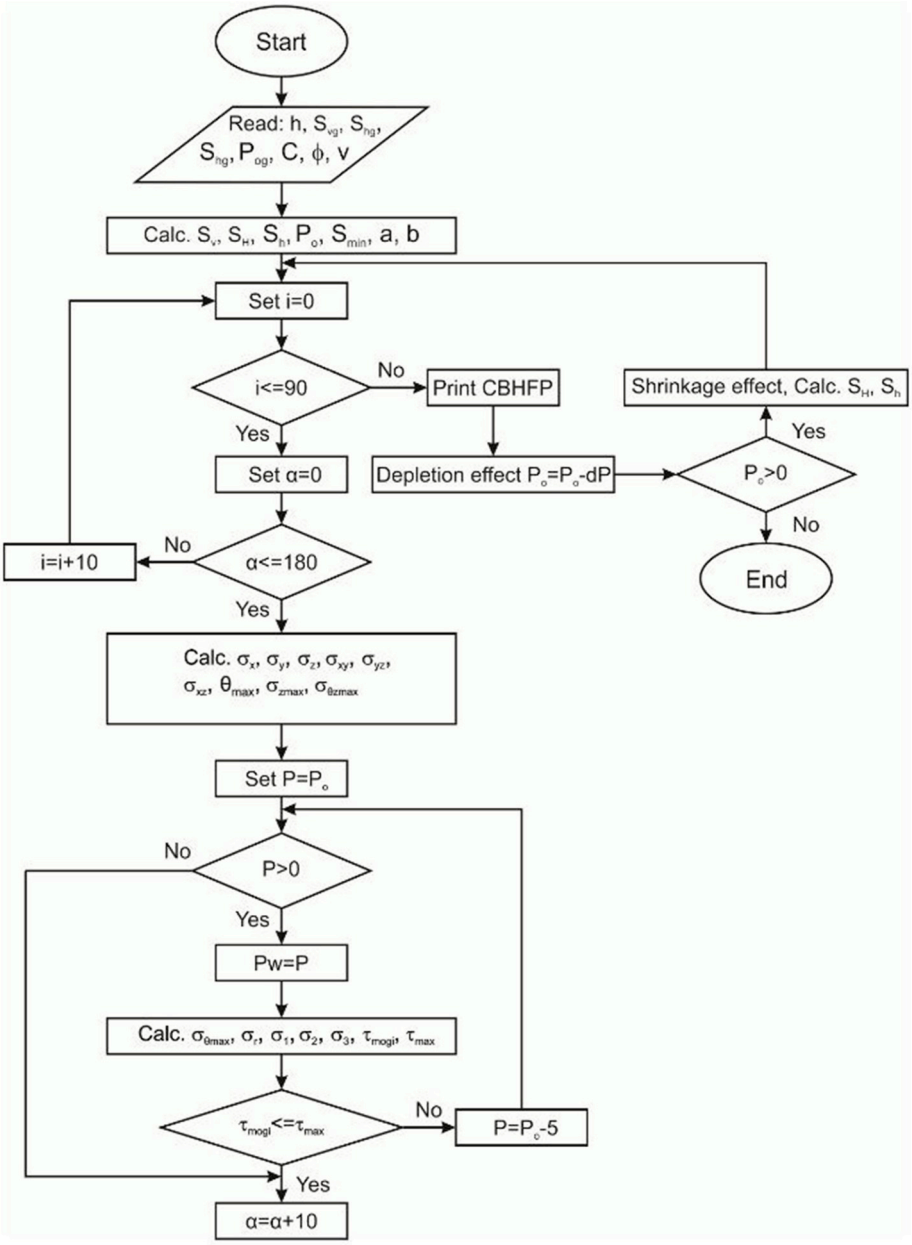

Fig. 4. The developed workflow for coal failure prediction.

$$\sigma_y^o = S_H sin^2\alpha + S_h cos^2\alpha,$$

$$\sigma_z^o = \left(S_H cos^2\alpha + S_h sin^2\alpha\right) sin^2 i + S_v cos^2 i, \quad (17)$$

$$\sigma_{xy}^o = 0.5(S_h - S_H) sin2\alpha cosi,$$

$$\sigma_{yz}^o = 0.5(S_h - S_H) sin2\alpha sini,$$

$$\sigma_{xz}^o = 0.5\left(S_H cos^2\alpha + S_h sin^2\alpha - S_v\right) sin2i,$$

Here i is wellbore inclination, α is wellbore azimuth respect to the maximum principal horizontal stress direction, S_v is total vertical stress and S_h and S_H are the total principal minimum and maximum horizontal stress respectively.

As equations (16) and (17) indicate, the stress around the borehole depends on in situ stresses, reservoir pressure, bottom-hole pressure, wellbore trajectory and angular location on wellbore wall. In order to consider the effect of matrix shrinkage and depletion on stress distribution in CSG reservoirs, the following equation is considered for both maximum and minimum horizontal stresses after Shi and Durucan[29]:

$$S_H - S_{Ho} = S_h - S_{ho} = \beta \frac{1-2\nu}{1-\upsilon}\Delta P + \frac{E}{3(1-\upsilon)}\varepsilon_l \left(\frac{P}{P+P_\varepsilon} - \frac{P_o}{P_o+P_\varepsilon}\right) \quad (18)$$

We used β in the first term of the right-hand side of the equation, to consider the effect of poroelasticity in stress path. The isotropic stress changes are assumed here and the changes of both maximum and minimum horizontal stresses are considered the same. In the case of vertical wellbores, since the shear stresses around the wellbore are zero, therefore S_r, S_θ and S_z are principal stresses. However, in deviated and horizontal wells, the principal stresses will be determined from equation (19) to include the effects of both normal and shear stresses[34]:

$$S_{1,2} = 0.5\,(S_\theta + S_z) \pm \sqrt{(S_\theta + S_z)^2 + \tau_{\theta z}^2} \quad (19)$$

Table 1
Parameters and properties of San Juan coal basin from literature.

Parameter	Value	Source
Young's modulus (psi)	464122	[39]
	319084	[40]
	420610	[29]
	522136	[41]
	304580	[42]
Poisson's ratio	0.34	[39]
	0.3	[40]
	0.35	[29]
	0.21	[41]
	0.35	[42]
Biot coefficient	0.8	[43]
Maximum swelling strain	0.0127	[29]
	0.0083–0.033	[42]
Langmuir-type shrinkage pressure, p_ε (psi)	625	[29]
	495	[42]
Depth (ft)	2756	[43]
	2700–2900	[42]
Minimum total horizontal stress (psi)	2321	[44]
	1813	[42]
Maximum total horizontal stress (psi)	2466	[43]
Total vertical horizontal stress (psi)	2756	[43]
	2800	[42]
Initial reservoir pressure (psi)	1000	[45]
	957	[29]
	1450	[42]

By knowing the principal stresses and coal strength, coal failure can be predicted by applying a failure criterion. There are a number of failure criteria in literature for wellbore stability analysis and sand production, among them, Mohr-Coulomb is the most commonly used. However, this failure criterion does not consider the effect of the intermediate principal stress on failure. Al-Ajmi and Zimmerman[35] developed the Mogi-Coulomb failure criterion, which also considers the effect of intermediate principal stress. This failure criterion has been used in wellbore stability analysis and sand production and it is found that its failure predictions matching well with field data.[26,36,37] In the rest of this paper, the Mogi-Coulomb failure criterion is used as the failure criterion to predict coal failure during production.

$$\tau_{mogi} = a + b\frac{S_1 + S_3}{2} - \beta P_w \tag{20}$$

$$a = \frac{2\sqrt{2}\, C cos\varphi}{3} \tag{21}$$

$$b = \frac{2\sqrt{2} sin\varphi}{3} \tag{22}$$

$$\tau_{oct} = \frac{1}{3}\sqrt{(S_2 - S_3)^2 + (S_3 - S_1)^2 + (S_1 - S_2)^2} \tag{23}$$

Here φ is the friction angle and C is the rock cohesion.

Based on the Mogi failure criterion, the shear failure happens as $\tau_{oct} > \tau_{Mogi}$. As equation (16) indicates the radial, tangential and axial stresses depend on bottom-hole pressure, reservoir pressure and in situ stresses. We developed a workflow (Fig. 4) with an iterative loop to consider the effect of bottom-hole pressure on stress distribution for a given reservoir pressure and calculate the critical bottom-hole pressure which satisfies the failure equation considering the effect of pressure depletion, matrix shrinkage and well inclination and azimuth on stress path and coal failure pressure. Critical Bottom Hole Flowing Pressure (*CBHFP*) is defined as the minimum allowable bottom hole pressure without any coal failure and therefore the Maximum Coal Free Drawdown Pressure (*MCFDP*) will be the difference between reservoir pressure and the Critical Flowing bottom hole pressure:

MCFDP = Current reservoir pressure – *CBHFP*

Table 2
Input data for coal failure analysis in San Juan Basin.

Parameter	Value
Vertical Stress Gradient (psi/ft)	1
Maximum Horizontal Stress Gradient (psi/ft)	0.88
Minimum Horizontal Stress Gradient (psi/ft)	0.7
Initial Pore Pressure Gradient (psi)	1260
Depth (ft)	2800
Cohesion (psi)	500
Friction Angle (degree)	38
Langmuir-type shrinkage pressure (psi)	560
Maximum swelling strain	0.0083
Young's modulus (psi)	406105
Poisson's ratio	0.31
Biot coefficient	0.8
Reservoir pressure at time of failure (psi)	260

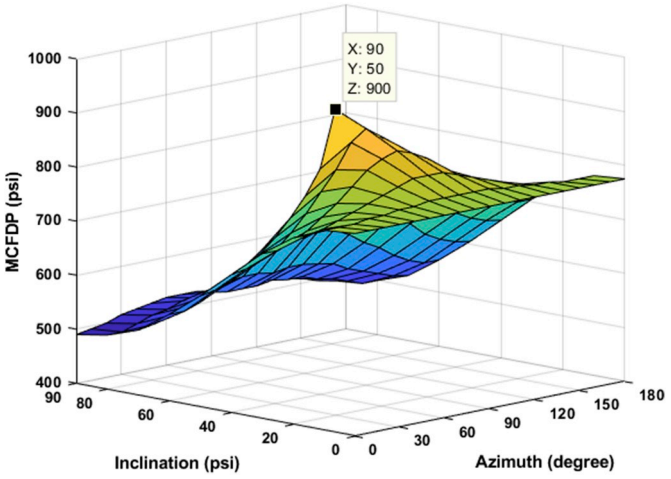

Fig. 5. The *MCFDP* in San Juan Basin at the early stage of production, zero depletion.

The higher values of *MCFDP* will represent a more stable case regarding coal failure.

3. Model validation

In order to validate the developed model, field data and observed coal failure pressure in San Juan Basin in USA are utilized. The San Juan Basin spans across the northwest of New Mexico through southwestern Colorado and is one of the oldest CSG productive areas in the world. The commercial gas production was established in 1977 from Fruitland coal formation and as of 2010, there were more than 7200 active wells in the Basin.[12] At the early stage of gas production, there was no coal production problem, but after more than 20 years of production when the reservoir pressure reduced to 250–300 psi from the original pressure of 1260 psi, the massive production of coal fines became a challenge.[10,12] We will apply the developed methodology to evaluate the coal failure in this basin for a vertical wellbore.

Table 1 lists the range input data required for the coal failure modelling exercise extracted from different sources. Triaxial experimental data from Saurabh and Harpalani[38] are utilized as the cohesion and friction angle of coal seams. Table 2 shows the input parameters for the coal failure model (from triaxial data and average values in Table 1). The minimum value of Longmuir type parameter (maximum swelling strain) in the literature was utilized.

Fig. 5 shows the coal failure analysis results for different well inclination and azimuth in San Juan basin in the early stage of production. It shows a 3D plot of *MCFDP* in vertical axis versus different wellbore inclination and azimuth in horizontal axes. It should be noted that

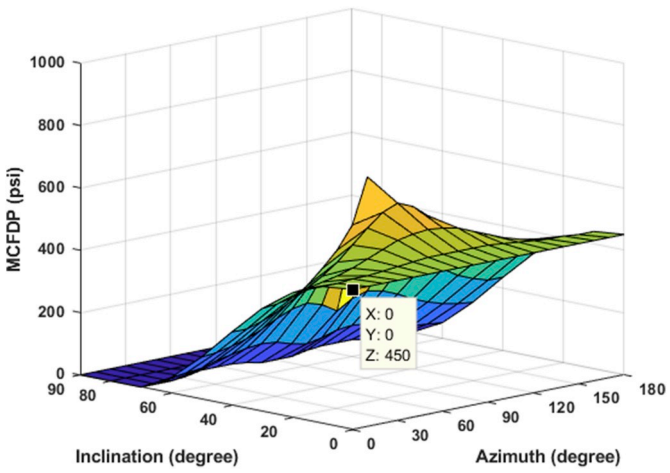

Fig. 6. The *MCFDP* in San Juan Basin with depletion = 400 psi.

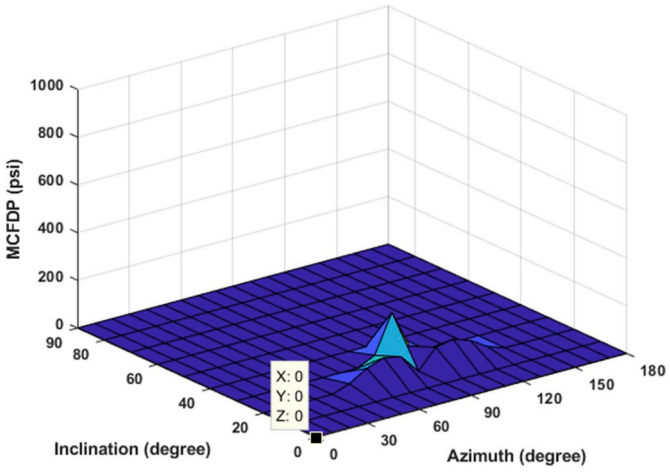

Fig. 7. The *MCFDP* in San Juan Basin with depletion = 1000 psi.

azimuth values are regarding to the direction of maximum horizontal stress, therefore azimuth = 0° means a well that its trajectory is in the direction of maximum horizontal stress and azimuth = 90° means drilling trajectory is parallel to the direction of minimum horizontal stress. No coal failure is predicted for any combination of inclination and azimuth in the early stage of production. The figure indicates that for this coal reservoir, the vertical wellbores are much safer than horizontal wells and a drawdown pressure up to 900 psi for a 50° deviated wells in direction of minimum horizontal stress is reachable without any risk of coal production. However, as the reservoir is depressurized and by 400 psi some horizontal wells could start to produce coal fine as the coal failure happens, but the vertical wellbores are still remained stable and free of coal fines problems if the drawdown pressure is maintained below 450 psi (Fig. 6). The results of a case when the reservoir pressure reaches 280 psi (1000 psi depletion) have been presented in Fig. 7. The developed model proposes that as the reservoir pressure reduces to 280 psi, the vertical wellbores are not coal failure free anymore and the coal failure will happen in this situation, which is consistent with the field

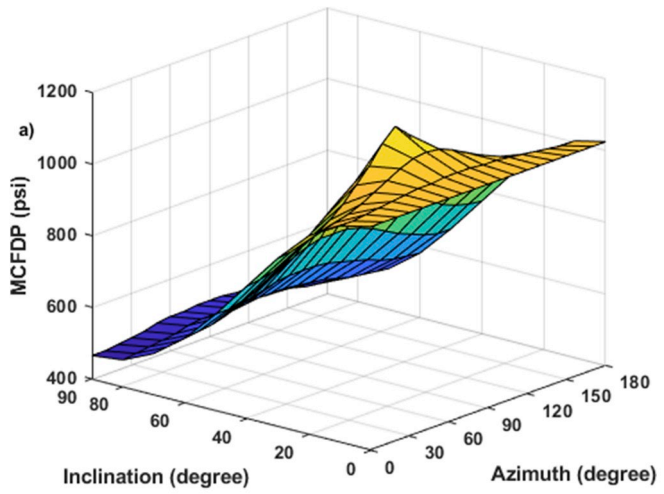

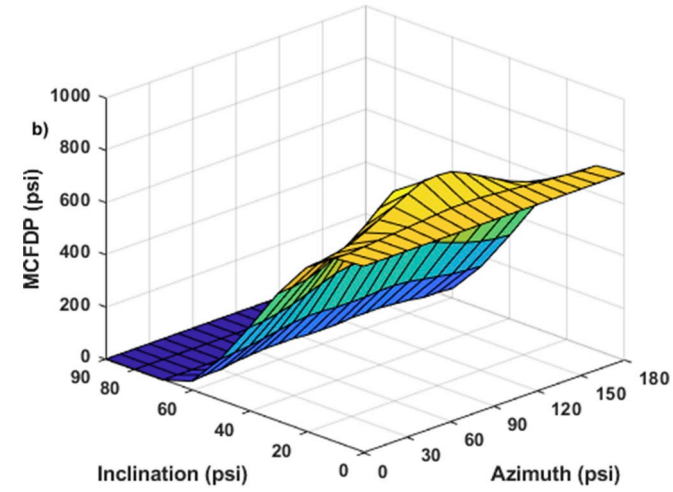

Fig. 8. The *MCFDP* for different azimuth and inclination in a normal faulting stress regime a) at the early stage of production with no pressure depletion b) with depletion = 400 psi.

data in the San Juan Basin reported by Okotie and Moore[12] and Moore, Loftin.[10]

4. Coal failure in different stress regimes

The developed methodology is applied in three different stress regimes to investigate the coal failure in CSG reservoirs. Table 3 presents the typical input data used for the analysis of coal failure in normal, strike-slip and reverse faulting stress regimes.

4.1. Normal faulting stress regime

Fig. 8 indicates the results of the coal failure model in a normal stress regime. The results indicate that the *MCFDP* in an early stage of production for a vertical well in this stress regime is 1025 psi (Fig. 8a). However, for a horizontal well drilled in the direction of maximum

Table 3
Input data for coal failure analysis in three different in situ stress regimes.

Stress Regime	S_v psi/ft	S_H psi/ft	S_h psi/ft	P_o psi/ft	Depth ft	C psi	Φ degree	ν	β	E psi	P_ε psi	ε_l
NF	1	0.8	0.7	0.46	3000	700	32	0.35	0.8	420609	625.1	0.0127
SS	1	1.1	0.9	0.46	3000	700	32	0.35	0.8	420609	625.1	0.0127
RF	1	1.3	1.1	0.46	3000	700	32	0.35	0.8	420609	625.1	0.0127

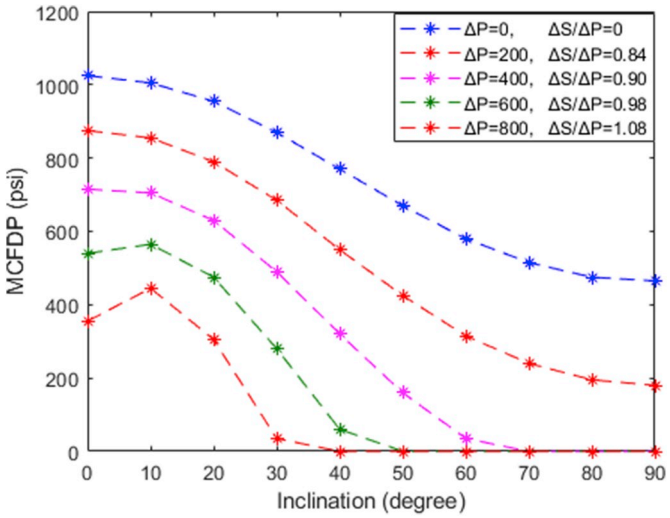

Fig. 9. The effect of depletion and desorption on *MCFDP* in a normal faulting stress regime, for wells drilled in the direction of maximum horizontal stress.

horizontal stress, the *MCFDP* decreases to 465 psi. It is shown that in this case, a vertical producing well is less susceptible to coal failure and coal production than a horizontal well or any deviated wellbores. This figure also indicates that producing from the wells in direction of the minimum horizontal stress (azimuth = 90°), leads the maximum *MCFDP* and it is the best drilling trajectory for deviated wells. Fig. 8. b shows *MCFDP* when the reservoir has been depleted by 400 psi and the effect of depletion and desorption on coal failure have been considered. It shows that as the reservoir is depleted by 400 psi, the producing horizontal wells and highly deviated wells are not stable anymore in any direction and they can produce coal particles as a result of rock failure with pressure depletion. In addition, the results indicate that for vertical wells the *MCFDP* will decrease to 715 psi which in comparison with no depletion and desorption is 410 psi less. This means that in order to prevent coal failure, the production constraint should change through the life of the CSG reservoir and the bottom hole flowing pressure should be adjusted to avoid coal failure.

Fig. 9 shows the effect of depletion on coal failure in CSG reservoirs for depletion values from 0 to 800 psi. The depicted values represent producing wells with different inclinations drilled parallel to the direction of maximum horizontal stress. As this figure shows, depletion and induced matrix shrinkage make the coal more susceptible to failure and as the depletion increases the *MCFDP* decreases. The effect of depletion and desorption on *MCFDP* for horizontal and highly deviated wellbores is more than vertical wells. It's because of that when the well is drilled horizontal or highly deviated parallel to maximum horizontal stress, the stress on the wellbore plane are vertical and minimum horizontal stresses, and based on uniaxial strain condition there are different changes in these two stresses during depletion. In a normal faulting stress regime, the vertical stress is the maximum principal stress and the minimum horizontal stress is the least principal stress, and as the pressure depletion and shrinkage lead to the reduction of effective horizontal stress, the difference between the stresses will increase by production. However, for a vertical wellbore, both applied stresses on the plane of the wellbore are horizontal stresses which have the same level of changes with pressure depletion and desorption. As Fig. 9 indicates, because of the shrinkage effect, the stress path value is not constant and it increases from 0.84 to 1.08 with depletion. However, for conventional reservoirs, as there is no shrinkage, there would be just a poromechanical effect and the stress path value remains constant and equal to 0.37 in this case.

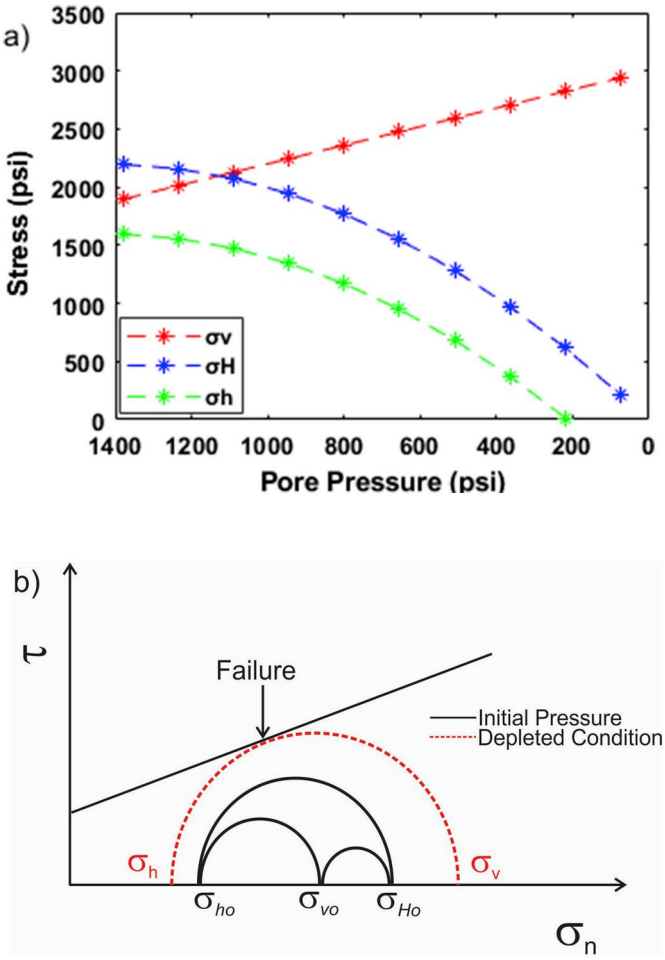

Fig. 10. a) The effect of depletion and desorption on effective stress, and b) Schematic of the coal failure in a strike-slip faulting stress regime during production.

4.2. Strike-slip faulting stress regime

Fig. 10 shows the effective stresses change in a strike-slip stress regime by depletion and desorption. During the early stage of production, the vertical stress is the intermediate stress and the maximum horizontal stress is the maximum in situ stress. By production from the CSG reservoir, the pressure depletion, desorption and matrix shrinkage effect lead the effective horizontal stresses to decrease, whilst the vertical effective stress will increase. It means that at a particular reservoir pressure level (here around 400 psi depletion), the in situ stress regime will change from strike-slip to normal stress regime. As Fig. 10. b shows, these stress changes may result in coal failure. It should be noticed that only the field scale stress changes have been considered in the depicted failure envelope in this figure and the effect of near-wellbore stress changes has not been taken into account. The effect of stress distribution around the wellbore has been considered in the developed analytical model and the results of *MCFDP* coal failure in a strike-slip regime have been depicted in Fig. 11. In comparison with the normal stress regime case showed in the previous section, the *MCFDP* values are lower in the strike-slip regime and the wells are more susceptible to failure. Fig. 11. a shows that in the strike-slip regime, the horizontal and near horizontal wells are less susceptible to failure than the vertical boreholes and a horizontal well drilled in direction of the maximum horizontal stress would be the most stable wells. In this case, coal failure will start if the drawdown is more than 670 psi. Contrary to the normal faulting stress regime, for wells drilled in direction of the minimum horizontal stress,

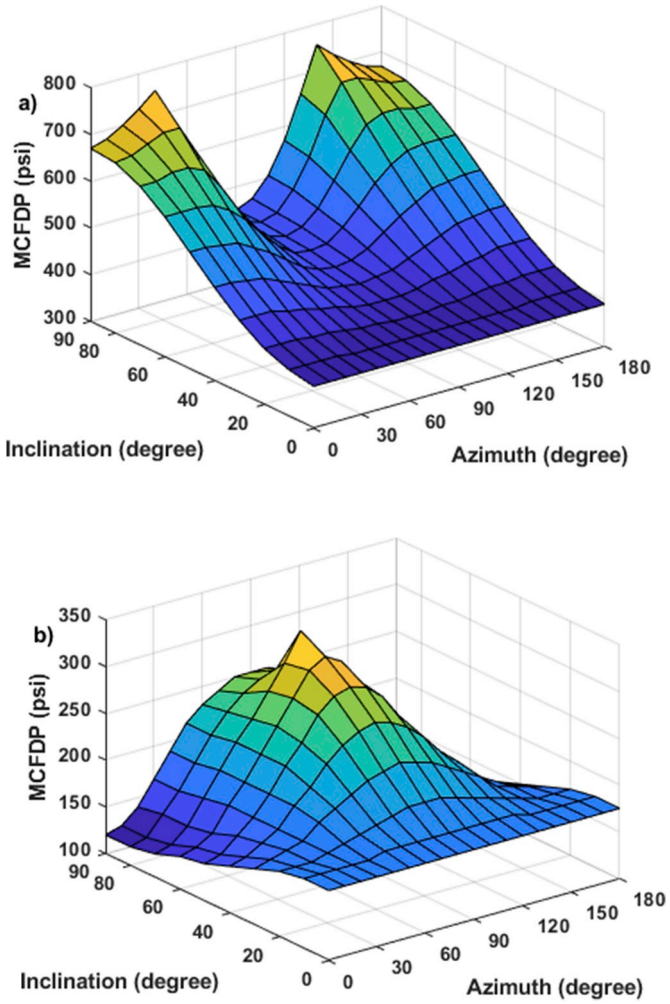

Fig. 11. The *MCFDP* for different azimuth and inclination in a strike-slip faulting stress regime a) at the early stage of production b) with depletion = 400 psi.

the *MCFDP* is not too sensitive to inclination in this case. However, for wells in direction of the maximum horizontal stress, the *MCFDP* will change with the inclination.

The effects of pressure depletion and desorption on coal failure in a strike-slip stress regime are shown in Fig. 11. b. It is shown that the *MCFDP* will decrease as the reservoir is depleted and shrinkage occurs. Moreover, the consequent stress regime's change from strike-slip to normal with depletion and its associated shrinkage will affect the *MCFDP* trend. For example, a horizontal well in direction of the maximum horizontal stress (Azimuth = 0°) is very susceptible to coal failure and coal fine production. As Fig. 11. b exhibits after 400 psi depletion, wells in direction of the minimum horizontal stress (azimuth = 90°) will become more stable, whilst this direction was the worst case in the early stage of production. This figure also indicates that after 400 psi depletion, the stable production with no coal failure is still reachable for different wells with any combination of inclination and azimuth, which wasn't possible in the case of normal faulting stress regime in spite of the fact that *MCFDP* at initial stage of production in the normal stress regime were higher than the strike-slip stress regime.

4.3. Reverse faulting stress regime

The final case is the coal failure analysis of wells in a reverse faulting stress regime. Fig. 12.a shows the effective stresses profile change during depletion. At the early stage of production with no pressure depletion,

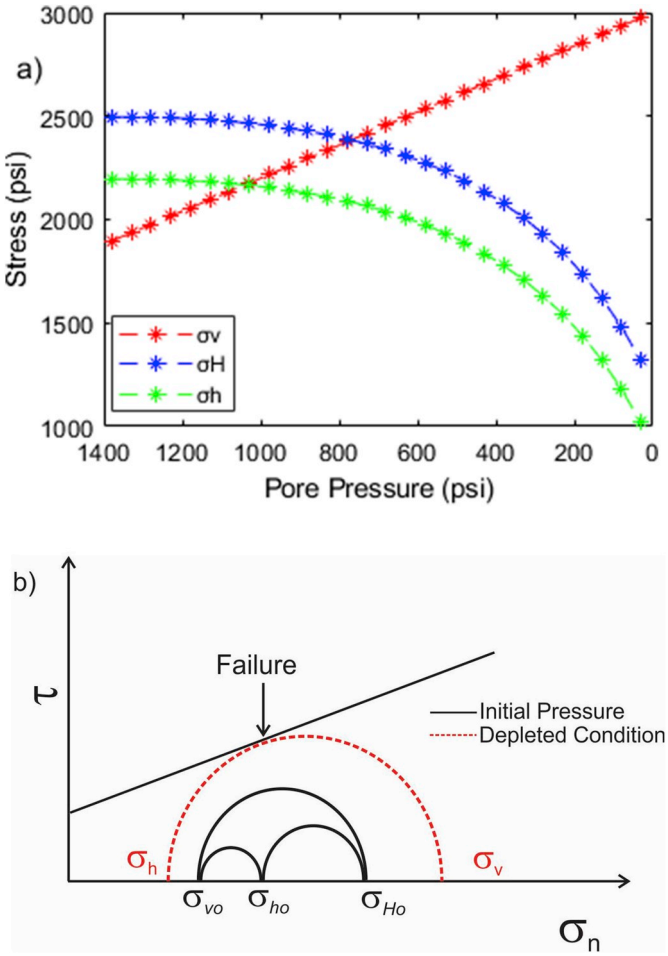

Fig. 12. a) The effect of depletion and desorption on effective stress, and b) Schematic of coal failure during production in a reverse faulting stress regime.

the vertical stress is the least principal stress, however, with depletion the effective horizontal stresses increase, whilst the effective vertical stress will increase because the shrinkage term of stress will outweigh the poromechanical term. After an approximately 300 psi pressure depletion, the stress regime changes from reverse to strike-slip and with continuing production, the stress regime becomes normal stress regime at reservoir pressure of 600 psi. Fig. 12.b shows the effect of this stress change on coal failure in field scale. Similar to the strike-slip stress regime case showed in the previous section, failure becomes more susceptible by production from CSG reservoirs and the stress change with depletion could be accompanied by coal failure.

Fig. 13.a shows the 3D plot of coal failure analysis in a reverse stress regime at the early stage of production. Same as the strike-slip regime case, horizontal wells in the direction of maximum horizontal stress are the most stable while vertical wells are the least stable and most susceptible to coal failure and coal production at the early stage of production. Fig. 13. b shows that by depleting the reservoir by 600 psi the stress regime changes to normal faulting and the *MCFDP* values decrease significantly. In this case, like the strike-slip regime case, the most stable well trajectory will change with depletion as the stress regime changes.

Fig. 14 shows the change of *MCFDP* with pressure depletion from 0 to 800 psi in a reverse stress regime. The depicted values represent wells drilled parallel to the direction of minimum horizontal stress. Like the normal faulting stress regime case, pressure depletion and induced matrix shrinkage increase the risk of coal failure and with depletion increases the *MCFDP* decreases. In contrast to the normal stress regime, in this case, the effect of depletion and desorption on *MCFDP* for vertical wellbores is more than highly deviated and horizontal wells. If there is

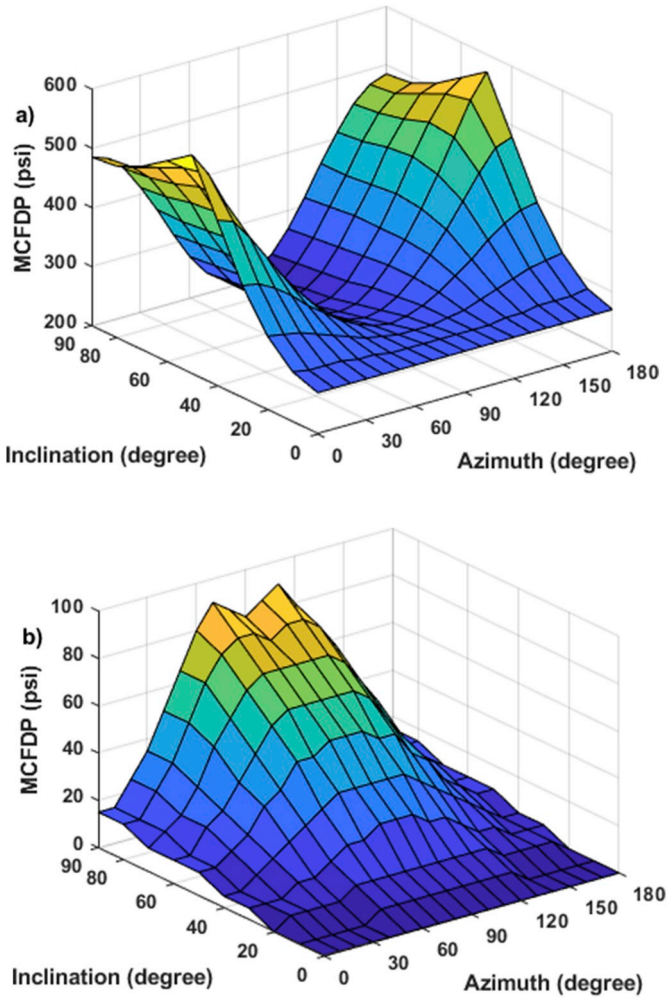

Fig. 13. The *MCFDP* for different well azimuth and inclination in a reverse faulting stress regime a) at the early stage of production b)with depletion = 600 psi.

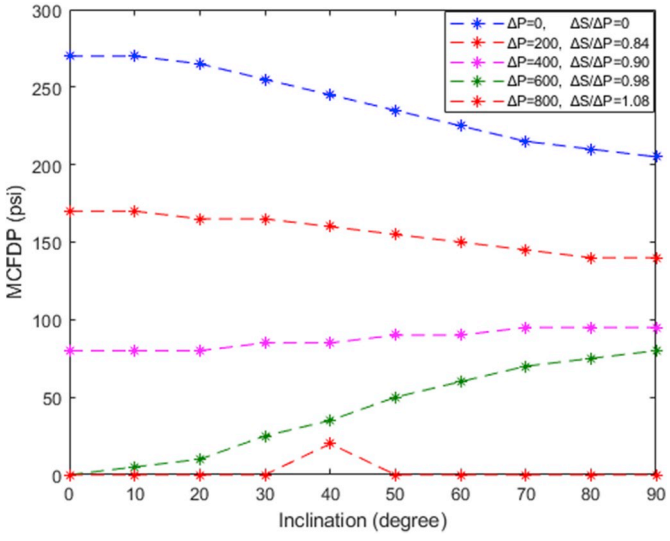

Fig. 14. The effect of pressure depletion and desorption on *MCFDP* in a reverse faulting stress regime.

no desorption during depletion (like conventional reservoirs), the effect of production on failure drawdown would be almost the same for any combination of inclination and azimuth. In this stress regime case also the stress path value is changing and it increases from 0.84 to 1.08 by increasing depletion, whereas the stress path due to the poromechanical effect will be constant (0.37) during depletion.

5. Conclusions

This study presented an analytical model for coal failure prediction in CSG reservoirs in different in situ stress regimes by applying the Mogi-Coulomb failure criterion. The developed model enables quantitative estimation of maximum coal free drawdown pressure in different pressure conditions. It considers the combined effects of matrix shrinkage, pressure depletion, initial in situ stress and wellbore trajectory on stress distribution around the wellbore simultaneously. The model prediction is consistent with the coal fines production from the San Juan Basin. The matrix shrinkage causes the greater stress path in CSG reservoirs than the conventional reservoirs with depletion. Thus, the new stress distribution around the wellbore may result in the reduction of Maximum Coal Free Drawdown Pressure and leads to coal failure with depletion.

The effect of depletion on *MCFDP* for horizontal and highly deviated wellbores is more than vertical wells in a normal faulting stress regime. It has been concluded that the wells in a strike-slip stress regime are more susceptible to failure compared to the normal fault regime. Moreover, horizontal and deviated wells are less prone to coal failure than vertical wells in strike-slip stress regime. In this case, depletion could change the in situ stress regime from strike-slip to normal stress regime. This stress change makes coal more susceptible to failure.

In a reverse faulting stress regime, horizontal wells in direction of maximum horizontal stress are the most stable and least susceptible to coal failure at the early stage of production. However, with pressure depletion and the change of stress regime to normal fault regime, the optimum production trajectory will change and deviated wells in minimum horizontal stress direction will be less susceptible to coal failure. In contrary to the normal fault stress regime, in a reverse fault regime, the influence of depletion on *MCFDP* for vertical wells is more than horizontal and highly deviated wellbores.

Declaration of competing interest

The authors declare that they have no known competing financial interests or personal relationships that could have appeared to influence the work reported in this paper.

Appendix A. Supplementary data

Supplementary data to this article can be found online at https://doi.org/10.1016/j.ijrmms.2020.104259.

References

1 Liu J, Chen Z, Elsworth D, Qu H, Chen D. Interactions of multiple processes during CBM extraction: a critical review. *Int J Coal Geol.* 2011;87:175–189.
2 Palmer I. Coalbed methane completions: a world view. *Int J Coal Geol.* 2010;82:184–195.
3 Espinoza DN, Pereira JM, Vandamme M, Dangla P, Vidal-Gilbert S. Desorption-induced shear failure of coal bed seams during gas depletion. *Int J Coal Geol.* 2015;137:142–151.
4 Day S, Fry R, Sakurovs R. Swelling of Australian coals in supercritical CO2. *Int J Coal Geol.* 2008;74:41–52.
5 Fan L, Liu S. Numerical prediction of in situ horizontal stress evolution in coalbed methane reservoirs by considering both poroelastic and sorption induced strain effects. *Int J Rock Mech Min Sci.* 2018;104:156–164.
6 Gentzis T. Review of Mannville coal geomechanical properties: application to coalbed methane drilling in the Central Alberta Plains, Canada. *Energy Sources, Part A: Recovery, Util. Environ Effect.* 2009;32:355–369.
7 Lu M, Connell L. Coal failure during primary and enhanced coalbed methane production — theory and approximate analyses. *Int J Coal Geol.* 2016;154–155:275–285.

8 Yang Y, Cui S, Ni Y, Wang F, Yang Y, Lang S. A new attempt of a CBM tree-like horizontal well: a pilot case of Well ZS 1P-5H in the Qinshui Basin. *Nat Gas Ind B*. 2014;1:205–209.
9 Puspitasari R, Gan T, Pallikathekathil ZJ, Luft J. Wellbore stability modelling for horizontal and multi-branch lateral wells in CBM: practical solution to better understand the uncertainty in rock strength and coal heterogeneity. In: *SPE Asia Pacific Oil & Gas Conference and Exhibition*. Adelaide, Australia: Society of Petroleum Engineers; 2014.
10 Moore RL, Loftin DF, Palmer ID. History matching and permeability increases of mature coalbed methane wells in San Juan Basin. In: *SPE Asia Pacific Oil and Gas Conference and Exhibition*. Jakarta, Indonesia: Society of Petroleum Engineers; 2011.
11 Palmer ID, Moschovidis ZA, Cameron JR. Coal failure and consequences for coalbed methane wells. In: *SPE Annual Technical Conference and Exhibition*. Dallas, Texas: Society of Petroleum Engineers; 2005.
12 Okotie VU, Moore RL. *Well-Production Challenges and Solutions in a Mature, Very-Low-Pressure Coalbed-Methane Reservoir*. 2011.
13 Keshavarz A, Badalyan A, Carageorgos T, Bedrikovetsky P, Johnson R. Stimulation of coal seam permeability by micro-sized graded proppant placement using selective fluid properties. *Fuel*. 2015;144:228–236.
14 Wei C, Zou M, Sun Y, Cai Z, Qi Y. Experimental and applied analyses of particle migration in fractures of coalbed methane reservoirs. *J Nat Gas Sci Eng*. 2015;23:399–406.
15 Bai T, Chen Z, Aminossadati SM, Li L, Liu J, Lu H. Dimensional analysis and prediction of coal fines generation under two-phase flow conditions. *Fuel*. 2017;194:460–479.
16 Liu S, Harpalani S. Evaluation of in situ stress changes with gas depletion of coalbed methane reservoirs. *J Geophys Res: Solid Earth*. 2014;119:6263–6276.
17 Bai T, Chen Z, Aminossadati SM, Pan Z, Liu J, Li L. Characterization of coal fines generation: a micro-scale investigation. *J Nat Gas Sci Eng*. 2015;27:862–875.
18 Saurabh S, Harpalani S, Singh VK. Implications of stress re-distribution and rock failure with continued gas depletion in coalbed methane reservoirs. *Int J Coal Geol*. 2016;162:183–192.
19 Geertsma J. *The Effect of Fluid Pressure Decline on Volumetric Changes of Porous Rocks*. Society of Petroleum Engineers; 1957:10.
20 Olson JE, Laubach SE, Lander RH. Natural fracture characterization in tight gas sandstones: integrating mechanics and diagenesis. *AAPG (Am Assoc Pet Geol) Bull*. 2009;93:1535–1549.
21 Zoback MD, Zinke JC. Production-induced normal faulting in the Valhall and Ekofisk oil fields. *Pure Appl Geophys*. 2002;159:403–420.
22 Addis MA. The stress-depletion response of reservoirs. In: *SPE Annual Technical Conference and Exhibition*. San Antonio, Texas: Society of Petroleum Engineers; 1997:11.
23 Teufel LW, Rhett DW, Farrell HE. Effect of reservoir depletion and pore pressure drawdown on in situ stress and deformation in the Ekofisk field, North Sea. In: *The 32nd US Symposium on Rock Mechanics (USRMS)*. Norman, Oklahoma: American Rock Mechanics Association; 1991:10.
24 Behnoud far P, Hassani AH, Al-Ajmi AM, Heydari H. A novel model for wellbore stability analysis during reservoir depletion. *J Nat Gas Sci Eng*. 2016;35:935–943.
25 Zhang R, Shi X, Zhu R, et al. Critical drawdown pressure of sanding onset for offshore depleted and water cut gas reservoirs: modeling and application. *J Nat Gas Sci Eng*. 2016;34:159–169.
26 Kaffash A, Zare-Reisabadi MR. Borehole stability evaluation in overbalanced and underbalanced drilling: based on 3D failure criteria. *Geosyst Eng*. 2013;16:175–182.
27 Zare-Reisabadi M, Parvazdavani M, Sharifi H. Numerical stability analysis OF drilled wells IN Maroun oilfield. *Petroleum & Coal*. 2016;58:292–298.
28 Feng R, Harpalani S, Saurabh S. Experimental investigation of in situ stress relaxation on deformation behavior and permeability variation of coalbed methane reservoirs during primary depletion. *J Nat Gas Sci Eng*. 2018;53:1–11.
29 Shi JQ, Durucan S. Drawdown induced changes in permeability of Coalbeds: a new interpretation of the reservoir response to primary recovery. *Transport Porous Media*. 2004;56:1–16.
30 Mitra A, Harpalani S, Liu S. Laboratory measurement and modeling of coal permeability with continued methane production: Part 1 – laboratory results. *Fuel*. 2012;94:110–116.
31 Saurabh S, Harpalani S. Stress path with depletion in coalbed methane reservoirs and stress based permeability modeling. *Int J Coal Geol*. 2018;185:12–22.
32 Cui X, Bustin RM. Volumetric strain associated with methane desorption and its impact on coalbed gas production from deep coal seams. *AAPG (Am Assoc Pet Geol) Bull*. 2005;89:1181–1202.
33 Zare-Reisabadi MR, Kaffash A, Shadizadeh SR. Determination of optimal well trajectory during drilling and production based on borehole stability. *Int J Rock Mech Min Sci*. 2012;56:77–87.
34 Fjær E, Holt RM, Horsrud P, Raaen AM, Risnes R. Chapter 2 failure mechanics. In: Fjær E, Holt RM, Horsrud P, Raaen AM, Risnes R, eds. *Developments in Petroleum Science*. Elsevier; 2008:55–102.
35 Al-Ajmi AM, Zimmerman RW. Relation between the Mogi and the Coulomb failure criteria. *Int J Rock Mech Min Sci*. 2005;42:431–439.
36 Zare MR, Shadizadeh SR, Habibnia B. Mechanical stability analysis of directional wells: a case study in Ahwaz oilfield. In: *Nigeria Annual International Conference and Exhibition. Tinapa - Calabar*. Nigeria: Society of Petroleum Engineers; 2010:10.
37 Al-Ajmi AM, Zimmerman RW. Stability analysis of vertical boreholes using the Mogi–Coulomb failure criterion. *Int J Rock Mech Min Sci*. 2006;43:1200–1211.
38 Saurabh S, Harpalani S. Stress-Dependent permeability of sorptive reservoirs incorporating postfailure behavior. In: *51st US Rock Mechanics/Geomechanics Symposium*. San Francisco, California, USA: American Rock Mechanics Association; 2017.
39 Ian Palmer JM. *How Permeability Depends on Stress and Pore Pressure in Coalbeds: A New Model*. 1998.
40 Liu S, Harpalani S. Permeability prediction of coalbed methane reservoirs during primary depletion. *Int J Coal Geol*. 2013;113:1–10.
41 Mavor MJ, Vaughn JE. Increasing coal absolute permeability in the San Juan Basin Fruitland formation. *SPE-96018-PA*. 1998;1:201–206.
42 Palmer I. Permeability changes in coal: analytical modeling. *Int J Coal Geol*. 2009;77:119–126.
43 Shovkun I, Espinoza DN. Coupled fluid flow-geomechanics simulation in stress-sensitive coal and shale reservoirs: impact of desorption-induced stresses, shear failure, and fines migration. *Fuel*. 2017;195:260–272.
44 Ramurthy M, Rogers RE, Weida D. Analysis of the success of cavity completions in the fairway zone of the San Juan Basin. In: *SPE Rocky Mountain Regional Meeting*. Gillette, Wyoming: Society of Petroleum Engineers; 1999:8.
45 Min K-B, Rutqvist J, Tsang C-F, Jing L. Stress-dependent permeability of fractured rock masses: a numerical study. *Int J Rock Mech Min Sci*. 2004;41:1191–1210.

4 Effect of matrix shrinkage and wellbore trajectory on coal failure in Bowen Basin

4.1 Effect of matrix shrinkage on wellbore stresses in coal seam gas: An example from Bowen Basin, east Australia

Zare Reisabadi M, Haghighi M, Sayyafzadeh M, Khaksar A., Journal of Natural Gas Science and Engineering. 2020; 77:103280.

Statement of Authorship

Title of Paper	Effect of matrix shrinkage on wellbore stresses in coal seam gas: An example from Bowen Basin, east Australia
Publication Status	☑ Published ☐ Accepted for Publication ☐ Submitted for Publication ☐ Unpublished and Unsubmitted w ork w ritten in manuscript style
Publication Details	Zare Reisabadi M, Haghighi M, Sayyafzadeh M, Khaksar A., Journal of Natural Gas Science and Engineering. 2020; 77:103280.

Principal Author

Name of Principal Author (Candidate)	Mohammadreza Zare Reisabadi
Contribution to the Paper	Literature review, Model development, Analysis of results, wiring the manuscript.
Overall percentage (%)	70
Certification:	This paper reports on original research I conducted during the period of my Higher Degree by Research candidature and is not subject to any obligations or contractual agreements with a third party that would constrain its inclusion in this thesis. I am the primary author of this paper.
Signature	Date: 09/03/2021

Co-Author Contributions

By signing the Statement of Authorship, each author certifies that:

i. the candidate's stated contribution to the publication is accurate (as detailed above);

ii. permission is granted for the candidate in include the publication in the thesis; and

iii. the sum of all co-author contributions is equal to 100% less the candidate's stated contribution.

Name of Co-Author	Manouchehr Haghighi
Contribution to the Paper	Support in analysis of results
Signature	Date: 9/3/21

Name of Co-Author	Mohammad Sayyafzadeh
Contribution to the Paper	Support in analysis of results, Reviewing the manuscript
Signature	Date: 9/3/2021

Name of Co-Author	Abbas Khaksar		
Contribution to the Paper	Support in analysis of results		
Signature		Date	15/3/2021

Journal of Natural Gas Science and Engineering 77 (2020) 103280

Contents lists available at ScienceDirect

Journal of Natural Gas Science and Engineering

journal homepage: http://www.elsevier.com/locate/jngse

Effect of matrix shrinkage on wellbore stresses in coal seam gas: An example from Bowen Basin, east Australia

Mohammadreza Zare Reisabadi [a,*], Manouchehr Haghighi [a], Mohammad Sayyafzadeh [a], Abbas Khaksar [b]

[a] Australian School of Petroleum, The University of Adelaide, Australia
[b] Baker Hughes, Australia

ARTICLE INFO

Keywords:
Matrix shrinkage
Stress path
Stress distribution
Coal failure
Bowen basin

ABSTRACT

Coal matrix is subjected to shrinkage as a result of gas desorption. This can contribute to the stress distribution changes around the wellbore during the exploitation of Coal Seam Gas (CSG) resources. The knowledge of these stresses is essential for coal shear failure prediction and assessing coal fines production risks, particularly in horizontal wells which nowadays are becoming common in CSG fields.

This study introduces an analytical model to estimate the stress distribution around the wellbore by coupling the effects of depletion, matrix shrinkage, and wellbore trajectory. The model is applied for coal failure analysis in both vertical and horizontal wells in Moranbah Coal Measures, in the Bowen Basin eastern Australia. The results reveal that the stress path value in CSG reservoirs, is not constant during production and it can even be more than one due to the matrix shrinkage. The shrinkage effect can significantly alter the effective horizontal stresses which accordingly can cause a considerable change to the near-wellbore stress distribution. It is shown that the stress differential may increase or decrease, depending on shrinkage/swelling magnitude and wellbore trajectory. In a normal fault stress regime, the matrix shrinkage decreases stress differential on the wellbore wall in vertical wells and consequently, reduces the coal failure potentials. However, in highly deviated and horizontal wells, the matrix shrinkage causes an extra increase of the tangential stress and reduction of radial stress on the wellbore wall (i.e., greater stress differentials on the wellbore wall). This increases the coal failure risks with depletion. The model was verified versus the observed coal failure pressure in the San Juan Basin, USA.

1. Introduction

During the past decades, CSG or Coal Bed Methane (CBM) reservoirs have increasingly become an important part of natural gas resources. Particularly in eastern Australia, CSG is the main part of the gas industry where 97 percent of produced CSG of Australia is coming from Bowen and Surat basins in Queensland and the remainder from New South Wales (GA and BREE, 2012).

Coals are typically weak rocks and preventing coal failure during production, particularly in horizontal wells is a challenging task (Espinoza et al., 2015b; Moore et al., 2011; Yang et al., 2014; Lu and Connell, 2016). Some of the recently drilled horizontal wells in the Moranbah Coal Measures, Bowen Basin have experienced unexpected solid production during production from coal layers (Puspitasari et al., 2014; Mazumder et al., 2012; Alboub et al., 2013) and rock failure problems could become more pervasive with further depletion. Coal failure has several detrimental consequences and it causes damage to pumps, tubing, surface facilities, and compressors. A comprehensive stress model is necessary for the accurate prediction of coal failure in the horizontal wells.

Associated matrix shrinkage with methane desorption results in a unique stress path, and contrary to conventional reservoirs, its value will change during depletion. This originates the changes of tangential, axial and radial stresses near the producing wells and within the coal seams. The effect of depletion on stress distribution around the wellbore in conventional reservoirs has been extensively studied in the literature (Li and Gray, 2015; Tohidi et al., 2018; Gao and Gray, 2019; Rafieepour et al., 2017; Davison et al., 2016; Behnoud far et al., 2016; Zare et al., 2010). Palmer et al. (2005) studied coal failure during the life of CSG well, but they utilized the conventional stress modelling and they did not consider the effect of matrix shrinkage. However, there are few studies that consider the effect of depletion and consequent matrix

* Corresponding author.
E-mail address: mohammadreza.zarereisabadi@adelaide.edu.au (M.Z. Reisabadi).

https://doi.org/10.1016/j.jngse.2020.103280
Received 3 January 2020; Received in revised form 24 March 2020; Accepted 24 March 2020
Available online 29 March 2020

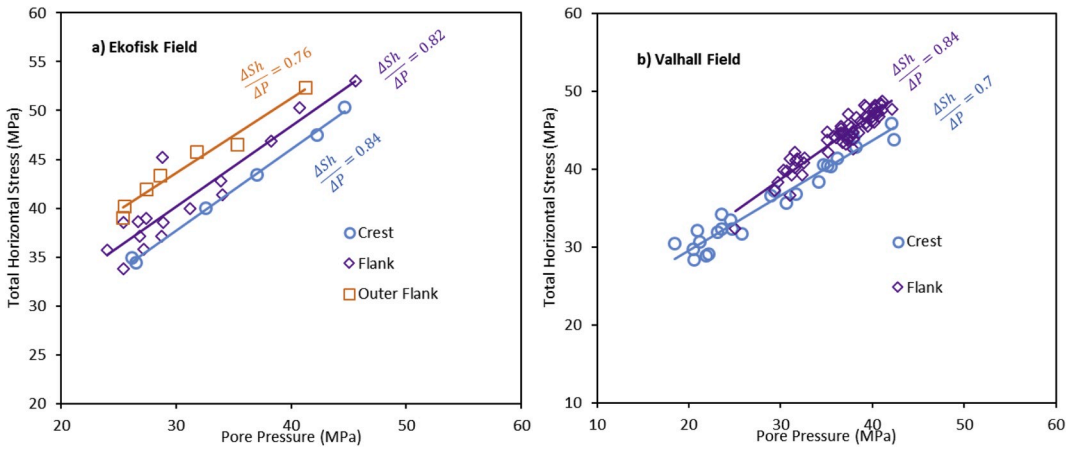

Fig. 1. Total horizontal stress path with depletion in conventional reservoirs. Data points in (a) from (Teufel et al., 1991) and data points in (b) from (Zoback and Zinke, 2002).

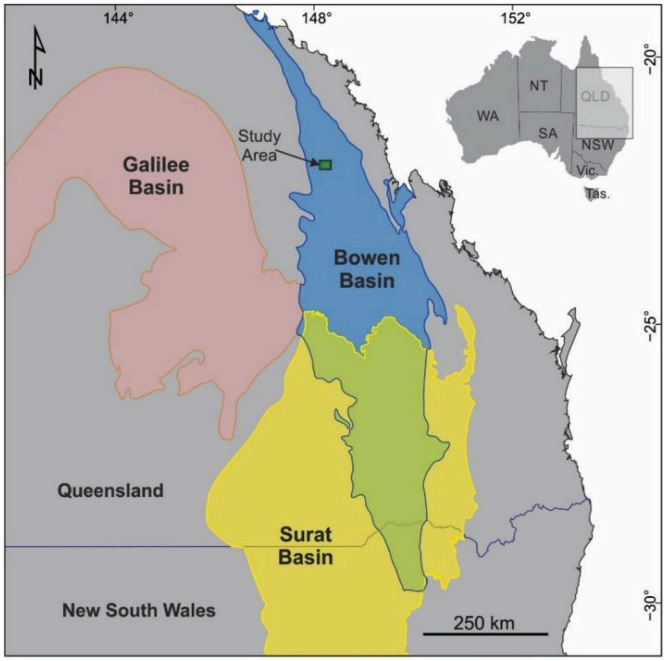

Fig. 2. Location of the Permo-Triassic Bowen Basin, eastern Australia.

shrinkage. Cui et al. (2007) developed an analytical model for stress distribution around a vertical CSG well by considering the impacts of adsorption-induced swelling. Masoudian and Hashemi (2016) considered elastoplastic formation around an axisymmetric CSG vertical well to develop an analytical model for stress distribution. Lu and Connell (2016) presented the reservoir-scale coal failure during production from CSG by considering the effect of desorption on stress distribution. In their study, they did not take into account the effect of the wellbore trajectory on stress redistribution around the wellbore.

Previously developed analytical models for CSG wells were mainly focused on vertical wells and they do not consider the effect of wellbore trajectory, pressure distribution and matrix shrinkage on the stress distribution at the same time. Therefore, these models cannot be applied to the deviated or horizontal wells. In this study, an analytical model is developed to evaluate the stress distribution around both vertical and horizontal wells by including pressure depletion and matrix shrinkage effects. The developed stress model is then used to assess the coal failure in both vertical and horizontal wells in the Bowen Basin.

2. Stress path in conventional reservoirs

Uniaxial strain conditions and constant vertical stress are widely used to determine the change in original stresses during depletion in conventional reservoirs. The stress path is defined as the following:

$$\frac{\Delta\sigma_H}{\Delta P}=\frac{\Delta\sigma_h}{\Delta P}=\beta\frac{1-2\nu}{1-\nu} \tag{1}$$

$$\frac{\Delta\sigma_H'}{\Delta P}=\frac{\Delta\sigma_h'}{\Delta P}=-\beta\frac{\nu}{1-\nu} \tag{2}$$

Where σ_H and σ_h are the total maximum and minimum horizontal stress respectively in MPa, P is pore pressure in MPa, β is Biot's coefficient and ν is Poisson's ratio, $'$ and Δ indicate effective stress and incremental values respectively. Since the Poisson's ratio is always less than 0.5, the stress path based on equation (1), will be less than one. Therefore, the reservoir depletion is expected to be accompanied by a linear reduction of both total horizontal stresses, i.e., the increase of the effective horizontal stresses. This has been confirmed by field observations in various conventional reservoirs worldwide (Zoback and Zinke, 2002; Addis, 1997; Teufel et al., 1991). Fig. 1 shows the observed changes of total horizontal stress by pore pressure depletion in the Ekofisk and Valhall field in the North Sea respectively. It indicates that the stress path is constant during depletion and the total horizontal stress decreases linearly during production. However, the stress path in CSG reservoirs is different from conventional reservoirs which is derived in the next section (equations (17) and (18)).

3. Stress modelling

To evaluate stress distribution around deviated or horizontal wells with anisotropic horizontal stresses, general poroelastic solution with varying pore pressure is considered. Given the fact that the radius of the reservoir is much larger than wellbore radius ($R_o \gg R_w$), the resulting radial, tangential and axial stress components are as follows (Fjær et al., 2008):

$$\sigma_r=\frac{\sigma_x^o+\sigma_y^o}{2}\left(1-\frac{R_w^2}{r^2}\right)+\frac{\sigma_x^o-\sigma_y^o}{2}\left(1+3\frac{R_w^4}{r^4}-4\frac{R_w^2}{r^2}\right)\cos 2\theta+\tau_{xy}^o\left(1+3\frac{R_w^4}{r^4}-4\frac{R_w^2}{r^2}\right)\sin 2\theta+\frac{2\eta}{r^2}\left(\int_{R_w}^{r} r\Delta p_f(r)dr\right)+p_w\frac{R_w^2}{r^2} \tag{3}$$

$$\sigma_\theta = \frac{\sigma_x^o + \sigma_y^o}{2}\left(1+\frac{R_w^2}{r^2}\right) - \frac{\sigma_x^o - \sigma_y^o}{2}\left(1+3\frac{R_w^4}{r^4}\right)\cos 2\,\theta - \tau_{xy}^o\left(1+3\frac{R_w^4}{r^4}\right)\sin 2\,\theta - \frac{2\eta}{r^2}\left(\int_{R_w}^{r} r\Delta p_f(r)dr - r^2\Delta p_f(r)\right) - p_w\frac{R_w^2}{r^2} \tag{4}$$

$$p_f(r) = p_{f0} + \frac{p_{f0}-p_w}{\ln\left(\frac{R_0}{R_w}\right)}\ln\left(\frac{r}{R_0}\right) \tag{8}$$

$$\int_{R_w}^{r} r\Delta p_f(r)dr = \frac{p_{f0}-p_w}{4\ln\left(\frac{R_0}{R_w}\right)}\left[\left(R_w^2-r^2\right)+2r^2\ln\left(\frac{r}{R_0}\right)-2R_w^2\ln\left(\frac{R_w}{R_0}\right)\right] \tag{9}$$

Where p_{fo} is initial reservoir pressure in psi, R_o is Reservoir radius in feet.

By substitution of equation (9) into equations (3)–(5), the stress distribution is:

$$\sigma_r = \frac{\sigma_x^o + \sigma_y^o}{2}\left(1-\frac{R_w^2}{r^2}\right) + \frac{\sigma_x^o - \sigma_y^o}{2}\left(1+3\frac{R_w^4}{r^4}-4\frac{R_w^2}{r^2}\right)\cos 2\,\theta + \tau_{xy}^o\left(1+3\frac{R_w^4}{r^4}-4\frac{R_w^2}{r^2}\right)\sin 2\,\theta + \frac{2\eta}{r^2}\left(\frac{p_{f0}-p_w}{4\ln\left(\frac{R_0}{R_w}\right)}\left[\left(R_w^2-r^2\right)+2r^2\ln\left(\frac{r}{R_0}\right)-2R_w^2\ln\left(\frac{R_w}{R_0}\right)\right]\right) + p_w\frac{R_w^2}{r^2} \tag{10}$$

$$\sigma_z = \sigma_z^o - \upsilon\left[2\left(\sigma_x^o-\sigma_y^o\right)\frac{R_w^2}{r^2}\cos 2\,\theta + 4\tau_{xy}^o\frac{R_w^2}{r^2}\sin 2\,\theta\right] + 2\eta\Delta p_f(r) \tag{5}$$

$$\begin{aligned}\sigma_x^o &= \left(\sigma_H\cos^2\alpha + \sigma_h\sin^2\alpha\right)\cos^2 i + \sigma_v\sin^2 i\\ \sigma_y^o &= \sigma_H\sin^2\alpha + \sigma_h\cos^2\alpha\\ \sigma_z^o &= \left(\sigma_H\cos^2\alpha + \sigma_h\sin^2\alpha\right)\sin^2 i + \sigma_v\cos^2 i\\ \tau_{xy}^o &= 0.5(\sigma_h-\sigma_H)\sin 2\,\alpha\cos i\end{aligned} \tag{6}$$

And $\eta = \frac{\beta(1-2\upsilon)}{2(1-\upsilon)}$.

Where σ_r is radial stress in psi, σ_θ is tangential stress in psi, σ_z is axial stress in psi, R_w is wellbore radius, r is the radial distance from the wellbore in feet, θ is the angular position around the wellbore in degree, p_w is bottom-hole pressure in psi, i is wellbore inclination in degree, α is wellbore azimuth respect to the maximum principal horizontal stress direction, σ_v is total vertical stress in psi.

Based on the assumption of steady state flow equation, the pore pressure profile in equations (3)–(5) is derived (Cui et al., 2007):

$$\Delta p_f(r) = p_f(r) - p_{f0} \tag{7}$$

Table 1
Input parameters for stress distribution in MCM, Bowen Basin.

Parameters	Symbol	Value	Reference
Vertical stress gradient	S_v (psi/ft)	1.014	Alboub et al. (2013)
Maximum horizontal stress gradient	S_H (psi/ft)	0.959	Alboub et al. (2013)
Minimum horizontal stress gradient	S_h (psi/ft)	0.817	Alboub et al. (2013)
Pore pressure gradient	P_o (psi/ft)	0.45	Alboub et al. (2013)
Depth	D (ft)	1758	Alboub et al. (2013)
Cohesion	C (psi)	536.6	Alboub et al. (2013)
Friction angle	φ(degree)	29.4	Alboub et al. (2013)
Langmuir pressure	$P\varepsilon$(psi)	885	Connell et al. (2016)
Maximum swelling strain	ε_l	0.0138	Connell et al. (2016)
Young's modulus	E (psi)	389,000	Alboub et al. (2013)
Poisson's ratio	ν	0.326	Alboub et al. (2013)
Biot's coefficient	β	0.8	–
Wellbore radius	Rw (ft)	0.333	Puspitasari et al. (2014)
Outer radius	Ro (ft)	333	–

$$\sigma_\theta = \frac{\sigma_x^o + \sigma_y^o}{2}\left(1+\frac{R_w^2}{r^2}\right) - \frac{\sigma_x^o - \sigma_y^o}{2}\left(1+3\frac{R_w^4}{r^4}\right)\cos 2\,\theta - \tau_{xy}^o\left(1+3\frac{R_w^4}{r^4}\right)\sin 2\,\theta - \frac{2\eta}{r^2}\left(\frac{p_{f0}-p_w}{4\ln\left(\frac{R_0}{R_w}\right)}\left[\left(R_w^2-r^2\right)-2r^2\ln\left(\frac{r}{R_0}\right)-2R_w^2\ln\left(\frac{R_w}{R_0}\right)\right]\right) - p_w\frac{R_w^2}{r^2} \tag{11}$$

$$\sigma_z = \sigma_z^o - \upsilon\left[2\left(\sigma_x^o-\sigma_y^o\right)\frac{R_w^2}{r^2}\cos 2\,\theta + 4\tau_{xy}^o\frac{R_w^2}{r^2}\sin 2\,\theta\right] + \frac{2\eta\left(p_{f0}-p_w\right)}{\ln\left(\frac{R_0}{R_w}\right)}\ln\left(\frac{r}{R_0}\right) \tag{12}$$

Equations (10)–(12) indicate that the stresses around the wellbore and in the reservoir are related to in-situ stresses, wellbore and reservoir radius, pore pressure profile, elastic properties of rock and wellbore trajectory. The experimental studies (Saurabh and Harpalani, 2018, Espinoza et al., 2015b, a, Liu and Harpalani, 2014, Mitra et al., 2012, Saurabh et al., 2016, Liu et al., 2020) have shown that the conventional stress path equations (equations (1) and (2)) cannot explain the observed situation in CSG, and because of the matrix shrinkage, the stress path values is not constant, and it can be greater than one. The effective horizontal stress change during depletion and methane desorption can be determined using a linear elasticity model developed by Shi and Durucan (2004):

$$\sigma_{ij}' = 2G\varepsilon_{ij} + \lambda\varepsilon\delta_{ij} + k\varepsilon_s\delta_{ij} \tag{13}$$

Where σ_{ij}' is effective stress, G is shear modulus, ε_{ij} is Incremental strain, δ_{ij} is Kronecker delta, and ε_s is incremental volumetric shrinkage strain.

In term of total stress, it is as equation (14)–(16):

$$\sigma_{ij} = 2G\varepsilon_{ij} + \lambda\varepsilon\delta_{ij} + k\varepsilon_s\delta_{ij} + \beta p\delta_{ij} \tag{14}$$

$$\varepsilon = \varepsilon_x + \varepsilon_y + \varepsilon_z, \quad \varepsilon_s = \varepsilon_l\frac{p}{p+p_\varepsilon} \tag{15}$$

$$G = \frac{E}{2(1+\nu)}, \quad \lambda = \frac{E\nu}{(1+\nu)(1-2\nu)}, \quad k = \frac{E}{3(1-2\nu)} \tag{16}$$

Where ε_l is Langmuir shrinkage strain, p_s is Langmuir pressure in psi, and E is Modulus of elasticity in psi.

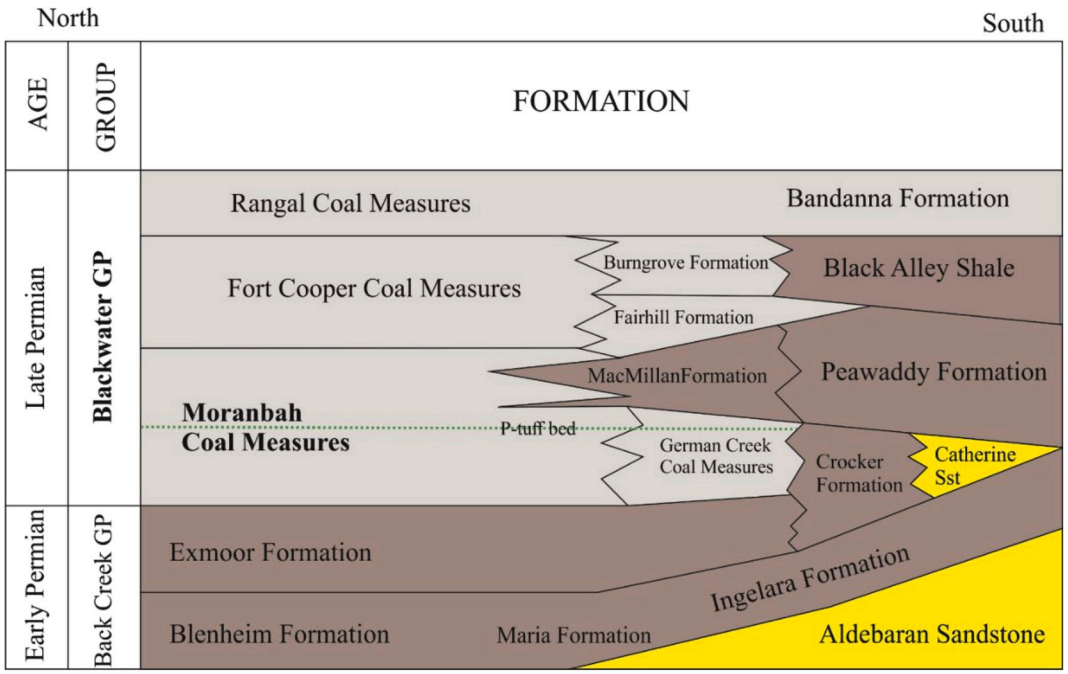

Fig. 3. Stratigraphic framework of Blackwater Group (shaded in gray) and associated formations, modified after Michaelsen and Henderson (2000).

By considering uniaxial strain condition and fitting the matrix shrinkage strain to the Langmuir type curves, the total horizontal stress and effective horizontal stress will be as follows:

$$\Delta\sigma_H = \Delta\sigma_h = \frac{1-2\upsilon}{1-\upsilon}\Delta p + \frac{E}{3(1-\upsilon)}\varepsilon_l\left(\frac{p}{p+p_\varepsilon} - \frac{p_{fo}}{p_{fo}+p_\varepsilon}\right) \tag{17}$$

$$\Delta\sigma'_H = \Delta\sigma'_h = \frac{-\upsilon}{1-\upsilon}\Delta p + \frac{E}{3(1-\upsilon)}\varepsilon_l\left(\frac{p}{p+p_\varepsilon} - \frac{p_{fo}}{p_{fo}+p_\varepsilon}\right) \tag{18}$$

New horizontal stresses from equation (17), are substituted into equation (6) to calculate the stress distribution near the CSG wellbore. To evaluate the coal failure potential, the principal stresses on the wellbore wall are calculated and then a failure criterion is applied. The Mogi-Coulomb criterion showed a better prediction of rock failure than the conventional Mohr-Coulomb criterion (Al-Ajmi and Zimmerman, 2006; Kaffash and Zare-Reisabadi, 2013). Therefore, it is used to analyze coal failure which is as follows:

$$\begin{aligned}
&\tau_{mogi} = a + b\frac{\sigma_1+\sigma_3}{2} - \beta p_w \\
&a = \frac{2\sqrt{2}C\cos\varphi}{3}, b = \frac{2\sqrt{2}\sin\varphi}{3} \\
&\tau_{oct} = \frac{1}{3}\sqrt{(\sigma_2-\sigma_3)^2+(\sigma_3-\sigma_1)^2+(\sigma_1-\sigma_2)^2}
\end{aligned} \tag{19}$$

Where ϕ is friction angle in degree, and C is cohesion in psi.

4. Study area: Bowen Basin

The Bowen Basin is a north-south trending Permo-Triassic basin in east-central Queensland and northern New South Wales, Australia (Fig. 2). It covers an area of approximately 200,000 km^2 contains up to 10 km of variably deformed shallow marine and fluvio-deltaic silici-clastic sedimentary rocks, which are unconformably overlain in the south by relatively flat-lying Jurassic and Cretaceous rocks of the Surat Basin (Pattison et al., 1996; Alboub et al., 2013).

The Blackwater Group in the northern Bowen Basin is the most

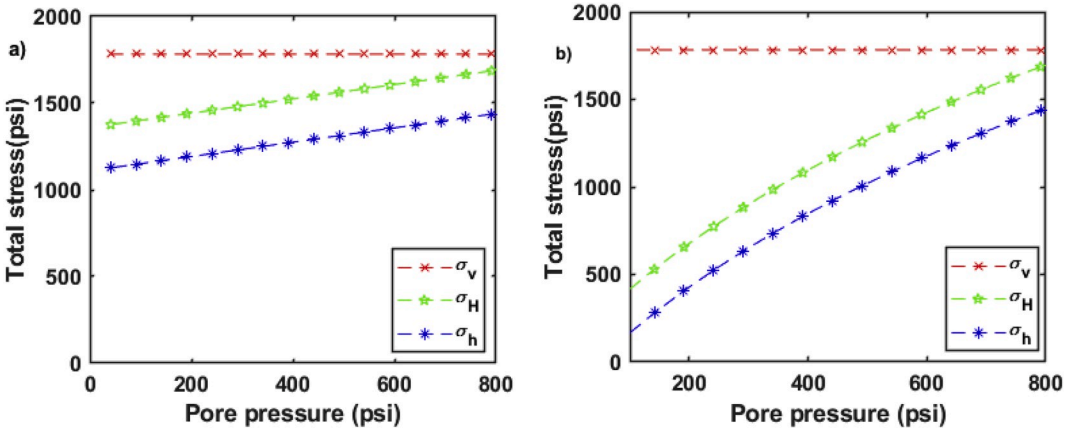

Fig. 4. Total stress changes during depletion in MCM, Bowen Basin. a) Conventional stress path with no matrix shrinkage effect, b) Stress path with matrix shrinkage effect.

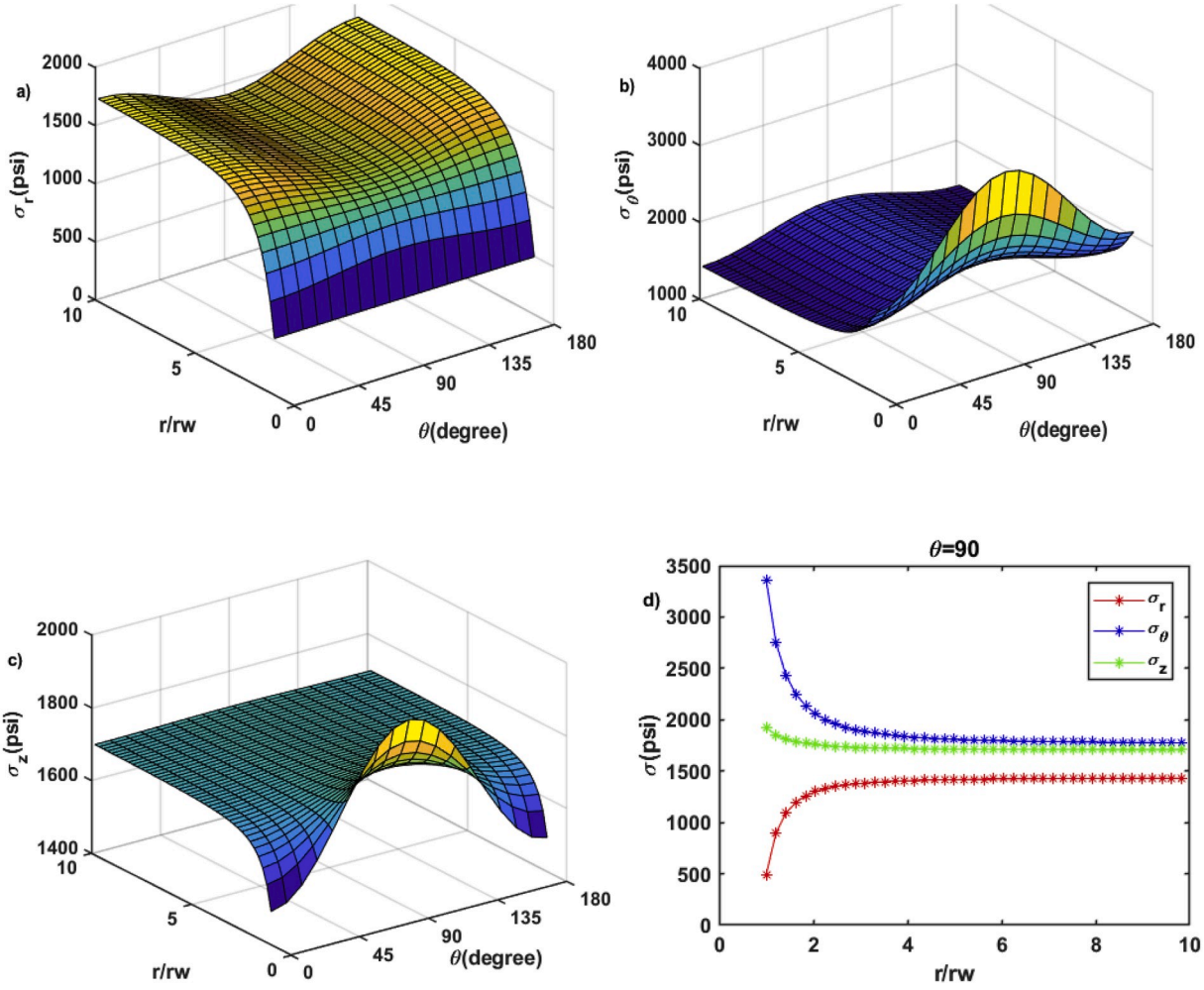

Fig. 5. Stress distribution in a vertical well with no depletion for MCM, Bowen Basin, a) Radial stress, b) Tangential stress, c) Axial stress, d) all stress at θ = 90°.

prolific coal-bearing unit and consists, Moranbah Coal Measures, Fort Cooper Coal Measures and Rangal Coal Measures (Fig. 3). The focus of this study is in the Moranbah Coal Measures (MCM) which is located approximately 400 km south of Townsville and 170 km west of Mackay and includes the most extensive coal measure in this area. The MCM comprises multiple coal layers of Q, P, GM and GML which are placed between sandstone layers. The seams thickness generally ranges from 2 to 10 m with an accumulative thickness of up to 25 m. The seams depth ranging from 100 to 700 m, hydrostatically pressured, and average gas saturation of 75% and permeability range of 0.01–1 mD (Mazumder et al., 2012; Alboub et al., 2013; Michaelsen and Henderson, 2000).

5. Results and discussion

5.1. Input data and stress path in MCM

Table 1 shows the input parameters are used to evaluate the stresses distribution around the vertical and horizontal wellbores in MCM of Bowen Basin.

Fig. 4 shows the stress path in MCM, Bowen Basin using input data in Table 1 for both cases of with and without matrix shrinkage effect. Fig. 4a shows the conventional stress path, where the poromechanical effect is the only affecting parameter and the effect of matrix shrinkage is not considered. Thereby, the stress path factor is constant and equal to 0.41 regardless of the depletion level. Based on uniaxial strain condition and constant vertical stress, the overburden stress is assumed not to change with depletion. However, both total maximum and minimum horizontal stresses are decreasing at a constant rate. Fig. 4b illustrates the stress path by including the methane desorption effect. As this figure shows, the matrix shrinkage effect will increase the stress path value with a nonlinear profile and it causes the stress path to change with depletion rather than being a constant value like conventional reservoirs.

5.2. Vertical well

The stress distribution near the vertical well and in the reservoir are evaluated using equations (10)–(16). The poroelastic stress distribution for a vertical well at the initial stage of production with no depletion is shown in Fig. 5. The radial stress at the angular position of θ equal to 90° is the minimum where the tangential and axial stresses will reach their maximum value (maximum differential stress). The radial stress is the minimum on the wellbore wall, and it increases in the reservoir, whereas the tangential stress is decreasing from its peak on the wellbore toward the reservoir. The effect of depletion and matrix shrinkage on tangential and radial stresses at an angular position of θ equal to 90° is discussed here as the differential stress is at its maximum level and hence the highest possibility of coal failure.

Fig. 6 shows the effect of matrix shrinkage on radial stress near the wellbore wall and in the seam layer for a vertical well. The reservoir pressure reduces from its initial value (~800 psia) during production. Fig. 6a shows the radial stress distribution far from the wellbore where the matrix shrinkage is not considered and a constant stress path is assumed, whereas Fig. 6b shows the stress distribution far from the

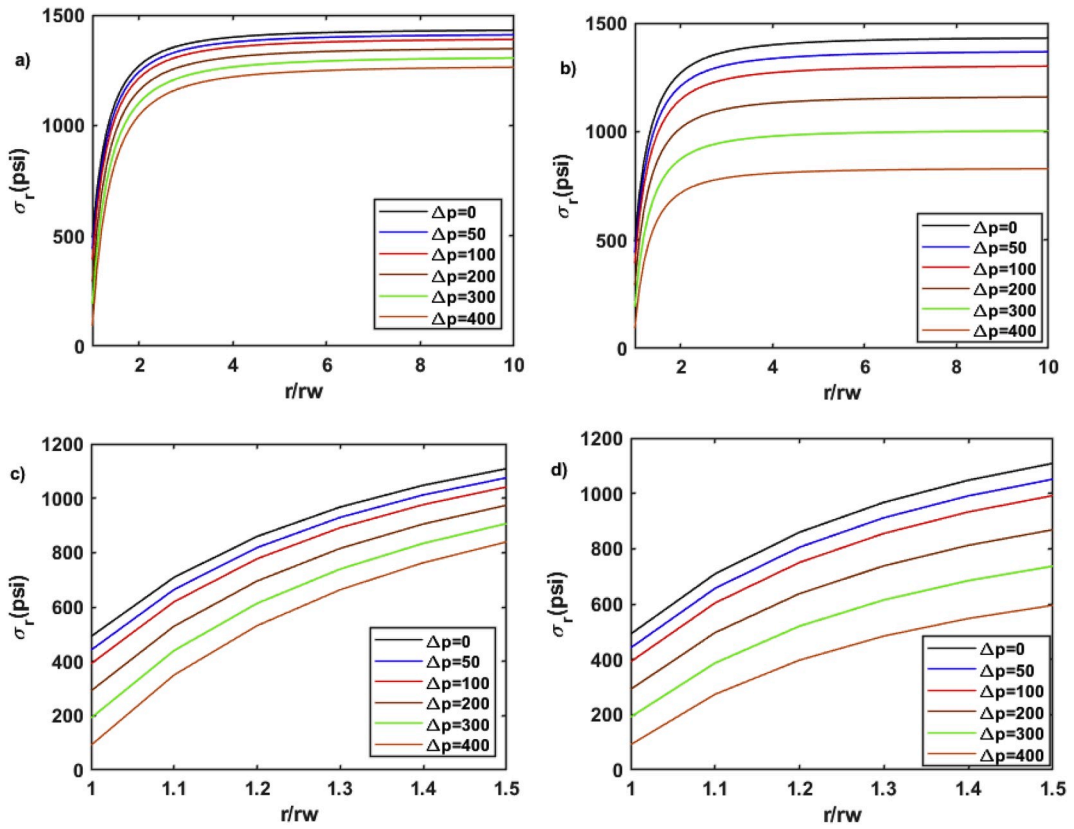

Fig. 6. Radial stress distribution for a vertical well in MCM, a) in the reservoir without the shrinkage effect, b) in the reservoir with the shrinkage effect, c) near the wellbore wall without the shrinkage d) near the wellbore wall with the shrinkage effect.

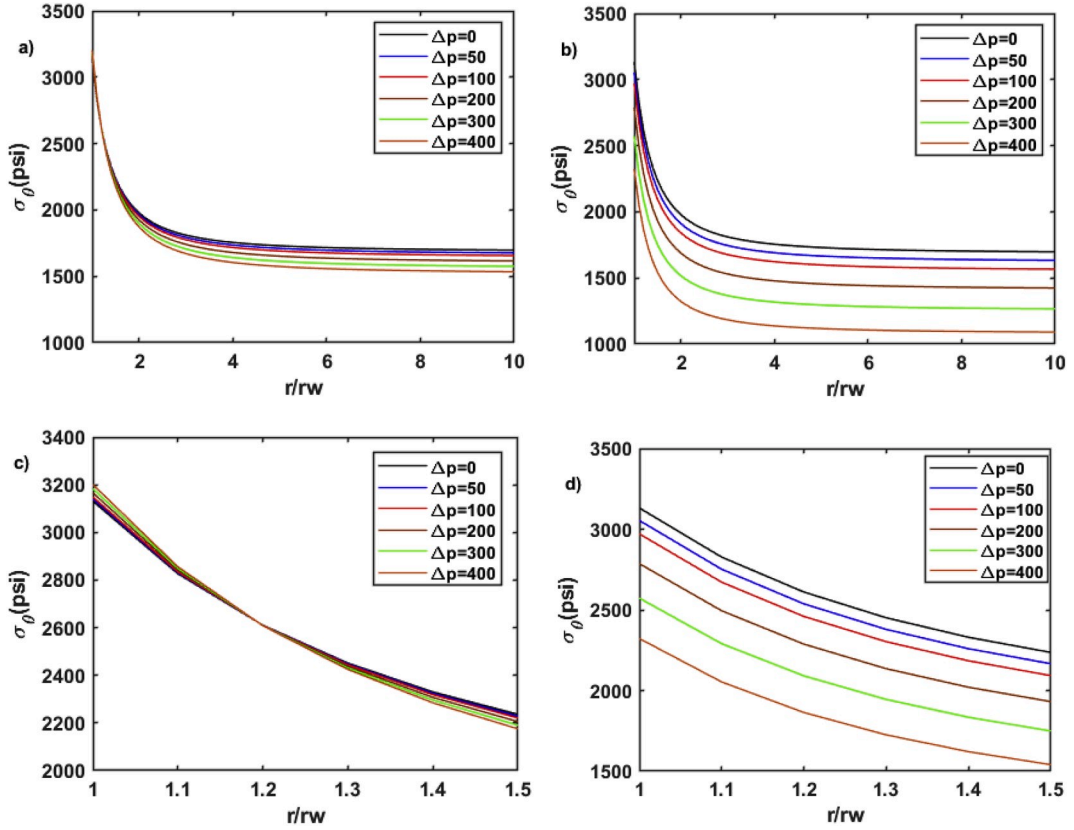

Fig. 7. Tangential stress distribution for a vertical well in MCM, a) in the reservoir and without the shrinkage effect, b) in the reservoir and with the shrinkage effect, c) near the wellbore wall and without the shrinkage, d) near the wellbore wall with the shrinkage effect.

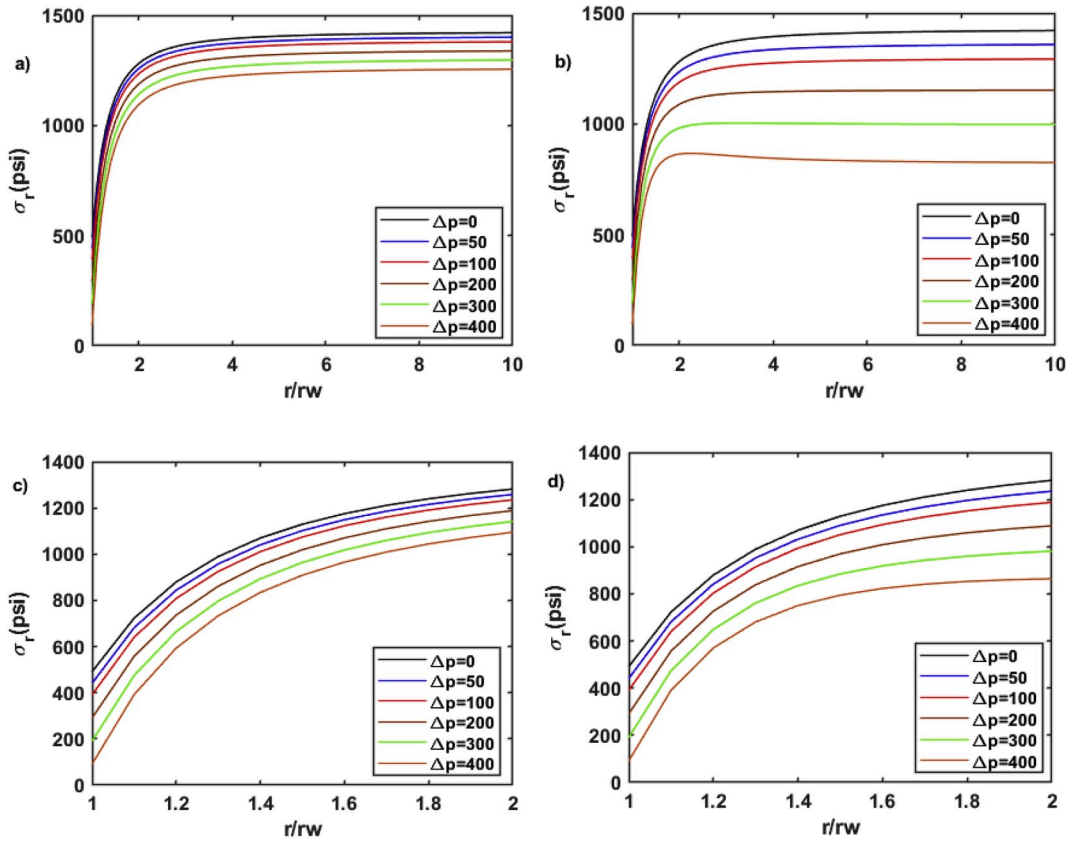

Fig. 8. Radial stress distribution for a horizontal well in MCM, a) in the reservoir without the shrinkage effect, b) in the reservoir with the shrinkage effect, c) near the wellbore wall without the shrinkage d) near the wellbore wall with the shrinkage effect.

wellbore by considering the matrix shrinkage effect. The radial stresses near the wellbore wall without and with shrinkage effect are shown in Fig. 6c and d respectively. In general, the radial stress in a vertical well will decrease during depletion which is consistent with the Masoudian and Hashemi (2016) study. However, the matrix shrinkage and the nonlinear stress path in coal seam gas result in more reduction of radial stress during depletion in the reservoir away from the borehole wall and into the reservoir. It is exactly at the wellbore wall r = Rw and substituting this in equation (10) gives radial stress equal to the bottom-hole flowing pressure. Therefore, as Fig. 6 indicates the radial stress values at the wellbore wall for both conventional and unconventional cases are the same and the matrix shrinkage does not affect them.

The tangential stress distribution in the reservoir and near a vertical wellbore wall in MCM is shown in Fig. 7. The tangential stress in the conventional reservoir without matrix shrinkage effect does not change significantly during depletion (Fig. 7a), while the matrix shrinkage effect and the resulting variable stress path cause a significant decrease of tangential stress by production (Fig. 7b). The effects of depletion and matrix shrinkage on tangential stress near the vertical wellbore wall are shown in Fig. 7c and d respectively. Fig. 7c shows that tangential stress will increase slightly during depletion in a conventional case, whilst Fig. 7d shows that considering the matrix shrinkage effect causes a reduction of the tangential stress during depletion. Therefore, there will be less stress differential on a vertical well wall for a CSG reservoir where the shrinkage effect is considered. In this case, the matrix shrinkage lowers the risk of coal failure and assists the wellbore wall stability. This is consistent with the field operation observations in MCM, Bowen Basin by Puspitasari et al. (2014) and Alboub et al. (2013), where there is no serious coal failure in vertical wells, whereas the coal failure and solids production could be a concern for horizontal wells which is discussed in next section.

5.3. Horizontal well

For a horizontal well, the radial stress distribution around the wellbore and in the reservoir is shown in Fig. 8. The radial stress similar to vertical wells is decreasing by production for both scenarios of with and without shrinkage. It is clear from Fig. 8b and d that the matrix shrinkage reduces the radial stress near the wellbore and in the reservoir significantly. However, the effect of matrix shrinkage on the radial stress inside the reservoir is more significant than on the wellbore wall.

The change of tangential stress during depletion for a horizontal well is different from a vertical well. Fig. 9a and Fig. 9b show the tangential stress distribution inside the reservoir without and with matrix shrinkage effect respectively. The tangential stress without matrix shrinkage effect does not change significantly during production, however, the matrix shrinkage effect causes the reduction of tangential stress inside the reservoir (Fig. 9b). Considering the near wellbore wall stress, the tangential stress during production increases in both scenarios with and without matrix shrinkage. However, the matrix shrinkage causes more increase in the tangential stress in comparison with the conventional case.

The deviatoric stress values on the wellbore wall (r/rw = 1) versus depletion are shown in Fig. 10 for the vertical and horizontal wells respectively. Fig. 10a shows the deviatoric stress will increase by depletion for a vertical well in the conventional reservoirs with no matrix shrinkage. However, the matrix shrinkage effect causes the reduction of deviatoric stress for vertical CSG well. Conversely, in a horizontal well, the matrix shrinkage results in higher deviatoric stress and hence a higher risk of coal failure with depletion (Fig. 10b).

5.4. Coal failure

The principal stresses acting on the wellbore wall and the Mogi-

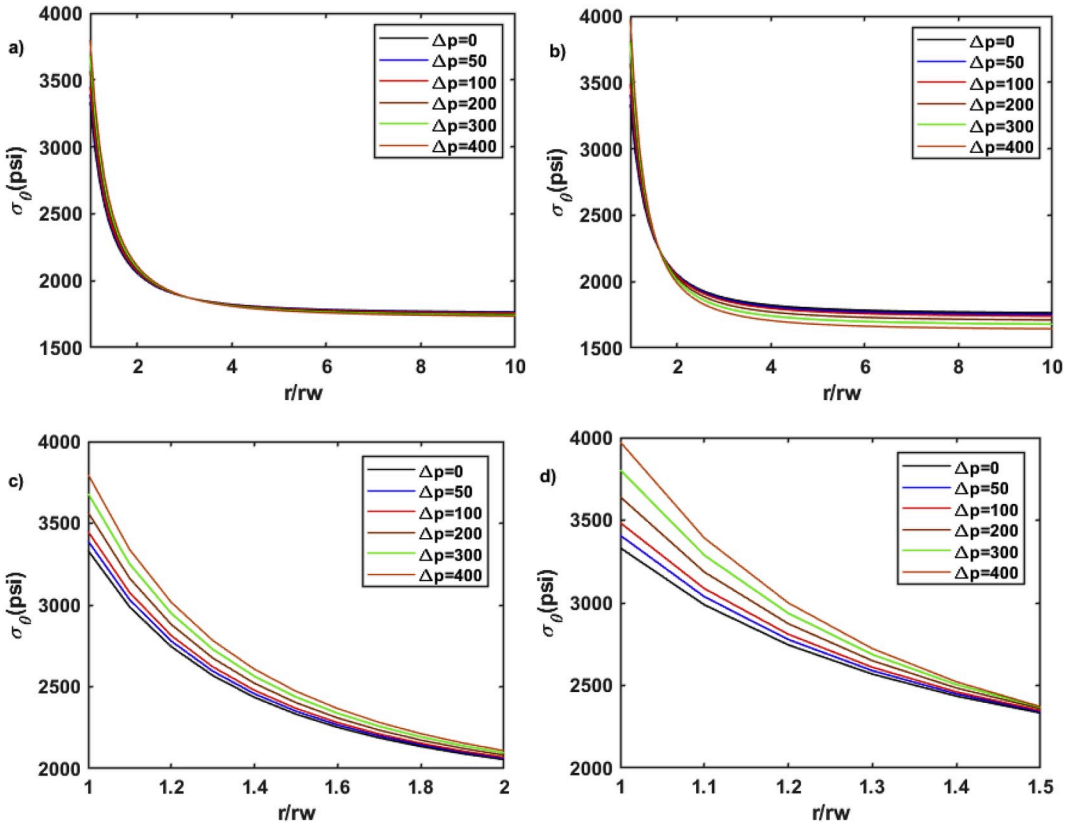

Fig. 9. Tangential stress distribution for a horizontal well in MCM, a) in the reservoir without the shrinkage effect, b) with shrinkage effect in the reservoir, c) near the wellbore wall without the shrinkage d) near the wellbore wall with the shrinkage effect.

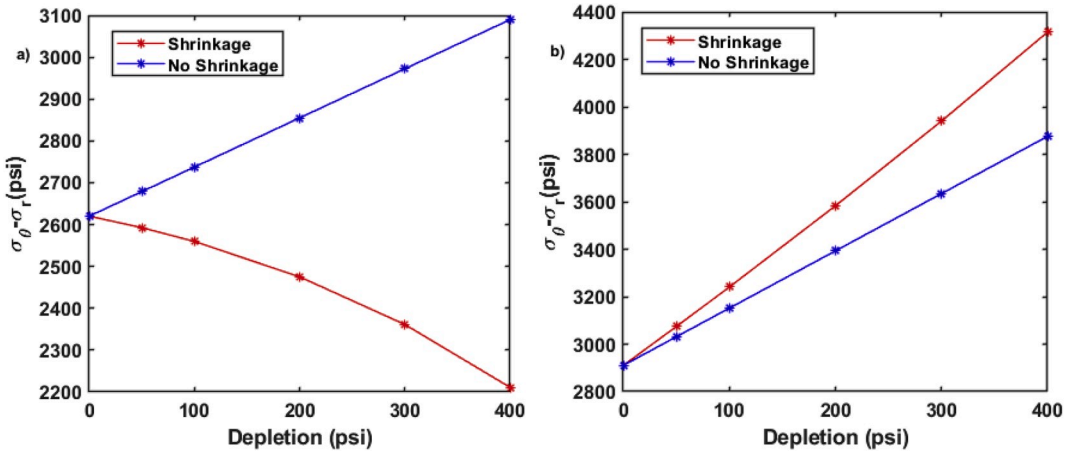

Fig. 10. Deviatoric stress on the wellbore wall in MCM, a) Vertica well, b) Horizontal well.

Coulomb failure criterion are utilized to calculate the Maximum Coal Free Drawdown Pressure (MCFDP). Equations (10)–(12) indicate that the stresses are related to the bottom hole flowing pressure and reservoir pressure. In every step of depletion and for a specific wellbore trajectory, the model will calculate the Critical Bottom Hole Flowing Pressure (CBHFP) by having stress around the wellbore and utilizing Mogi-Coulomb failure criterion. The CBHFP is the bottom hole pressure which satisfies $\tau oct > \tau mogi$ in equation (19). In this situation, the applied stress is more than the rock strength and accordingly the coal failure occurs (see Zare-Reisabadi et al. (2012) and Zare Reisabadi et al. (2020) for details). MCFDP is the difference between reservoir pressure and CBHFP.

Fig. 11a shows the coal failure analysis without considering the matrix shrinkage effect in MCM with a normal faulting stress regime. The higher values of MCFDP represent a more stable case as the rock fails later and allows applying greater drawdown pressure without failure. Fig. 11a indicates that for the case without the matrix shrinkage, the effect of depletion on MCFDP is fairly the same for vertical and horizontal wells. The higher depletion causes higher coal failure potential, which is consistent with previous studies for sand production in conventional reservoirs (Zare-Reisabadi et al., 2012; Kaffash and Zare-Reisabadi, 2013). Fig. 11b shows the MCFDP during depletion for different well inclinations by considering the matrix shrinkage effect. It indicates that the MCFDP for a horizontal well will significantly decrease during depletion, whereas there is a slight change in a vertical well.

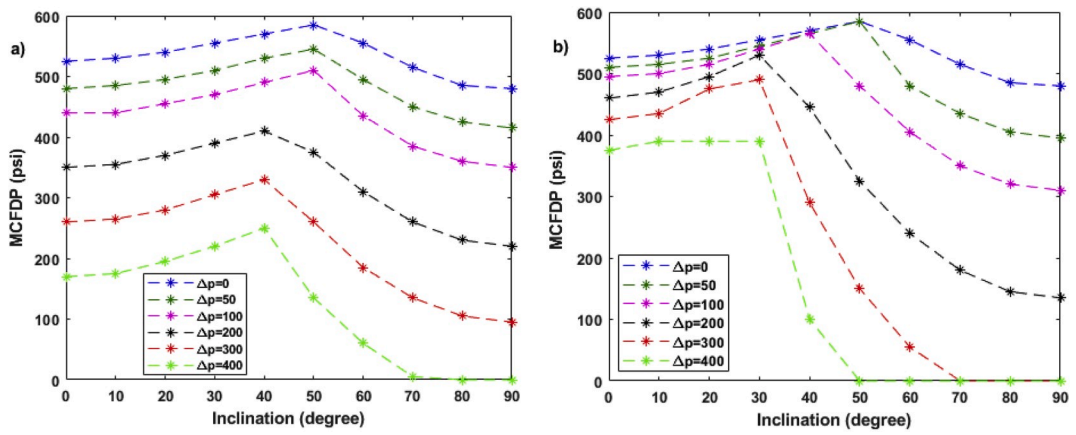

Fig. 11. Coal failure analysis in MCM, a) without matrix shrinkage effect, b) with matrix shrinkage effect.

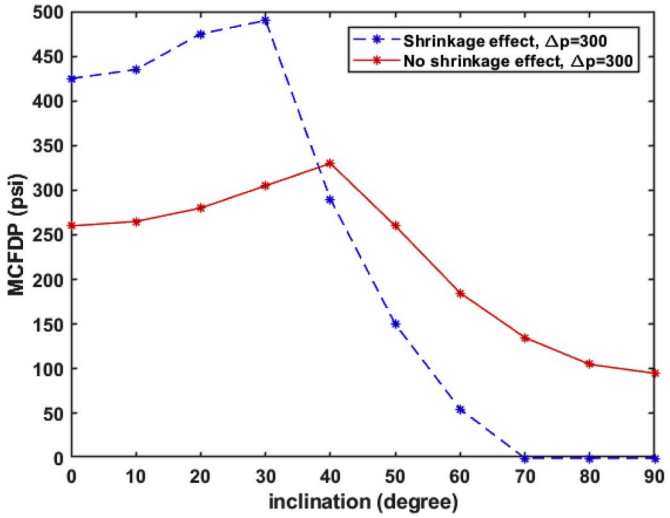

Fig. 12. The effect of matrix shrinkage on coal failure for different inclinations.

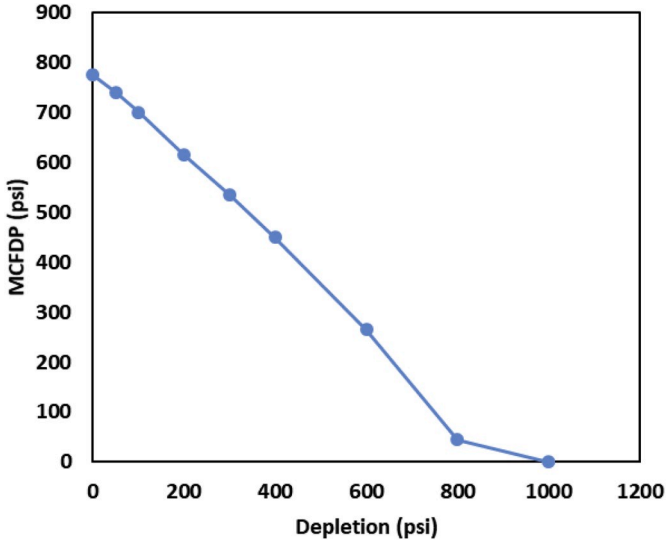

Fig. 13. Coal failure analysis in the San Juan Basin.

Table 2
Parameters for coal failure analysis in the San Juan Basin.

Parameter	Value	Source
S_v (psi)	2800	(Palmer, 2009; Shovkun and Espinoza, 2017)
S_H (psi)	2464	Shovkun and Espinoza (2017)
S_h (psi)	1960	(Palmer, 2009; Ramurthy et al., 1999)
P_o (psi)	1260	(Shi and Durucan, 2004; Palmer, 2009)
C (psi)	500	Saurabh and Harpalani (2017)
φ(degree)	38	Saurabh and Harpalani (2017)
$P\varepsilon$(psi)	560	(Shi and Durucan, 2004; Palmer, 2009)
ε_l	0.0083	(Shi and Durucan, 2004; Palmer, 2009)
E (psi)	406,105	(Shi and Durucan, 2004; Palmer, 2009; Liu and Harpalani, 2013)
N	0.31	(Shi and Durucan, 2004; Palmer, 2009; Liu and Harpalani, 2013)
B	0.8	Shovkun and Espinoza (2017)

Fig. 12 shows the effect of matrix shrinkage on MCFDP in MCM, Bowen Basin after 300 psi depletion from its initial reservoir pressure. It indicates that in a vertical wellbore, the resultant matrix shrinkage makes the wellbore stable and increases the MCFDP from 250 psi to 430 psi. It is concluded that in a vertical well, the matrix shrinkage effect will lower the coal failure potential during production. However, for the highly deviated or horizontal wells, the effect of matrix shrinkage is different. The matrix shrinkage can cause inevitable coal failure and coal production for a horizontal well by 300 psi pressure drop from the initial reservoir pressure. This outcome is consistent with coal failure and solids production in recently drilled horizontal wells in the Bowen Basin (Puspitasari et al., 2014). It should be noted that the results shown in this paper are valid for a normal stress regime only.

6. Model verification, limitations, and future work

The coal failure situation in Fruitland coal formation of the San Juan Basin is utilized to validate the model. The vertical wells were producing for more than 15 years without serious coal failure problem, but as the reservoir pressure reduces to 300-250 psi (960–1010 psi depletion) from its original reservoir pressure of 1260 psi, the coal failure became a serious challenge (Moore et al., 2011; Okotie and Moore, 2011). The input data in Table 2 were utilized to evaluate coal failure in the San Juan Basin. It should be noted the values in Table 2 are averaged over different measurements in the literature. Fig. 13 shows the MCFDP versus depletion for the vertical wells in the San Juan Basin. It indicates that as long as the depletion is less than 1000 psi, methane can produce without coal failure (if the applied drawdown pressure is less than calculated MCFDP). However, beyond 1000 psi depletion, there is no applicable drawdown pressure to avoid coal failure which is in agreement with field observation by Okotie and Moore (2011) and Moore et al. (2011).

The presented model utilizes the general poroelastic solution which enables stress distribution evaluation for deviated and horizontal wells. However, other constitutive models such as elastoplastic, elastic-brittle-plastic, and elastic softening models are developed for vertical wells and cannot predict the coal failure in deviated and horizontal wells (Lv et al., 2018; Masoudian, 2018; Li et al., 2015). The proposed model in this study does not consider the effect of the cleat system on the stress path for simplicity, which is an important research topic for further investigation. However, it is quite clear that depletion causes the reduction of effective stress and consequently will increase the cleat aperture and permeability (Saurabh and Harpalani, 2018; Palmer, 2009). The other limitation of the model is about the anisotropy as the model assumes the isotropic rock properties and isotropic matrix shrinkage for simplicity.

7. Conclusions

A stress model is developed to investigate the impact of matrix shrinkage on stress distribution around the vertical and horizontal CSG wells during primary production. Based on the developed model, the following conclusions can be drawn:

- For a vertical well, the radial stress decreases during depletion and the matrix shrinkage leads to more reduction of radial stress.
- The matrix shrinkage causes the reduction of tangential stress near the vertical wellbore wall (unlike the conventional reservoirs). Therefore, there will be less stress differential on the wellbore wall for a CSG reservoir than a case without the matrix shrinkage.
- In a horizontal well, the radial stress decreases during production irrespective of matrix shrinkage; however, the reduction of radial stress is more significant if the matrix shrinkage effect is considered.
- For a horizontal well, the matrix shrinkage will cause an increase of the near wellbore wall tangential stress. The increase of tangential stress and reduction of radial stress near the CSG's horizontal wellbore wall result in more deviatoric stress compare to the conventional case.
- In a vertical wellbore, the matrix shrinkage help the stability of wellbore during depletion (which is not the case if consider the matrix shrinkage). Conversely, for a horizontal wellbore or a highly deviated well, the matrix shrinkage will cause the reduction of MCFDP during depletion, hence a higher risk of coal failure.

Declaration of competing interest

The authors declare that they have no known competing financial interests or personal relationships that could have appeared to influence the work reported in this paper.

CRediT authorship contribution statement

Mohammadreza Zare Reisabadi: Conceptualization, Methodology, Software, Writing - original draft. **Manouchehr Haghighi:** Supervision. **Mohammad Sayyafzadeh:** Writing - review & editing. **Abbas Khaksar:** Supervision.

Appendix A. Supplementary data

Supplementary data to this article can be found online at https://doi.org/10.1016/j.jngse.2020.103280.

References

Addis, M.A., 1997. The stress-depletion response of reservoirs. In: Proc., SPE Annual Technical Conference and Exhibition, San Antonio, Texas, p. 11.

Al-Ajmi, A.M., Zimmerman, R.W., 2006. Stability analysis of vertical boreholes using the Mogi–Coulomb failure criterion. Int. J. Rock Mech. Min. Sci. 43 (8), 1200–1211. http://www.sciencedirect.com/science/article/pii/S1365160906000669.

Alboub, Mohamed, Scott, Michael, John Pallikathekathil, Zachariah, et al., 2013. Calibrated mechanical earth models answer questions on hydraulic fracture containment and wellbore stability in some of the CSG wells in the Bowen Basin. In: Proc., SPE Unconventional Resources Conference and Exhibition-Asia Pacific, Brisbane, Australia.

Behnoud far, Pouria, Hassani, Amir Hossein, Al-Ajmi, Adel M., et al., 2016. A novel model for wellbore stability analysis during reservoir depletion. J. Nat. Gas Sci. Eng. 35, 935–943.

Connell, Luke D., Mazumder, S., Sander, Regina, et al., 2016. Laboratory characterisation of coal matrix shrinkage, cleat compressibility and the geomechanical properties determining reservoir permeability. Fuel 165, 499–512. http://www.sciencedirect.com/science/article/pii/S0016236115010601.

Cui, Xiaojun, Bustin, R. Marc, Chikatamarla, Laxmi, 2007. Adsorption-induced coal swelling and stress: implications for methane production and acid gas sequestration into coal seams. J. Geophys. Res.: Solid Earth 112 (B10). https://doi.org/10.1029/2004JB003482.

Davison, J.M., Foo, I., Ellis, F., et al., 2016. The in-situ stress response of reservoirs to pressure reduction followed by pressure increase: depletion and rebound stress paths from two case studies. In: Proc., 50th U.S. Rock Mechanics/Geomechanics Symposium, Houston, Texas, vol. 8.

Espinoza, D.N., Pereira, J.M., Vandamme, M., et al., 2015a. Desorption-induced shear failure of coal bed seams during gas depletion. Int. J. Coal Geol. 137, 142–151.

Espinoza, D.N., Pereira, J.M., Vandamme, M., et al., 2015b. Stress path of coal seams during depletion: the effect of desorption on coal failure. In: Proc., 49th U.S. Rock Mechanics/Geomechanics Symposium, San Francisco, California, vol. 6.

Fjær, E., Holt, R.M., Horsrud, P., et al., 2008. Chapter 4 Stresses around boreholes. Borehole failure criteria. In: Fjær, E., Holt, R.M., Horsrud, P., Raaen, A.M., Risnes, R. (Eds.), Petroleum Related Rock Mechanics. Elsevier, pp. 135–174.

GA, BREE, 2012. Australian Gas Resource Assessment. Department of Resources, Energy and Tourism, Geoscience Australia and Bureau of Resources and Energy Economics, Canberra.

Gao, Chao, Gray, K.E., 2019. A workflow for infill well design: wellbore stability analysis through a coupled geomechanics and reservoir simulator. J. Petrol. Sci. Eng. 176, 279–290. http://www.sciencedirect.com/science/article/pii/S0920410518311860.

Kaffash, Amin, Zare-Reisabadi, M.R., 2013. Borehole stability evaluation in overbalanced and underbalanced drilling: based on 3D failure criteria. Geosyst. Eng. 16 (2), 175–182. https://doi.org/10.1080/12269328.2013.806047.

Li, Xiaorong, Gray, K.E., 2015. Wellbore stability of deviated wells in depleted reservoir. In: Proc., SPE Annual Technical Conference and Exhibition, Houston, Texas, USA, vol. 14.

Li, Yong, Cao, Shugang, Fantuzzi, Nicholas, et al., 2015. Elasto-plastic analysis of a circular borehole in elastic-strain softening coal seams. Int. J. Rock Mech. Min. Sci. $V 80, 316–324.

Liu, Shimin, Harpalani, Satya, 2013. Permeability prediction of coalbed methane reservoirs during primary depletion. Int. J. Coal Geol. 113, 1–10.

Liu, Shimin, Harpalani, Satya, 2014. Evaluation of in situ stress changes with gas depletion of coalbed methane reservoirs. J. Geophys. Res.: Solid Earth 119 (8), 6263–6276.

Liu, Ting, Liu, Shimin, Lin, Baiquan, et al., 2020. Stress response during in-situ gas depletion and its impact on permeability and stability of CBM reservoir. Fuel 266, 117083. http://www.sciencedirect.com/science/article/pii/S0016236120300788.

Lu, Meng, Connell, Luke, 2016. Coal failure during primary and enhanced coalbed methane production — theory and approximate analyses. Int. J. Coal Geol. 154–155, 275–285.

Lv, Adelina, Masoumi, Hossein, Stuart, D., Walsh, C., et al., 2018. Elastic-softening-plasticity around a borehole: an analytical and experimental study. Rock Mech. Rock Eng. https://doi.org/10.1007/s00603-018-1650-7.

Masoudian, Mohsen S., Amid Hashemi, Mir, Tasalloti, Ali, et al., 2018. Elastic–brittle–plastic behaviour of shale reservoirs and its implications on fracture permeability variation: an analytical approach. Rock Mech. Rock Eng. 51 (5), 1565–1582. https://doi.org/10.1007/s00603-017-1392-y.

Masoudian, Mohsen S., Hashemi, Mir Amid, 2016. Analytical solution of a circular opening in an axisymmetric elastic-brittle-plastic swelling rock. J. Nat. Gas Sci. Eng. 35, 483–496. http://www.sciencedirect.com/science/article/pii/S1875510016306370.

Mazumder, Saikat, Scott, Michael, Jiang, Jessica, 2012. Permeability increase in Bowen Basin coal as a result of matrix shrinkage during primary depletion. Int. J. Coal Geol. 96–97, 109–119. http://www.sciencedirect.com/science/article/pii/S0166516212000420.

Michaelsen, Per, Henderson, Robert A., 2000. Facies relationships and cyclicity of high-latitude, Late Permian coal measures, Bowen Basin, Australia. Int. J. Coal Geol. 44 (1), 19–48. http://www.sciencedirect.com/science/article/pii/S0166516299000488.

Mitra, Abhijit, Harpalani, Satya, Liu, Shimin, 2012. Laboratory measurement and modeling of coal permeability with continued methane production: Part 1 – laboratory results. Fuel 94, 110–116. http://www.sciencedirect.com/science/article/pii/S0016236111006703.

Moore, Robert Lloyd, Fay Loftin, Debbie, Palmer, Ian D., 2011. History matching and permeability increases of mature coalbed methane wells in san Juan Basin. In: Proc., SPE Asia Pacific Oil and Gas Conference and Exhibition, Jakarta, Indonesia.

Okotie, Victoria U., Moore, Robert L., 2011. Well-Production Challenges and Solutions in a Mature, Very-Low-Pressure Coalbed-Methane Reservoir.

Palmer, Ian D., Zissis Andrew, Moschovidis, John Robert, Cameron, 2005. Coal failure and consequences for coalbed methane wells. In: Proc., SPE Annual Technical Conference and Exhibition, Dallas, Texas.

Palmer, Ian, 2009. Permeability changes in coal: analytical modeling. Int. J. Coal Geol. 77 (1), 119–126. http://www.sciencedirect.com/science/article/pii/S0166516208001857.

Pattison, C.I., Fielding, C.R., McWatters, R.H., et al., 1996. Nature and origin of fractures in permian coals from the Bowen Basin, Queensland, Australia. Geol. Soc. Lond. Spec. Publ. 109 (1), 133. https://sp.lyellcollection.org/content/109/1/133.abstract.

Puspitasari, Ratih, Gan, Thomas, John Pallikathekathil, Zachariah, et al., 2014. Wellbore stability modelling for horizontal and multi-branch lateral wells in CBM: practical solution to better understand the uncertainty in rock strength and coal heterogeneity. In: Proc., SPE Asia Pacific Oil & Gas Conference and Exhibition, Adelaide, Australia.

Rafieepour, Saeed, Miska, Stefan Z., Ozbayoglu, Evren, et al., 2017. Experimental study of reservoir stress path and hysteresis during depletion and injection under different deformational conditions. In: Proc., 51st U.S. Rock Mechanics/Geomechanics Symposium, San Francisco, California, USA.

Ramurthy, Muthukumarappan, Rogers, Rudy E., Dana, Weida, 1999. Analysis of the success of cavity completions in the fairway zone of the san Juan Basin. In: Proc., SPE Rocky Mountain Regional Meeting, Gillette, Wyoming, p. 8.

Reisabadi, Zare, Mohammadreza, Haghighi, Manouchehr, Salmachi, Alireza, et al., 2020. Analytical modelling of coal failure in coal seam gas reservoirs in different stress regimes. Int. J. Rock Mech. Min. Sci. 128, 104259. http://www.sciencedirect.com/science/article/pii/S1365160919308408.

Saurabh, S., Harpalani, S., 2017. Stress-dependent permeability of sorptive reservoirs incorporating postfailure behavior. In: Proc., 51st U.S. Rock Mechanics/Geomechanics Symposium, San Francisco, California, USA.

Saurabh, Suman, Harpalani, Satya, 2018. Stress path with depletion in coalbed methane reservoirs and stress based permeability modeling. Int. J. Coal Geol. 185, 12–22.

Saurabh, S., Harpalani, S., Singh, V.K., 2016. Implications of stress re-distribution and rock failure with continued gas depletion in coalbed methane reservoirs. Int. J. Coal Geol. 162, 183–192.

Shi, J.Q., Durucan, S., 2004. Drawdown induced changes in permeability of coalbeds: a new interpretation of the reservoir response to primary recovery. Transport Porous Media 56 (1), 1–16. https://doi.org/10.1023/B:TIPM.0000018398.19928.5a.

Shovkun, Igor, Espinoza, D. Nicolas, 2017. Coupled fluid flow-geomechanics simulation in stress-sensitive coal and shale reservoirs: impact of desorption-induced stresses, shear failure, and fines migration. Fuel 195, 260–272.

Teufel, Lawrence W., Rhett, Douglas W., Farrell, Helen E., 1991. Effect of reservoir depletion and pore pressure drawdown on in situ stress and deformation in the Ekofisk field, North Sea. In: Proc., the 32nd U.S. Symposium on Rock Mechanics (USRMS), Norman, Oklahoma, p. 10.

Tohidi, Amin, Ahmad, Fahimifar, Rasouli, Vamegh, 2018. Analytical solution to study depletion/injection rate on induced wellbore stresses in an anisotropic stress field. Geotech. Geol. Eng. 36 (3), 1735–1744. https://doi.org/10.1007/s10706-017-0429-z.

Yang, Yong, Cui, Shuqing, Ni, Yuanyong, et al., 2014. A new attempt of a CBM tree-like horizontal well: a pilot case of Well ZS 1P-5H in the Qinshui Basin. Nat. Gas. Ind. B 1 (2), 205–209. http://www.sciencedirect.com/science/article/pii/S2352854014000308.

Zare, M.R., Shadizadeh, S.R., Habibnia, B., 2010. Mechanical stability analysis of directional wells: a case study in ahwaz oilfield. In: Proc., Nigeria Annual International Conference and Exhibition, Tinapa - Calabar, Nigeria, p. 10.

Zare-Reisabadi, M.R., Kaffash, A., Shadizadeh, S.R., 2012. Determination of optimal well trajectory during drilling and production based on borehole stability. Int. J. Rock Mech. Min. Sci. 56, 77–87. http://www.sciencedirect.com/science/article/pii/S1365160912001554.

Zoback, M.D., Zinke, J.C., 2002. Production-induced normal faulting in the Valhall and Ekofisk oil fields. Pure Appl. Geophys. 159 (1), 403–420. https://doi.org/10.1007/PL00001258.

4.2 Stress Changes and Coal Failure Analysis in Coal Seam Gas Wells Accounting for Matrix Shrinkage: An Example from Bowen Basin, East Australia

Zare Reisabadi M, Haghighi M, Khaksar A., SPE/AAPG/SEG Asia Pacific Unconventional Resources Technology Conference. Brisbane, Australia: Unconventional Resources Technology Conference; 2019. p. 11.

Statement of Authorship

Title of Paper	Stress Changes and Coal Failure Analysis in Coal Seam Gas Wells Accounting for Matrix Shrinkage: An Example from Bowen Basin, East Australia
Publication Status	☑ Published ☐ Accepted for Publication ☐ Submitted for Publication ☐ Unpublished and Unsubmitted w ork w ritten in manuscript style
Publication Details	Zare Reisabadi M, Haghighi M, Khaksar A., SPE/AAPG/SEG Asia Pacific Unconventional Resources Technology Conference. Brisbane, Australia: Unconventional Resources Technology Conference; 2019. p. 11.

Principal Author

Name of Principal Author (Candidate)	Mohammadreza Zare Reisabadi
Contribution to the Paper	Literature review, Model development, Analysis of results, wiring the manuscript.
Overall percentage (%)	80
Certification:	This paper reports on original research I conducted during the period of my Higher Degree by Research candidature and is not subject to any obligations or contractual agreements with a third party that would constrain its inclusion in this thesis. I am the primary author of this paper.
Signature	Date: 09/03/2021

Co-Author Contributions

By signing the Statement of Authorship, each author certifies that:

i. the candidate's stated contribution to the publication is accurate (as detailed above);

ii. permission is granted for the candidate in include the publication in the thesis; and

iii. the sum of all co-author contributions is equal to 100% less the candidate's stated contribution.

Name of Co-Author	Manouchehr Haghighi
Contribution to the Paper	Support in analysis of results, Reviewing the manuscript
Signature	Date: 9/3/21

Name of Co-Author	Abbas Khaksar
Contribution to the Paper	Support in analysis of results, Reviewing the manuscript
Signature	Date: 15/3/2021

UNCONVENTIONAL RESOURCES TECHNOLOGY CONFERENCE
FUELED BY SPE • AAPG • SEG

URTEC-198309-MS

Stress Changes and Coal Failure Analysis in Coal Seam Gas Wells Accounting for Matrix Shrinkage: An Example from Bowen Basin, East Australia

Mohammadreza Zare Reisabadi and Manouchehr Haghighi, Australian School of Petroleum, The University of Adelaide; Abbas Khaksar, Baker Hughes

This paper was prepared for presentation at the SPE/AAPG/SEG Asia Pacific Unconventional Resources Technology Conference held in Brisbane, Australia, 18 – 19 November 2019.

Abstract

Coal Seam Gas (CSG) has increasingly become an important part of natural gas resources for both domestic use and LNG export in Eastern Australia. The matrix shrinkage during primary production results in a unique stress path and new near-wellbore stress distribution in CSG reservoirs. The knowledge of these stresses is essential for coal shear failure prediction and assessing coal fines production risks, particularly in horizontal wells which nowadays are becoming common in Australian CSG fields such as the Bowen Basin.

In this study, an analytical model is developed to evaluate the stress distribution around both vertical and horizontal wells by coupling the effects of depletion, matrix shrinkage, and wellbore trajectory. Then, the model is applied for coal failure analysis in both vertical and horizontal wells in Moranbah Coal Measures, in the Bowen Basin eastern Australia.

The results of the model reveal that the stress path factor in CSG reservoirs, contrary to conventional reservoirs, is not constant during production and it can even be more than one due to the matrix shrinkage effect of coal seams with depletion. Production from these reservoirs will significantly alter the effective horizontal stresses which result in a considerable change to the near-wellbore stress distribution. The results also indicate that in a normal faulting stress regime, the matrix shrinkage will cause less stress differential on the wellbore wall for vertical wells and it is found that this mechanism reduces the coal failure potential during production. Conversely, for highly deviated and horizontal wells, the matrix shrinkage will cause an extra increase of tangential stress and reduction of radial stress on the wellbore wall. Therefore, it results in higher levels of stress differentials on horizontal wellbore wall and increase of the coal failure risks with depletion.

The results of this study can be used as a guide for assessing the risk of solids production, identifying the critical drawdown and depletion pressure and the effects of wellbore trajectory on optimizing coal fines production in CSG wells.

Introduction

During the past decades, Coal Seam Gas (CSG) or Coal Bed Methane (CBM) recourses have increasingly become an important part of natural gas resources. Particularly in Eastern Australia, CSG is the main part of the gas industry where 97 percent of produced CSG of Australia is coming from Bowen and Surat basins in Queensland and the remainder from New South Wales (GA and BREE 2012).

Some of the recently drilled horizontal and multilateral wells in the Bowen Basin have experienced unexpected fines and solid production during production from coal layers (Puspitasari et al. 2014, Mazumder, Scott, and Jiang 2012, Alboub et al. 2013) and rock failure problems could become more pervasive with further depletion. Coal failure has several detrimental consequences and it causes damage to pumps and compressors.

Depressurizing water production and associated depletion is a pre-requisite for commercial production from CSG reservoirs. This results in changes of horizontal in-situ stresses and consequent changes of tangential, axial, and radial stresses distribution around the producing wells and within the coal seam layer. The effect of depletion on stress distribution around the wellbore in conventional reservoirs has been extensively studied in the literature (Li and Gray 2015, Rafieepour et al. 2017, Davison et al. 2016, Behnoud far et al. 2016, Zare, Shadizadeh, and Habibnia 2010, Zare-Reisabadi, Kaffash, and Shadizadeh 2012). However, there are few studies that consider the effect of depletion and consequent matrix shrinkage on the stress distribution around the wellbore in unconventional reservoirs. Masoudian and Hashemi (2016) considered elastoplastic formation around an axisymmetric coal seam gas vertical wellbore to develop an analytical solution for stress distribution by including shrinkage effect.

Horizontal drilling is common in Bowen Basin where permeability is relatively low (Mazumder, Scott, and Jiang 2012). Nevertheless, the previously developed analytical models for CSG reservoirs were focused on vertical wells and they cannot apply to horizontal wells. Coals are typically weak rocks and preventing coal failure during production, particularly in depleted horizontal wells, could be challenging in CSG wells. There are reports of rock failure related drilling and production problem in CSG wells, particularly in depleted deviated and horizontal wells (Espinoza et al. 2015b, Moore, Loftin, and Palmer 2011, Yang et al. 2014, Lu and Connell 2016).

In this study, an analytical model is developed to evaluate the stress distribution around both vertical and horizontal wells by including pressure depletion and matrix shrinkage effects. The developed stress model is then used to asses coal failure in both vertical and horizontal wells in the Bowen Basin using regional and published in situ stresses, pore pressure, and rock properties.

Study Area: Bowen Basin

Coal measures of the Bowen Basin provide one of the main resources of CSG for domestic use and LNG export (GA and BREE 2014). The Bowen Basin is a north-south trending Permo-Triassic basin in East-Central Queensland and Northern New South Wales, Australia (figure 1). It covers an area of approximately 200,000 km^2 contains up to 10km of variably deformed shallow marine and fluvio-deltaic siliciclastic sedimentary rocks unconformably overlain in the South by relatively flat-lying Jurassic and Cretaceous rocks of the Surat Basin (Pattison et al. 1996, Alboub et al. 2013). The Blackwater Group in the Northern Bowen Basin is the most prolific coal-bearing unit and comprises (oldest to youngest), Moranbah Coal Measures, Fort Cooper Coal Measures and Rangal Coal Measures (Alboub et al. 2013). The focus of this study is in the Moranbah Coal Measures (MCM) which is comprised of multiple coal layers.

Figure 1—Location of the Permo-Triassic Bowen Basin, eastern Australia (Swindon and Moore 1989).

Mathematical Modeling

To evaluate stress distribution around deviated or horizontal wells with anisotropic horizontal stresses, the general poroelastic solution with varying pore pressure is considered. Assuming the radius of the reservoir to be much larger than the wellbore radius ($R_o >> R_w$) the resulting radial and tangential stress components are as following (Fjær et al. 2008):

$$\sigma_r = \frac{\sigma_x^o + \sigma_y^o}{2}\left(1 - \frac{R_w^2}{r^2}\right) + \frac{\sigma_x^o - \sigma_y^o}{2}\left(1 + 3\frac{R_w^4}{r^4} - 4\frac{R_w^2}{r^2}\right)\cos 2\theta + \tau_{xy}^o\left(1 + 3\frac{R_w^4}{r^4} - 4\frac{R_w^2}{r^2}\right)\sin 2\theta + \frac{2\eta}{r^2}\left(\int_{R_w}^{r} r\,\Delta p_f(r)dr\right) + p_w\frac{R_w^2}{r^2} \quad (1)$$

$$\sigma_\theta = \frac{\sigma_x^o + \sigma_y^o}{2}\left(1 + \frac{R_w^2}{r^2}\right) - \frac{\sigma_x^o - \sigma_y^o}{2}\left(1 + 3\frac{R_w^4}{r^4}\right)\cos 2\theta - \tau_{xy}^o\left(1 + 3\frac{R_w^4}{r^4}\right)\sin 2\theta - \frac{2\eta}{r^2}\left(\int_{R_w}^{r} r\,\Delta p_f(r)dr - r^2\,\Delta p_f(r)\right) - p_w\frac{R_w^2}{r^2} \quad (2)$$

Where

$$\begin{aligned}
\sigma_x^o &= \left(\sigma_H \cos^2\alpha + \sigma_h \sin^2\alpha\right)\cos^2 i + \sigma_v \sin^2 i \\
\sigma_y^o &= \sigma_H \sin^2\alpha + \sigma_h \cos^2\alpha \\
\tau_{xy}^o &= 0.5\left(\sigma_h - \sigma_H\right)\sin 2\alpha \cos i \\
\text{And } \eta &= \frac{\beta(1-2\upsilon)}{2(1-\upsilon)}
\end{aligned} \quad (3)$$

Based on the assumption of a steady state flow equation, the pore pressure profile in Equation 4 is derived (Cui, Bustin, and Chikatamarla 2007):

$$\int_{R_w}^{r} r\,\Delta p_f(r)dr = \frac{p_{f0} - p_w}{4\ln\left(\frac{R_0}{R_w}\right)}\left[\left(R_w^2 - r^2\right) + 2r^2\ln\left(\frac{r}{R_0}\right) - 2R_w^2\ln\left(\frac{R_w}{R_0}\right)\right] \quad (4)$$

By substitution of equation 4 into the equations 1-3 the following stresses distribution around the wellbore is obtained:

$$\sigma_r = \frac{\sigma_x^o+\sigma_y^o}{2}\left(1-\frac{R_w^2}{r2}\right)+\frac{\sigma_x^o-\sigma_y^o}{2}\left(1+3\frac{R_w^4}{r4}-4\frac{R_w^2}{r2}\right)\cos 2\theta+\tau_{xy}^o\left(1+3\frac{R_w^4}{r4}-4\frac{R_w^2}{r2}\right)\sin 2\theta$$
$$+\frac{2\eta}{r2}\left(\frac{p_{f0}-p_w}{4\ln\left(\frac{R_0}{R_w}\right)}\left[\left(R_w^2-r^2\right)+2r^2\ln\left(\frac{r}{R_0}\right)-2R_w^2\ln\left(\frac{R_w}{R_0}\right)\right]\right)+p_w\frac{R_w^2}{r2} \quad (5)$$

$$\sigma_\theta = \frac{\sigma_x^o+\sigma_y^o}{2}\left(1+\frac{R_w^2}{r2}\right)-\frac{\sigma_x^o-\sigma_y^o}{2}\left(1+3\frac{R_w^4}{r4}\right)\cos 2\theta-\tau_{xy}^o\left(1+3\frac{R_w^4}{r4}\right)\sin 2\theta$$
$$-\frac{2\eta}{r2}\left(\frac{p_{f0}-p_w}{4\ln\left(\frac{R_0}{R_w}\right)}\left[\left(R_w^2-r^2\right)-2r^2\ln\left(\frac{r}{R_0}\right)-2R_w^2\ln\left(\frac{R_w}{R_0}\right)\right]\right)-p_w\frac{R_w^2}{r2} \quad (6)$$

Equations 5 and 6 indicate the stresses around the wellbore are related to in-situ stresses, wellbore and reservoir radius, pore pressure profile, elastic properties of rock and wellbore trajectory.

In the case of conventional reservoirs, uniaxial strain condition and constant vertical stress are commonly assumed to determine in situ stresses changes with depletion and where the stress path is defined as the following:

$$\frac{\Delta\sigma_H}{\Delta P}=\frac{\Delta\sigma_h}{\Delta P}=\beta\frac{1-2v}{1-v} \quad (7)$$

$$\frac{\Delta\sigma'_H}{\Delta P}=\frac{\Delta\sigma'_h}{\Delta P}=-\beta\frac{v}{1-v} \quad (8)$$

Since the Poisson's ratio is always less than 0.5, the total stress path based on equation 7, will be less than one for typical reservoirs. Therefore, the reservoir depletion is expected to be accompanied by linear reduction of both total horizontal stresses and hereby, the increase of the effective horizontal stress which has been confirmed by field observations in various conventional reservoirs worldwide (Zoback and Zinke 2002, Addis 1997, Teufel, Rhett, and Farrell 1991). However, for CSG reservoirs, methane desorption is generally associated with matrix shrinkage thus resulting in a unique stress path. Experimental studies have shown that the conventional stress path equations cannot explain the observed values in CSG, as the stress path values could be greater than one (Saurabh and Harpalani 2018, Espinoza et al. 2015a, Liu and Harpalani 2014, Mitra, Harpalani, and Liu 2012, Saurabh, Harpalani, and Singh 2016, Cui, Bustin, and Chikatamarla 2007). The horizontal stress change by depletion and methane desorption can be determined using a linear elasticity model developed by Shi and Durucan (2004):

$$\Delta\sigma_H=\Delta\sigma_h=\frac{1-2\upsilon}{1-\upsilon}\Delta p+\frac{E}{3(1-\upsilon)}\varepsilon_l\left(\frac{p}{p+p_\varepsilon}-\frac{p_{fo}}{p_{fo}+p_\varepsilon}\right) \quad (9)$$

New horizontal stresses from equation 9, are substituted into equation 3 to calculate the stress distribution near the CSG wellbore.

A failure criterion should be applied to evaluate coal failure and particle production by knowing stress values and coal strength properties. The Mogi-Coulomb criterion is used to analyse coal failure:

$$\tau_{mogi}=a+b\frac{\sigma_1+\sigma_3}{2}-\beta p_w$$
$$a=\frac{2\sqrt{2}\,C\cos\phi}{3},\ b=\frac{2\sqrt{2}\sin\phi}{3} \quad (10)$$
$$\tau_{oct}=\frac{1}{3}\sqrt{\left(\sigma_2-\sigma_3\right)^2+\left(\sigma_3-\sigma_1\right)^2+\left(\sigma_1-\sigma_2\right)^2}$$

Results and Discussion

Inputs

The stress distribution around the vertical and horizontal wellbores in MCM of Bowen Basin are evaluated for two scenarios of with and without matrix shrinkage effect. Table 1 shows the input parameters.

Table 1—Input parameters for stress distribution in MCM, Bowen Basin

Parameters	Symbol	Value	Reference
Vertical stress gradient	S_v (psi/ft)	1.014	(Alboub et al. 2013)
Maximum horizontal stress gradient	S_H (psi/ft)	0.959	(Alboub et al. 2013)
Minimum horizontal stress gradient	S_h (psi/ft)	0.817	(Alboub et al. 2013)
Pore pressure gradient	P_o (psi/ft)	0.45	(Alboub et al. 2013)
Depth	D (ft)	1758	(Alboub et al. 2013)
Cohesion	C (psi)	536.6	(Alboub et al. 2013)
Friction angle	ϕ(degree)	29.4	(Alboub et al. 2013)
Langmuir pressure	$P\varepsilon$ (psi)	885	(Connell et al. 2016)
Maximum swelling strain	ε_l	0.0138	(Connell et al. 2016)
Young's modulus	E (psi)	389000	(Alboub et al. 2013)
Poisson's ratio	ν	0.326	(Alboub et al. 2013)
Biot's coefficient	β	0.8	-
Wellbore radius	Rw (ft)	0.333	(Puspitasari et al. 2014)
Outer radius	Ro (ft)	333	-

Results

Figure 2 shows the stress path in MCM, Bowen Basin using input data in table 1 for both cases of with and without matrix shrinkage effect. Figure 2.a shows the conventional stress path, where the poromechanical effect is the only affecting parameter and the effect of matrix shrinkage is not considered. Thereby, the stress path factor is constant and equal to 0.41 regardless of the depletion level. Based on uniaxial strain condition and constant vertical stress, the overburden stress is assumed not to change with depletion. However, both total maximum and minimum horizontal stresses are decreasing by a constant rate. Figure 2.b illustrates the stress path, by including the methane desorption effect. As this figure shows, the matrix shrinkage effect will increase the stress path value with a nonlinear profile and it causes the stress path to change with depletion rather than being a constant value like conventional reservoirs.

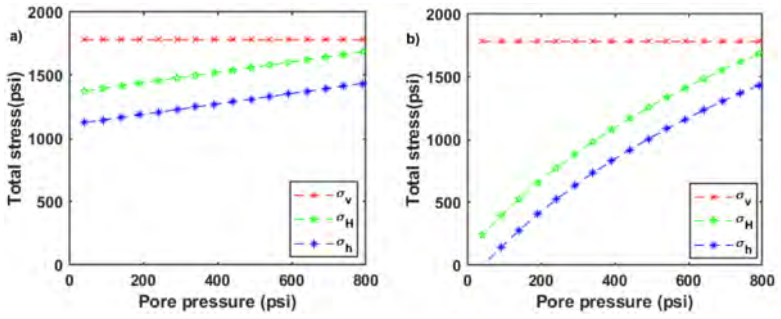

Figure 2—Total stress changes by depletion in MCM, Bowen Basin. a) Conventional stress path with no matrix shrinkage effect, b) Stress path with matrix shrinkage effect.

Equations 5 to 9 are used to evaluate the stress distribution near the vertical well for MCM. The poroelastic stress distribution for a vertical well at the initial stage of production with no depletion is shown in figure 3. The radial stress at the angular position of θ equal to 90° is the minimum where the tangential and axial stresses will reach their maximum value (maximum differential stress). The radial stress is the minimum on the wellbore wall, and it increases in the reservoir, whereas the tangential stress is decreasing from its peak on the wellbore toward the reservoir. The effect of depletion and matrix shrinkage on tangential and radial stresses at an angular position of θ equal to 90° is discussed here as the differential stress is at its maximum level and hence the highest possibility of coal failure.

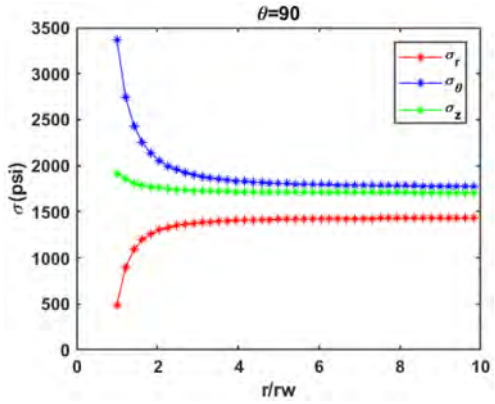

Figure 3—Stress distribution in a vertical well with no depletion in MCM, Bowen Basin.

Figure 4 shows the effect of matrix shrinkage on radial stress on the wellbore wall and the near-wellbore for a vertical well in MCM, Bowen Basin. The reservoir pressure reduces from its initial value (~800 psia) during production. The drawdown pressure of 300 psia was considered to evaluate all stresses in this section. Figure 4.a shows a constellation where the matrix shrinkage is not considered and a constant stress path is assumed, whereas in figure 4.b the stress distribution is shown by considering the matrix shrinkage's effect. In general, the radial stress in a vertical well will decrease during depletion which is consistent with the Masoudian and Hashemi (2016) study, however, the nonlinear stress path in coal seam gas results in more reduction of radial stress by depletion in the reservoir away from borehole wall and into the reservoirs (figure 4.b). Moreover, the radial stress values near the wellbore for both conventional and unconventional cases are almost the same and the matrix shrinkage does not significantly affect the radial stress near the vertical wellbore wall.

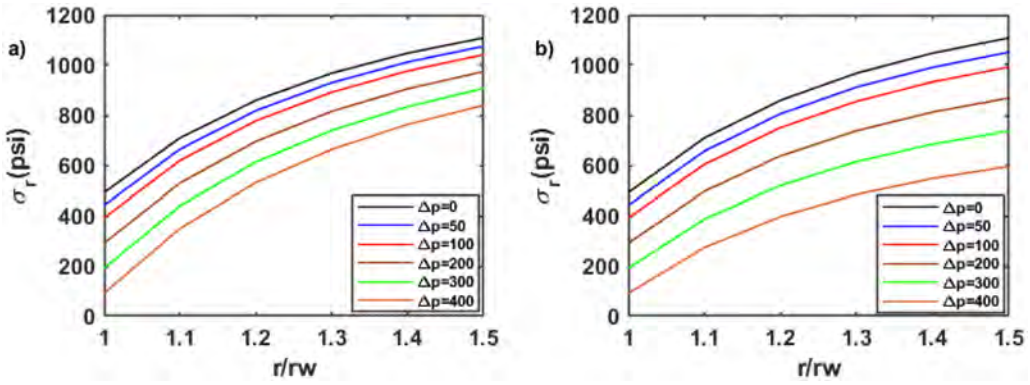

Figure 4—Radial stress distribution for a vertical well in MCM, a) near the wellbore wall and without the shrinkage effect, b) near the wellbore wall and with the shrinkage effect.

The tangential stress distribution near a vertical wellbore wall in MCM, Bowen Basin is shown in figure 5. The tangential stress in the conventional reservoir without the effect of matrix shrinkage does not change significantly during depletion (figure 5.a), while the matrix shrinkage effect and the resulting variable stress path cause a significant decrease of tangential stress (figure 5.b). Therefore, there will be less stress differential on a vertical well wall for a CSG reservoir where the shrinkage effect is considered. In this case, the matrix shrinkage lowers the risk of coal failure and assists the wellbore stability. This is consistent with the field operation observations in MCM, Bowen Basin by Puspitasari et al. (2014) and Alboub et al. (2013), where there is no serious coal failure in vertical wells, whereas the coal failure and solid production could be a concern for horizontal wells.

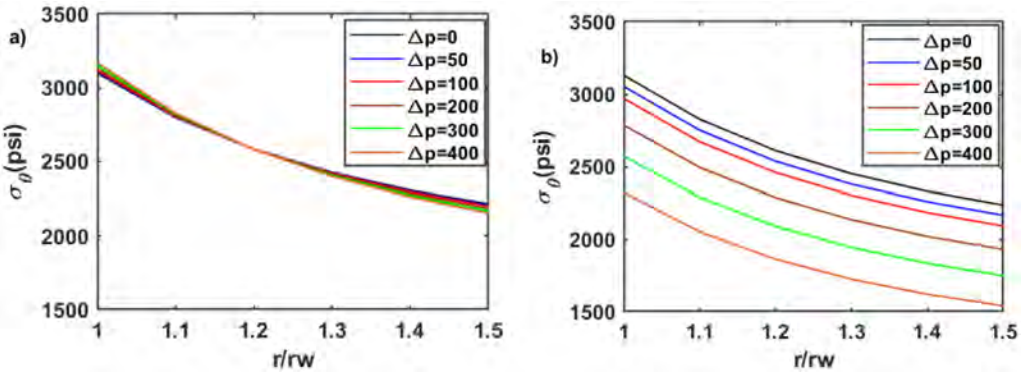

Figure 5—Tangential stress distribution for a vertical well in MCM, a) near the wellbore wall and without the shrinkage effect, b) near the wellbore wall and with the shrinkage effect.

The effect of matrix shrinkage on the stress distribution for horizontal wells is different from that in vertical wells. The radial stress distribution around a horizontal wellbore wall well in MCM, Bowen Basin is shown in figure 6. The radial stress similar to vertical wells is decreasing during production for both scenarios ie.with and without shrinkage (figure 4). It is clear from figure 6.b that matrix shrinkage will significantly reduce the radial stress around the wellbore wall.

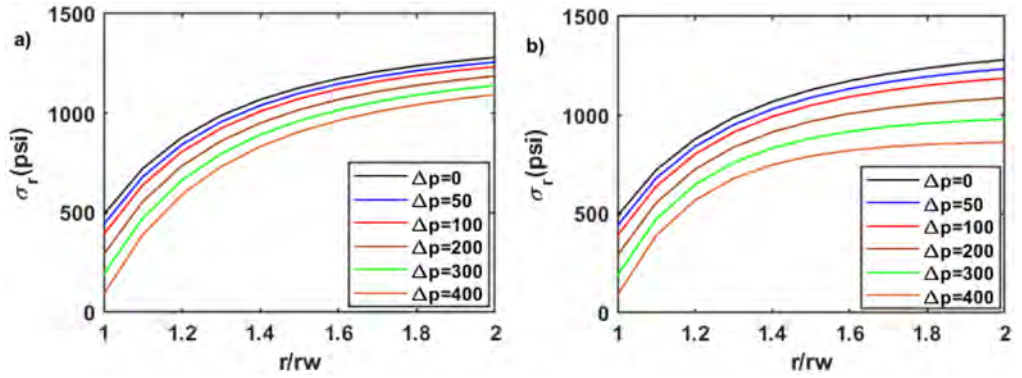

Figure 6—Radial stress distribution for a horizontal well in MCM, a) near the wellbore wall and without the shrinkage, b) near the wellbore wall and with the shrinkage effect.

The tangential stress changes during depletion for a horizontal well is different from a vertical wellbore. Figure 7.a and figure 7.b show the tangential stress changes around a horizontal wellbore wall considering matrix shrinkage and without shrinkage, respectively. The tangential stress during production will increase in both cases with and without matrix shrinkage. However, the matrix shrinkage causes more increase in the tangential stress in comparison with the conventional case. The increase of tangential stress and reduction of radial stress near the horizontal wellbore wall results in a higher deviatoric stress condition and hence a

higher risk of coal failure with depletion. In comparison with the vertical wellbores, where the shrinkage effect postpones the coal failure, in a horizontal wellbore, the matrix shrinkage will increase the likelihood of failure.

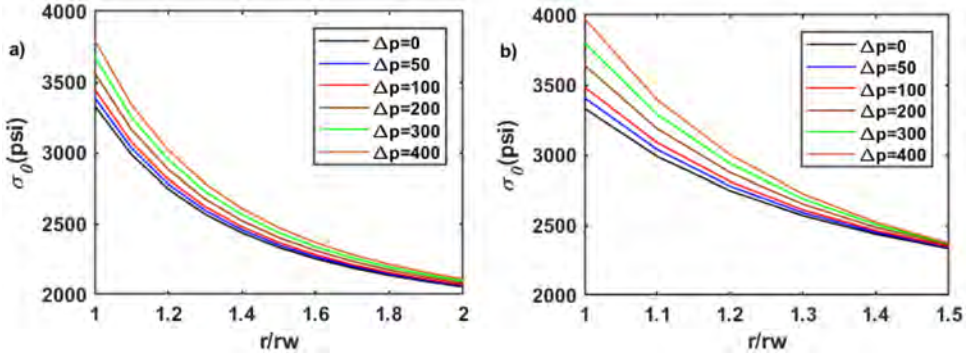

Figure 7—Tangential stress distribution for a horizontal well in MCM, a) near the wellbore wall and without the shrinkage, b) near the wellbore wall and with the shrinkage effect.

Application

The radial and tangential stresses acting on the wellbore wall, and the Mogi-Coulomb failure criterion are utilized to calculate the Maximum Coal Free Drawdown Pressure (MCFDP). Figure 8 shows the coal failure analysis for both condition of the conventional case without the matrix shrinkage effect and with the matrix shrinkage effect in MCM, Bowen Basin for different well inclinations. The figure indicates that for a normal faulting stress regime, in a vertical wellbore, considering the resultant matrix shrinkage after 300 psi depletion from its original reservoir pressure decreases the risk of wellbore instability and increases the MCFDP from 250 psi to 430 psi. It is concluded that in a vertical well, the matrix shrinkage effect will lower the coal failure risks during production. However, for highly deviated or horizontal wells, the effect of matrix shrinkage is different. The matrix shrinkage could cause inevitable coal failure and coal production for a horizontal well by 300 psi depletion from the initial reservoir pressure. This result is consistent with coal failure and coal production problem in the recently drilled horizontal and multilateral wells in Bowen Basin (Puspitasari et al. 2014). It should be noted that modeling results shown in this paper are valid for a normal stress regime and the results could be different in different stress and pressure regimes.

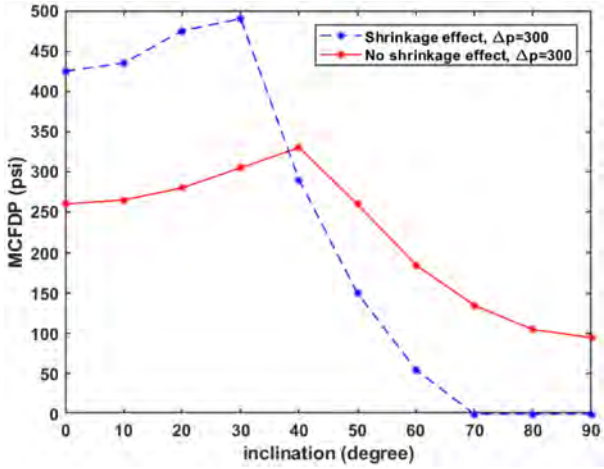

Figure 8—The effect of matrix shrinkage on coal failure for different inclinations.

Conclusions

An analytical model is developed to investigate the impact of matrix shrinkage on stress distribution around the vertical and horizontal CSG wells during primary production in Bowen Basin. It is concluded that the matrix shrinkage effect will increase the stress path value and it causes the stress path to change with depletion rather than being a constant value like conventional reservoirs.

It is concluded that for a vertical wellbore the radial stress will decrease with depletion, however, the matrix shrinkage effect and consequent nonlinear stress path results in more reduction of radial stress. The tangential stress around the vertical wellbore wall without considering the shrinkage effect will slightly increase during depletion. Conversely, the matrix shrinkage effect will cause the reduction of tangential stress on the wellbore wall. There will be less stress differential on a vertical well wall for CSG reservoir with shrinkage than the case without matrix shrinkage. It is concluded that matrix shrinkage and variable stress path could help the stability of vertical wells with depletion.

In a horizontal well, the radial stress on the wellbore wall always decreases during production irrespective of matrix shrinkage; however, the reduction of radial stress is more significant if the matrix shrinkage effect is considered. Considering the near-wellbore wall stress indicates that the matrix shrinkage will cause an increase of the tangential stress (unlike the vertical wellbore). The increase of tangential stress and reduction of radial stress near the CSG horizontal wellbore wall results in more deviatoric stress and hence higher risk of coal failure, i.e. wellbore instability and reduction of coal-free drawdown pressures.

Nomenclature

σ_r	*Radial stress*
σ_θ	*Tangential stress*
R_0	*Reservoir radius*
R_w	*Wellbore radius*
r	*Radius from the wellbore*
P_{f0}	*Initial reservoir pressure*
P_w	*Wellbore pressure*
P	*Current reservoir pressure*
θ	*Angular position around the wellbore*
σ_H	*Total maximum horizontal stress*
σ_h	*Total minimum horizontal stress*
σ_v	*Total vertical stress*
σ'_H	*Effective maximum horizontal stress*
σ'_h	*Effective minimum horizontal stress*
i	*Wellbore inclination*
α	*Wellbore azimuth*
β	*Biot's coefficient*
υ	*Poisson's ratio*
E	*Modulus of elasticity*
ϕ	*Internal friction angle*
C	*Cohesion*
ε_l	*Maximum swelling strain*
P_ε	*Langmuir pressure*

References

Addis, M. A. 1997. The Stress-Depletion Response Of Reservoirs. Proc., SPE Annual Technical Conference and Exhibition, San Antonio, Texas, 11.

Alboub, Mohamed, Michael Scott, Zachariah John Pallikathekathilet al.. 2013. Calibrated Mechanical Earth Models Answer Questions on Hydraulic Fracture Containment and Wellbore Stability in Some of the CSG Wells in the Bowen Basin. Proc., SPE Unconventional Resources Conference and Exhibition-Asia Pacific, Brisbane, Australia.

Behnoud far, Pouria, Amir Hossein Hassani, Adel M. Al-Ajmiet al.. 2016. A novel model for wellbore stability analysis during reservoir depletion. *Journal of Natural Gas Science and Engineering* **35**: 935–943.

Connell, Luke D., S. Mazumder, Regina Sanderet al.. 2016. Laboratory characterisation of coal matrix shrinkage, cleat compressibility and the geomechanical properties determining reservoir permeability. *Fuel* **165**: 499–512. http://www.sciencedirect.com/science/article/pii/S0016236115010601.

Cui, Xiaojun, R. Marc Bustin, Laxmi Chikatamarla. 2007. Adsorption-induced coal swelling and stress: Implications for methane production and acid gas sequestration into coal seams. *Journal of Geophysical Research: Solid Earth* **112** (B10). 10.1029/2004JB003482.

Davison, J. M., I. Foo, F. Elliset al.. 2016. The In-Situ Stress Response of Reservoirs to Pressure Reduction Followed by Pressure Increase: Depletion and Rebound Stress Paths from Two Case Studies. Proc., 50th U.S. Rock Mechanics/Geomechanics Symposium, Houston, Texas, 8.

Espinoza, D. N., J. M. Pereira, M. Vandammeet al.. 2015a. Desorption-induced shear failure of coal bed seams during gas depletion. *International Journal of Coal Geology* **137**: 142–151.

Espinoza, D. N., J. M. Pereira, M. Vandammeet al.. 2015b. Stress Path of Coal Seams During Depletion: The Effect of Desorption on Coal Failure. Proc., 49th U.S. Rock Mechanics/Geomechanics Symposium, San Francisco, California, 6.

Fjær, E., R. M. Holt, P. Horsrudet al.. 2008. Chapter 4 Stresses around boreholes. Borehole failure criteria. *In Petroleum Related Rock Mechanics*, ed. E. Fjær, R. M. Holt, P.Horsrud, A. M. Raaen and R. Risnes, 135–174. Elsevier.

GA, BREE. 2012. Australian gas resource assessment, Department of Resources, Energy and Tourism, Geoscience Australia and Bureau of Resources and Energy Economics, Canberra.

GA, BREE. 2014. Australian Energy Resource Assessment, Geoscience Australia, Canberra.

Li, Xiaorong, K. E. Gray. 2015. Wellbore Stability of Deviated Wells in Depleted Reservoir. Proc., SPE Annual Technical Conference and Exhibition, Houston, Texas, USA, 14.

Liu, Shimin, Satya Harpalani. 2014. Evaluation of in situ stress changes with gas depletion of coalbed methane reservoirs. *Journal of Geophysical Research: Solid Earth* **119** (8): 6263–6276.

Lu, Meng, Luke Connell. 2016. Coal failure during primary and enhanced coalbed methane production - Theory and approximate analyses. *International Journal of Coal Geology* **154-155**: 275–285.

Masoudian, Mohsen S., Mir Amid Hashemi. 2016. Analytical solution of a circular opening in an axisymmetric elastic-brittle-plastic swelling rock. *Journal of Natural Gas Science and Engineering* **35**: 483–496. http://www.sciencedirect.com/science/article/pii/S1875510016306370.

Mazumder, Saikat, Michael Scott, Jessica Jiang. 2012. Permeability increase in Bowen Basin coal as a result of matrix shrinkage during primary depletion. *International Journal of Coal Geology* **96-97**: 109–119. http://www.sciencedirect.com/science/article/pii/S0166516212000420.

Mitra, Abhijit, Satya Harpalani, Shimin Liu. 2012. Laboratory measurement and modeling of coal permeability with continued methane production: Part 1 - Laboratory results. *Fuel* **94**: 110–116. http://www.sciencedirect.com/science/article/pii/S0016236111006703.

Moore, Robert Lloyd, Debbie Fay Loftin, Ian D. Palmer. 2011. History Matching and Permeability Increases of Mature Coalbed Methane Wells in San Juan Basin. Proc., SPE Asia Pacific Oil and Gas Conference and Exhibition, Jakarta, Indonesia.

Pattison, C. I., C. R. Fielding, R. H. McWatterset al.. 1996. Nature and origin of fractures in Permian coals from the Bowen Basin, Queensland, Australia. *Geological Society, London, Special Publications* **109** (1): 133. https://sp.lyellcollection.org/content/109/1/133.abstract.

Puspitasari, Ratih, Thomas Gan, Zachariah John Pallikathekathilet al.. 2014. Wellbore Stability Modelling for Horizontal and Multi-Branch Lateral Wells in CBM: Practical Solution to Better Understand the Uncertainty in Rock Strength and Coal Heterogeneity. Proc., SPE Asia Pacific Oil & Gas Conference and Exhibition, Adelaide, Australia.

Rafieepour, Saeed, Stefan Z. Miska, Evren Ozbayogluet al.. 2017. Experimental Study of Reservoir Stress Path and Hysteresis during Depletion and Injection under Different Deformational Conditions. Proc., 51st U.S. Rock Mechanics/Geomechanics Symposium, San Francisco, California, USA.

Saurabh, S., S. Harpalani, V. K. Singh. 2016. Implications of stress re-distribution and rock failure with continued gas depletion in coalbed methane reservoirs. *International Journal of Coal Geology* **162**: 183–192.

Saurabh, Suman, Satya Harpalani. 2018. Stress path with depletion in coalbed methane reservoirs and stress based permeability modeling. *International Journal of Coal Geology* **185**: 12–22.

Shi, J. Q., S. Durucan. 2004. Drawdown Induced Changes in Permeability of Coalbeds: A New Interpretation of the Reservoir Response to Primary Recovery. *Transport in Porous Media* **56** (1): 1–16. 10.1023/B:TIPM.0000018398.19928.5a.

Swindon, V. G., P.S. Moore. 1989. EXPLORATION AND PRODUCTION IN THE EROMANGA BASIN, *CENTRAL AUSTRALIA Petroleum Resources of China and Related Subjects* **10**: 639–656.

Teufel, Lawrence W., Douglas W. Rhett, Helen E. Farrell. 1991. Effect of Reservoir Depletion And Pore Pressure Drawdown On In Situ Stress And Deformation In the Ekofisk Field, North Sea. Proc., The 32nd U.S. Symposium on Rock Mechanics (USRMS), Norman, Oklahoma, 10.

Yang, Yong, Shuqing Cui, Yuanyong Niet al.. 2014. A new attempt of a CBM tree-like horizontal well: A pilot case of Well ZS 1P-5H in the Qinshui Basin. *Natural Gas Industry B* **1** (2): 205–209. http://www.sciencedirect.com/science/article/pii/S2352854014000308.

Zare-Reisabadi, M. R., A. Kaffash, S. R. Shadizadeh. 2012. Determination of optimal well trajectory during drilling and production based on borehole stability. *International Journal of Rock Mechanics and Mining Sciences* **56**: 77–87. http://www.sciencedirect.com/science/article/pii/S1365160912001554.

Zare, M. R., S. R. Shadizadeh, B. Habibnia. 2010. Mechanical Stability Analysis of Directional Wells: A Case Study in Ahwaz Oilfield. Proc., Nigeria Annual International Conference and Exhibition, Tinapa - Calabar, Nigeria, 10.

Zoback, M. D., J. C. Zinke. 2002. Production-induced Normal Faulting in the Valhall and Ekofisk Oil Fields. *pure and applied geophysics* **159** (1): 403–420. 10.1007/PL00001258.

5 Stress distribution and permeability modelling in coalbed methane reservoirs by considering desorption radius expansion

5.1 Stress distribution and permeability modelling in coalbed methane reservoirs by considering desorption radius expansion

Zare Reisabadi M, Haghighi M, Sayyafzadeh M, Khaksar A., Fuel. 2021; 289:119951.

Statement of Authorship

Title of Paper	Stress distribution and permeability modelling in coalbed methane reservoirs by considering desorption radius expansion
Publication Status	☑ Published ☐ Accepted for Publication ☐ Submitted for Publication ☐ Unpublished and Unsubmitted w ork w ritten in manuscript style
Publication Details	Zare Reisabadi M, Haghighi M, Sayyafzadeh M, Khaksar A., Fuel. 2021; 289:119951.

Principal Author

Name of Principal Author (Candidate)	Mohammadreza Zare Reisabadi		
Contribution to the Paper	Literature review, Model development, Analysis of results, wiring the manuscript.		
Overall percentage (%)	80		
Certification:	This paper reports on original research I conducted during the period of my Higher Degree by Research candidature and is not subject to any obligations or contractual agreements with a third party that would constrain its inclusion in this thesis. I am the primary author of this paper.		
Signature		Date	09/03/2021

Co-Author Contributions

By signing the Statement of Authorship, each author certifies that:

i. the candidate's stated contribution to the publication is accurate (as detailed above);

ii. permission is granted for the candidate in include the publication in the thesis; and

iii. the sum of all co-author contributions is equal to 100% less the candidate's stated contribution.

Name of Co-Author	Manouchehr Haghighi		
Contribution to the Paper	Analytical model development, Support in analysis of results, Reviewing the manuscript		
Signature		Date	9/3/21

Name of Co-Author	Mohammad Sayyafzadeh		
Contribution to the Paper	Analytical model development, Support in analysis of results, Reviewing the manuscript		
Signature		Date	9/3/21

Name of Co-Author	Abbas Khaksar
Contribution to the Paper	Support in analysis of results
Signature	Date 15/3/2021

Fuel 289 (2021) 119951

Contents lists available at ScienceDirect

Fuel

journal homepage: www.elsevier.com/locate/fuel

Full Length Article

Stress distribution and permeability modelling in coalbed methane reservoirs by considering desorption radius expansion

Mohammadreza Zare Reisabadi [a,*], Manouchehr Haghighi [a], Mohammad Sayyafzadeh [a], Abbas Khaksar [b]

[a] Australian School of Petroleum, The University of Adelaide, Australia
[b] Baker Hughes, Australia

ARTICLE INFO

Keywords:
CBM reservoir
Desorption area
Analytical solution
Stress
Permeability modelling

ABSTRACT

Coal permeability is significantly stress-dependent and changes during gas production. In the previous studies, less attention has been paid to the impact of desorption radius and its expansion on the stress distribution and permeability changes. In this work, a mathematical model is developed to analytically evaluate the dynamic stress distribution and accordingly permeability by coupling the geomechanics, sorption and fluid flow in the cleat system. In this approach, the coalbed is divided into two regions: desorption area and non-desorption area. The desorption area represents the region with a low water–gas ratio, where the pressure squared (P^2) approach is applied for flow modelling. The non-desorption area represents the region with a high water–gas ratio with almost no desorption effect, where Darcy's equation (P approach) is used for flow modelling.

The results indicate that previous models, in which either uniform desorption or no desorption was assumed, cannot reflect the correct stress distribution in coalbed and accordingly overestimate or underestimate permeability, respectively. This is attributed to neglecting the varying desorption radius. The results demonstrate that this has a significant effect on stress distribution. The proposed model gives a more realistic evaluation of stress distribution and permeability as it only considers the effect of matrix shrinkage in the desorption area.

1. Introduction

Coal seam gas (CSG) reservoirs are considered as unconventional resources because of their unique characteristics. Unlike the conventional reservoirs in which gas is stored in the rock porosity, methane is mainly adsorbed on the internal surface of the coal matrix by adsorption mechanism. The gas production mechanism and performance from CSG is significantly different from conventional resources [11,22,24].

Depressurizing by water production is a pre-requisite to reduce the cleat pressure to a critical desorption pressure for commercial gas production from CSG reservoirs. During the methane production, coal matrix shrinks. The matrix shrinkage impacts the stress distribution and changes the tangential, axial and radial stresses distribution around the producing wells and within the coal seam layer [3,5,27,29].

In the stress-sensitive unconventional reservoirs such as CSG, permeability changes dynamically throughout the life of the reservoir, depending on the stress distribution around the well and within the reservoir. There exists a large number of experimental and theoretical studies that have evaluated the coal permeability by including the effective stress and matrix shrinkage effect [1,11,12,17,18,20,26]. In these models, the effective stress is not estimated as a function of distance from the wellbore, and therefore the permeability only changes by time not by the distance from the wellbore.

Several studies have developed analytical models to evaluate stress distribution in CSG [2,8,10,14,19,22,31,32]. Shi and Durucan [22] presented a model to evaluate the effective horizontal changes and permeability estimation in the field scale. Cui et al. [2] developed an analytical model for stress distribution around a vertical CSG well by considering the impacts of adsorption-induced swelling and applying different boundary conditions. Their study indicates the possibility of 10 times permeability enhancement around a CSG producing well due to matrix shrinkage and reservoir depletion. However, they did not consider the desorption radius and pressure squared approach for gas flow in the cleat. Masoudian and Hashemi [14] considered elastoplastic formation around an axisymmetric CSG vertical well to develop an analytical model for stress distribution. Zare Reisabadi et al. [30]

* Corresponding author.
E-mail address: mohammadreza.zarereisabadi@adelaide.edu.au (M. Zare Reisabadi).

https://doi.org/10.1016/j.fuel.2020.119951
Received 11 August 2020; Accepted 3 December 2020
Available online 21 December 2020

extended the previous models by considering the wellbore trajectory effect, matrix shrinkage, and different in situ stress regimes simultaneously. Their model enables stress distribution and coal failure analysis in the vertical, deviated, and horizontal wells.

These models neglect the effect of desorption radius. Dewatering and accordingly depressurizing during production result in the expansion of the desorption area outward. The significance of the desorption area has been presented in the literature and analytical models have been developed to evaluate desorption area expansion during production from CSG reservoirs [24,27]. Previously developed analytical models for stress distribution neglect the effect of desorption radius, and therefore the stress distribution as a result of the matrix shrinkage and depletion is explained by the same equation from the wellbore to the reservoir boundary, regardless of water–gas ratio. Additionally, in the previous stress models, the fluid flow was described by the same equation of pressure (P) approach for the entire area between the wellbore and reservoir boundary rather than the pressure squared (P^2) approach for gas flow in the desorption area.

In this paper, an analytical model is developed to evaluate stress distribution in two different zones, in which desorption and non-desorption areas and their corresponding pressure profile are considered proportionally. The permeability is then estimated based on the developed stress model, and it is compared with the previously developed models.

2. Problem description and assumptions

The production life of CSG reservoirs often consists of three stages, known as dewatering, stable production, and decline [15,27]. In the early stage of dewatering, since the Bottom-Hole Pressure (BHP) is higher than the critical desorption pressure, there is no desorption, and water is the dominant produced phase. This stage is recognized by a high Water-Gas Ratio (WGR) and almost no matrix shrinkage. The stress distribution for this stage is similar to the conventional reservoirs, and it widely has been discussed in the literature [6,9,28]. After a period of production, when the BHP drops below the critical desorption pressure, the gas desorption starts, and relative permeability to gas will start to increase causing WGR to be reduced from very high to a low value. This transition period is relatively short which has little influence on the pressure profile, and it can be neglected as discussed by Sun et al. [24]. However, continuing the production during the stable and decline stage (which are characterized by low WGR) results in the expansion of desorption radius from the wellbore towards the reservoir boundary.

To develop a stress distribution model for the stable and decline stage, the domain is split into two different regions, i.e., desorption area and non-desorption area as depicted in Fig. 1. Sun et al. [24] proposed this approach to estimate desorption area expansion during CSG production. Fig. 1 shows a wellbore under the in situ horizontal stress of σ_0 and the initial reservoir pressure of P_0 at the outer reservoir boundary (r_o). The wellbore is subjected to the BHP of P_w at r_w. The yellow region is characterized as the desorption area, where the pressure is below the critical desorption pressure and gas desorption takes place. Since WGR is very low in this region, the pressure squared approach is considered for pressure propagation (Eq. (22)), and there is a matrix shrinkage effect because of methane desorption. Desorption radius is characterized by r_{de}, where the reservoir pressure is equal to critical desorption pressure (P_{de}) and it will expand outward during production. The blue region between r_{de} to r_o includes the non-desorption area in which the reservoir pressure is higher than critical desorption pressure, and thus there is no gas desorption and matrix shrinkage. This area is considered as a high WGR area, and therefore a pressure approach for pressure propagation is used (Eq. (11)). It should be noted that for the simplicity of the problem, the two-phase transition flow due to capillary forces is not considered. In general, the following assumptions are made to simplify the problem:

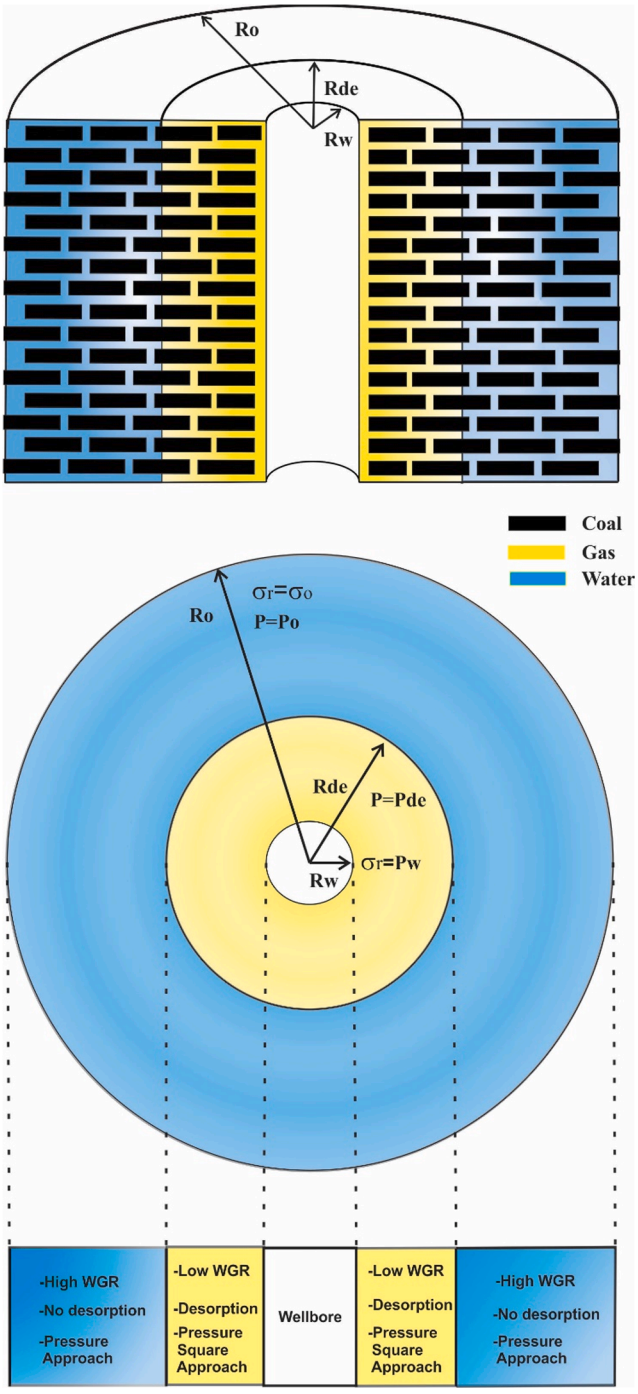

Fig. 1. Model geometry and boundary conditions.

1. The coal seam is isotropic, homogeneous, and the elastic properties remain constant during production.
2. There is a cylindrical reservoir with radial symmetry, and the wellbore is at its center.
3. The stress distribution near wellbores is a plane-strain problem.
4. Once the pressure drops below the critical desorption pressure because the WGR transits from high to low in the relatively very short period, the desorption area is assumed of low WGR and the non-desorption area is assumed of high WGR.

3. Mathematical model development

In this section, we present the derivation of an analytical model for

stress distribution around a CSG well and into the reservoir by considering the shrinkage effect and desorption radius. First, the solution in the non-desorption area is presented, and then the stress model in the desorption area is developed. Finally, we apply the boundary conditions to derive the equation constants.

3.1. Non-desorption area ($r_{de} \le r \le r_o$)

The effective stress (σ_{ij}) and strain (ε_{ij}) relation for the non-desorption area is described by Hooke's law as shown in Eq. (1):

$$\sigma_{ij}^{nd} = \frac{E}{1+\nu}\left(\varepsilon_{ij}^{nd} + \frac{\nu}{1-2\nu}\varepsilon_b^{nd}\delta_{ij}\right) + p^{nd}\delta_{ij} \tag{1}$$

Where superscript *nd* represents the non-desorption area, E is Young Modulus, ν is Poisson's Ratio, ε_b is the volumetric strain, δ is Kronecker's delta, and p^{nd} is pore pressure.

Considering a hollow cylinder wellbore and axisymmetric plane strain problem, the strain–displacement relations and corresponding equilibrium differential equation are given by:

$$\varepsilon_r^{nd} = \frac{\partial u^{nd}}{\partial r}, \qquad \varepsilon_\theta^{nd} = \frac{u^{nd}}{r}, \qquad \varepsilon_b^{nd} = \varepsilon_r^{nd} + \varepsilon_\theta^{nd} \tag{2}$$

$$\frac{d\sigma_r^{nd}}{dr} + \frac{\sigma_r^{nd} - \sigma_\theta^{nd}}{r} = 0 \tag{3}$$

Where u is the radial displacement, r is radial distance from the wellbore, and subscripts r and θ refer to the radial and tangential components, respectively.

Considering Eqs. (1) and (2), the elastic constitute between normal stress and strain becomes:

$$\sigma_r^{nd} = \frac{E}{1+\nu}\left(\frac{\partial u^{nd}}{\partial r} + \frac{\nu}{1-2\nu}\left(\frac{\partial u^{nd}}{\partial r} + \frac{u^{nd}}{r}\right)\right) + p^{nd} \tag{4}$$

$$\sigma_\theta^{nd} = \frac{E}{1+\nu}\left(\frac{u^{nd}}{r} + \frac{\nu}{1-2\nu}\left(\frac{\partial u^{nd}}{\partial r} + \frac{u^{nd}}{r}\right)\right) + p^{nd} \tag{5}$$

Substituting Eqs. (4) and (5) into Eq. (3) leads to:

$$\frac{\sigma_r^{nd} - \sigma_\theta^{nd}}{r} = \frac{E}{(1+\nu)r}\frac{\partial u^{nd}}{\partial r} - \frac{E}{(1+\nu)}\frac{u^{nd}}{r^2} \tag{6}$$

Replacing the stress in Eq. (6) with the radial displacement u using Eqs. (4) and (5) leads to:

$$\frac{\partial}{\partial r}\left(\frac{1}{r}\frac{\partial(ru^{nd})}{\partial r}\right) = -\frac{(1+\nu)(1-2\nu)}{E(1-\nu)}\frac{\partial p^{nd}}{\partial r} \tag{7}$$

And therefore the radial displacement equation becomes as follow:

$$u^{nd} = -\frac{(1+\nu)(1-2\nu)}{E(1-\nu)}\frac{F_p^{nd}}{r} + \frac{c_1 r}{2} + \frac{c_2}{r} \tag{8}$$

Where $F_p^{nd} = \int_{r_{de}}^{r} p^{nd} r dr$. The integration constants of C1 and C2 are determined by considering boundary conditions (section 3.3).

Radial and tangential stresses are derived by substituting Eq. (8) into the Eqs. (4) and (5):

$$\sigma_r^{nd} = \frac{1-2\nu}{1-\nu}\frac{F_p^{nd}}{r^2} + \frac{Ec_1}{2(1+\nu)(1-2\nu)} - \frac{Ec_2}{(1+\nu)r^2} \tag{9}$$

$$\sigma_\theta^{nd} = -\frac{1-2\nu}{1-\nu}\frac{F_p^{nd}}{r^2} + \frac{1-2\nu}{1-\nu}p^{nd} + \frac{Ec_1}{2(1+\nu)(1-2\nu)} + \frac{Ec_2}{(1+\nu)r^2} \tag{10}$$

As mentioned above, the pressure propagation in the non-desorption area with high WGR is described by the steady state flow and P approach as follows:

$$p^{nd} = p_o + \frac{p_{de} - p_o}{ln\left(\frac{r_{de}}{r_o}\right)} ln\left(\frac{r}{r_o}\right) \tag{11}$$

And therefore:

$$F_p^{nd} = \int_{r_{de}}^{r} p^{nd} r dr = -\frac{p_{de} - p_o}{ln\left(\frac{r_{de}}{r_o}\right)}\frac{r^2}{4} + p^{nd}\frac{r^2}{2} + \frac{p_{de} - p_o}{ln\left(\frac{r_{de}}{r_o}\right)}\frac{r_{de}^2}{4} - p_{de}\frac{r_{de}^2}{2} \tag{12}$$

3.2. Desorption area ($r \le r_{de}$)

The desorption region is the area between the wellbore wall and desorption radius where there are gas desorption and matrix shrinkage effect. The stress (σ_{ij}) strain (ε_{ij}) relation for this zone is described as:

$$\sigma_{ij}^{d} = \frac{E}{1+\nu}\left(\varepsilon_{ij}^{d} + \frac{\nu}{1-2\nu}\varepsilon_b^{d}\delta_{ij}\right) + p^{d}\delta_{ij} + k\varepsilon_v\delta_{ij} \tag{13}$$

Where superscript *d* represents desorption area, k is bulk modulus, and ε_v is the sorption-induced volumetric strain which is related to desorption properties as follow:

$$\varepsilon_v = \frac{\varepsilon_l p^d}{p^d + p_\varepsilon} \tag{14}$$

Where ε_l is Langmuir shrinkage strain, p_ε is Langmuir pressure.

Considering a hollow cylinder wellbore, axisymmetric plane strain, and the strain–displacement relations the elastic constitute between normal stress and strain in the desorption area becomes:

$$\sigma_r^{d} = \frac{E}{1+\nu}\left(\frac{\partial u^{d}}{\partial r} + \frac{\nu}{1-2\nu}\left(\frac{\partial u^{d}}{\partial r} + \frac{u^{d}}{r}\right)\right) + p^{d} + k\varepsilon_v \tag{15}$$

$$\sigma_\theta^{d} = \frac{E}{1+\nu}\left(\frac{u^{d}}{r} + \frac{\nu}{1-2\nu}\left(\frac{\partial u^{d}}{\partial r} + \frac{u^{d}}{r}\right)\right) + p^{d} + k\varepsilon_v \tag{16}$$

Substituting these equations into the equilibrium differential equation leads to:

$$\frac{\sigma_r^{d} - \sigma_\theta^{d}}{r} = \frac{E}{(1+\nu)r}\frac{\partial u^{d}}{\partial r} - \frac{E}{(1+\nu)r}\frac{u^{d}}{r} \tag{17}$$

Replacing the stresses in Eq. (17) with the radial displacement u leads to:

$$\frac{\partial}{\partial r}\left(\frac{1}{r}\frac{\partial(ru^{d})}{\partial r}\right) = -\frac{(1+\nu)(1-2\nu)}{E(1-\nu)}\frac{\partial p^{d}}{\partial r} - \frac{(1+\nu)}{3(1-\nu)}\frac{\partial \varepsilon_v}{\partial r} \tag{18}$$

And then after,

$$u^{d} = -\frac{(1+\nu)(1-2\nu)}{E(1-\nu)}\frac{F_p^{d}}{r} - \frac{(1+\nu)}{3(1-\nu)}\frac{F_s}{r} + \frac{c_3 r}{2} + \frac{c_4}{r} \tag{19}$$

Where $F_p^{d} = \int_{r_w}^{r} p^{d} r dr$ and $F_s = \int_{r_w}^{r} \varepsilon_v r dr$. The integration constants of C3 and C4 are determined by considering boundary conditions (section 3.3).

Radial and tangential stresses are derived by substituting Eq. (19) into Eqs. (15) and (16):

$$\sigma_r^{d} = \frac{1-2\nu}{1-\nu}\frac{F_p^{d}}{r^2} + \frac{E}{3(1-\nu)}\frac{F_s}{r^2} + \frac{Ec_3}{2(1+\nu)(1-2\nu)} - \frac{Ec_4}{(1+\nu)r^2} \tag{20}$$

$$\sigma_\theta^d = -\frac{1-2\nu}{1-\nu}\frac{F_p^d}{r^2} - \frac{E}{3(1-\nu)}\frac{F_s}{r^2} + \frac{1-2\nu}{1-\nu}p^d + \frac{E}{3(1-\nu)}\varepsilon_v + \frac{Ec_3}{2(1+\nu)(1-2\nu)} + \frac{Ec_4}{(1+\nu)r^2} \tag{21}$$

As the gas is the main flowing fluid in the desorption area, the pressure approach cannot explain the pressure propagation. The following pressure squared equation is used to describe the pressure profile in the desorption area [24,27]:

$$p^2 = p_w^2 + \frac{p_{de}^2 - p_w^2}{ln\left(\frac{r_{de}}{r_w}\right)} ln\left(\frac{r}{r_w}\right) \tag{22}$$

As a result,

$$F_p^d = \int_{r_w}^{r} p^d r dr = \frac{\sqrt{2\pi}bc^2 e^{-(2a)/b}\sqrt{-\frac{a+blog\left(\frac{r}{c}\right)}{b}}\left(erf\left(\sqrt{2}\sqrt{-\frac{a+blog\left(\frac{r}{c}\right)}{b}}\right) - 1\right) + 4r^2\left(a + blog\left(\frac{r}{c}\right)\right)}{8\sqrt{a+blog\left(\frac{r}{c}\right)}} - f_p^d(r_w) \tag{23}$$

$$a = p_w^2, \quad b = \frac{p_{de}^2 - p_w^2}{ln\left(\frac{r_{de}}{r_w}\right)}, \quad c = r_w$$

$$\text{And } F_s = \int_{r_w}^{r} \varepsilon_v r dr = \int_{r_w}^{r} \frac{\varepsilon_l p^d}{p^d + p_\varepsilon} r dr \tag{24}$$

F_s is related to the sorption-induced volumetric strain and will be solved numerically.

3.3. Boundary conditions

To determine σ_r and σ_θ, and integration constants C1-C4, the following four boundary conditions are applied. Radial stress at the wellbore wall is equal to BHP and its value reaches the horizontal stress at the outer boundary. These are the most commonly used boundary conditions to develop the stress distribution [6,10,13,14,16].

$$r = r_w, \quad \sigma_r^d = p_w; \qquad r = r_o, \quad \sigma_r^{nd} = \sigma_o \tag{25}$$

And at the desorption radius, the evaluated stresses by both non-desorption and desorption area equations should be the same,

$$r = r_{de}, \quad \sigma_r^{nd} = \sigma_r^d; \quad and \quad \sigma_\theta^{nd} = \sigma_\theta^d \tag{26}$$

Applying above boundary conditions to the Eqs. (9), (10), (20), and (21) leads the following values for integration constants:

$$c_1 = \frac{2(1+\nu)(1-2\nu)^2}{E(1-\nu)\left(r_w^2 - r_o^2\right)}\left(F_p^d(r_{de}) + F_p^{nd}(r_o)\right) + \frac{2(1+\nu)(1-2\nu)}{3(1-\nu)\left(r_w^2 - r_o^2\right)}F_s(r_{de}) + \frac{(1+\nu)(1-2\nu)\left(r_w^2 - r_{de}^2\right)}{3(1-\nu)\left(r_w^2 - r_o^2\right)}\varepsilon_{vde} + \frac{2(1-2\nu)(1+\nu)}{E\left(r_w^2 - r_o^2\right)}\left(r_w^2 p_w - r_o^2\sigma_o\right) \tag{27}$$

$$c_2 = \frac{(1+\nu)(1-2\nu)}{E(1-\nu)}F_p^{nd}(r_o) - \frac{(1+\nu)r_o^2}{E}\sigma_o + \frac{r_o^2}{2(1-2\nu)}c_1 \tag{28}$$

$$c_3 = c_1 - \frac{(1+\nu)(1-2\nu)}{3(1-\nu)}\varepsilon_{vde} \tag{29}$$

$$c_4 = \frac{r_w^2}{2(1-2\nu)}c_1 - \frac{(1+\nu)r_w^2}{6(1-\nu)}\varepsilon_{vde} - \frac{(1+\nu)r_w^2}{E}p_w \tag{30}$$

3.4. Permeability modelling

The estimated radial and tangential stresses from the developed model are used to evaluate the permeability distribution around the wellbore and within the reservoir. Assuming a bundled matchstick geometry, stress dependant coal permeability is given by [2,21,22]:

$$\frac{k}{k_0} = exp\left(-3c_f\Delta\sigma_h\right) \tag{31}$$

Where k_0 indicates the initial permeability, C_f is the cleat volume compressibility, and $\Delta\sigma_h$ is mean horizontal effective stress change and is given by

$$\Delta\sigma_h = (\sigma - p) - (\sigma_0 - p_0) \tag{32}$$

Where σ is the mean horizontal stress defined as $\sigma = (\sigma_r + \sigma_\theta)/2$.

Considering Eqs. (9), (10), (20), and (21), σ is given by following equations for no-desorption and desorption area respectively:

$$\sigma^{nd} = \frac{E}{2(1+\nu)(1-2\nu)}c_1 + \frac{1-2\nu}{2(1-\nu)}p^{nd} \tag{33}$$

$$\sigma^d = \frac{Ec_3}{2(1+\nu)(1-2\nu)} + \frac{(1-2\nu)}{2(1-\nu)}p^d + \frac{E}{6(1-\nu)}\varepsilon_v \tag{34}$$

Table 1
Input parameters for stress distribution analysis.

Parameters	Symbol	Value
In situ horizontal stress	σ_0 (psi)	1160
Initial reservoir pressure	P_o (psi/ft)	580
Langmuir pressure	Pε (psi)	261
Maximum swelling strain	ε_l	0.0092
Critical desorption pressure	P_{de} (psi)	508
Young's modulus	E (psi)	435,113
Poisson's ratio	ν	0.3
Wellbore pressure	P_w (psi)	140
Wellbore radius	Rw (ft)	0.328
Desorption radius	R_{de} (ft)	177
Outer radius	Ro (ft)	1010

Table 2
The input data for dynamic stress and permeability modelling.

Time of Production (days)	Boundary Pressure (psi)	BHP (psi)	Desorption Radius (ft)
150	580	160	127
200	580	140	177
250	565	120	226
300	536	100	275
500	522	72	472

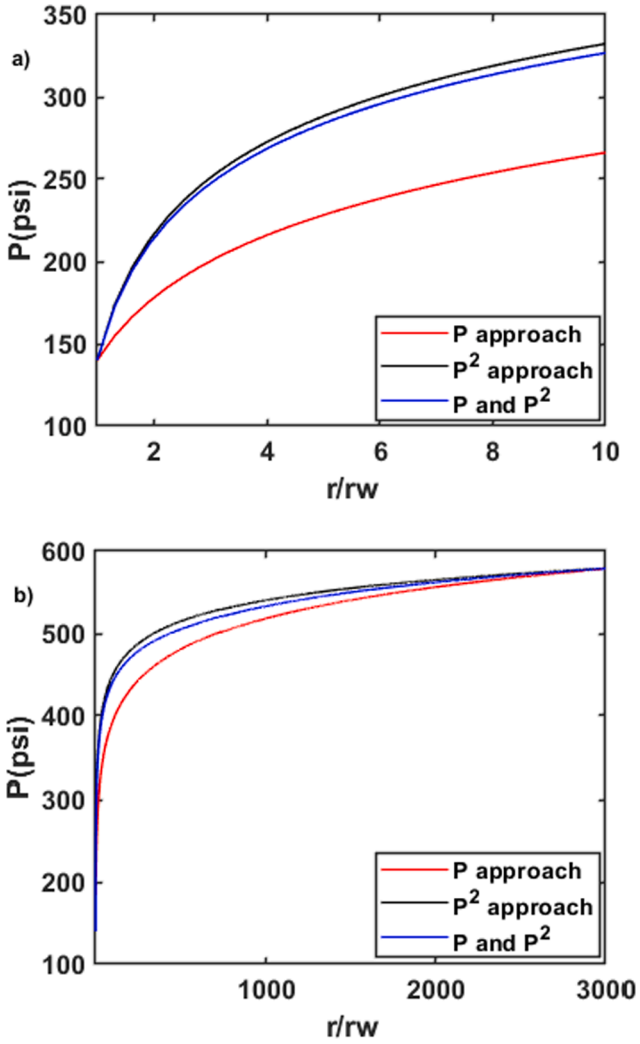

Fig. 2. Pressure distribution profile, a) near the wellbore, b) in the reservoir.

As Eq. (34) shows, the mean stress in the desorption area is closely coupled with reservoir pressure and associated matrix shrinkage effect and according to Eq. (33), it is only coupled with reservoir pressure in the non-desorption area.

4. Results and discussion

The values in Table 1 were used to present the practical application of the developed stress model and examine the permeability change around a CSG well and within the reservoir. Input values correspond to the desorption area expansion study by Sun et al. [24]. First, we compare the stress distribution results from the new model with previously developed models after 200 days of production when the desorption radius has reached 177 ft. later, desorption radius expansion in different time steps is considered to evaluate the dynamic stress and permeability

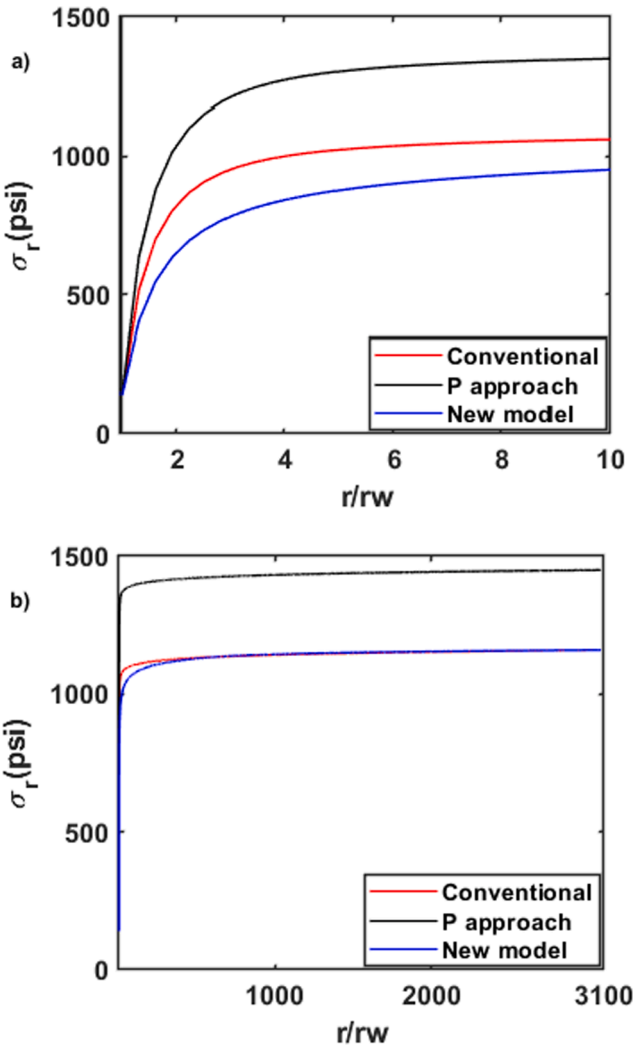

Fig. 3. Radial stress distribution, a) near the wellbore, b) in the reservoir.

changes during production (Table 2).

Fig. 2 compares the profile of different pressure approaches in the CSG reservoirs versus distance from the wellbore. P approach indicates the pressure profile estimated by Eq. (11) for the entire domain from the wellbore to the reservoir boundary, and the P^2 approach shows the pressure propagation calculated by Eq. (22). The blue line curve represents the pressure profile in this study, where the gas is dominant in the desorption area (Eq. (11)) and water is the main flowing fluid in the non-desorption area (Eq. (22)). As Fig. 2 indicates, there is a considerable difference between the diverse pressure profiles. Previously developed models by Cui et al. [2] and Huang et al. [8] considered P approach for the entire domain.

To present the practical application of the proposed model, Fig. 3 compares the radial stress distribution near the wellbore and within the reservoir by three different approaches versus distance from the wellbore wall. The conventional solution represents the stress distribution for a conventional reservoir where there is no matrix shrinkage effect (see Appendix A1). P approach indicates the stress distribution solution developed by Cui et al. [2] in a CSG reservoir, where the matrix shrinkage effect is considered for the entire domain, and the pressure approach is assumed for pressure distribution (Solution is presented in Appendix A2). The results indicate the radial stress increases from the wellbore to the reservoir boundary for all three different approaches. Fig. 3 demonstrates that the P approach model by Cui et al. [2] overestimates the effect of matrix shrinkage and results in a higher value of

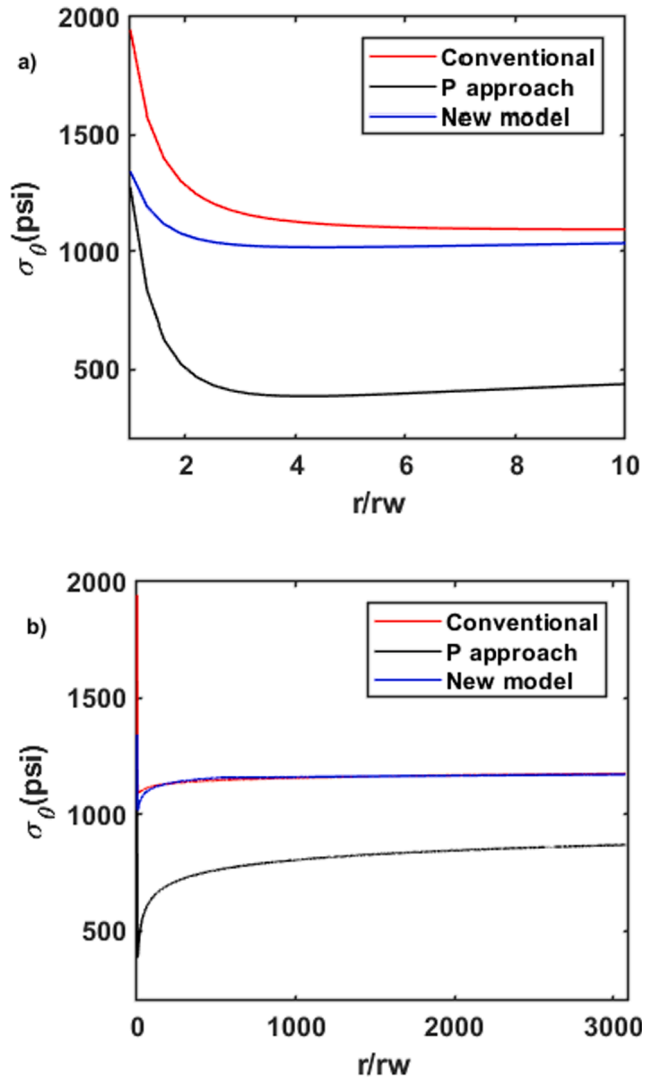

Fig. 4. Tangential stress distribution, a) near the wellbore, b) in the reservoir.

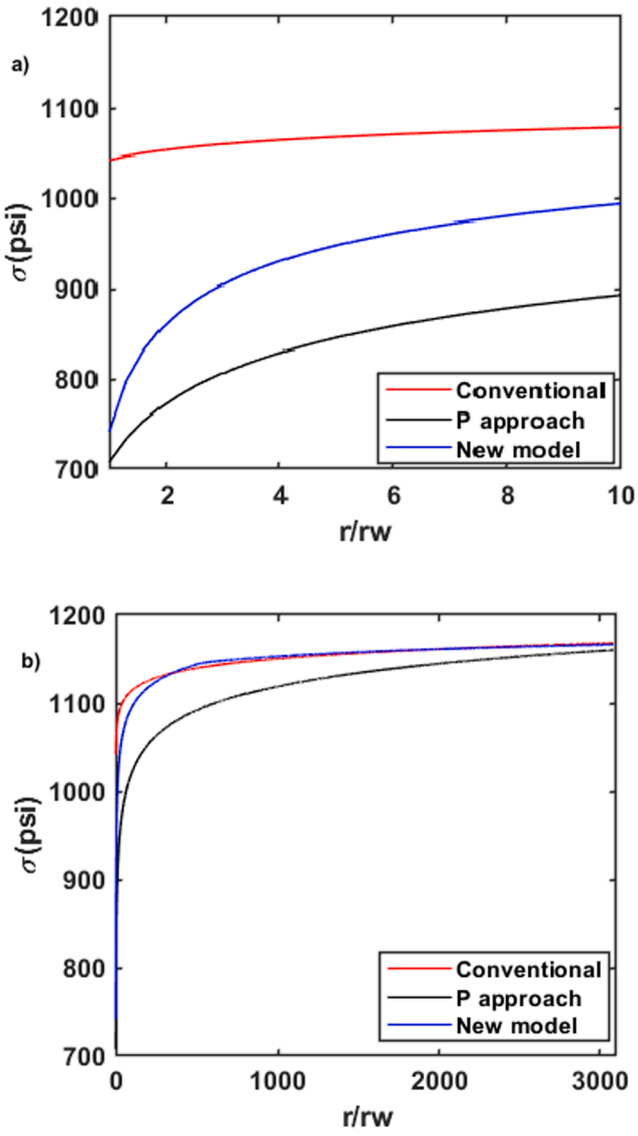

Fig. 5. Mean stress distribution, a) near the wellbore, b) in the reservoir.

radial stress. As the conventional model and newly developed model used the same boundary conditions at the outer boundary, the value of radial stress approaches to the horizontal stress at the outer radius for these two models. However, in the P approach, Cui et al. [2] considered different boundary conditions of the mean horizontal stress equal to the initial horizontal stress at the reservoir radius.

The tangential stresses near the wellbore and within the reservoir are depicted in Fig. 4a and b, respectively. As Eq. (21) indicates, the introduction of the matrix shrinkage in the desorption area produces a negative stress component which reduces the tangential stress values (blue line) in comparison with the conventional case (red line). It should be noted that because the P approach (dark line) considers the matrix shrinkage for the entire domain within the reservoir then it overestimates its effect and results in a really low value of tangential stress. Fig. 4b indicates that in desorption area (r/rw less than 540) with matrix shrinkage effect, the new model results in less tangential stress compare to the conventional solution. However, beyond the desorption radius where there is no matrix shrinkage effect, the tangential stress values from the new model approach to the conventional solution results.

The mean horizontal stress value is a key parameter to evaluate the coal seam gas permeability (Eq. (31)). To highlight the application of the new model, Fig. 5 compares the evaluated mean horizontal stress distribution versus distance from the wellbore by three approaches, and it is used to estimate the permeability of CSG as shown in Fig. 6. The mean horizontal stress decreases towards the wellbore for all models and therefore the rock is under minimum compression near the wellbore. However, Fig. 5a indicates the conventional approach overestimates the mean horizontal stress value near the wellbore as it does not consider desorption-induced stress. In contrast, the P approach underestimates the mean stress value as desorption-induced stress is considered for the whole domain. Finally, the new model leads a more realistic evaluation of mean stress by including the desorption-induced stress effect only in the desorption area rather than the entire domain.

Fig. 6 compares the permeability changes versus distance from the wellbore by three different models, where the permeability ratio is the ratio of current permeability to its initial value. It should be noted that CSG permeability depends on two opposing phenomena: poromechanical effect and desorption/shrinkage effect. The poromechanical effect relates to the reduction in reservoir pressure which causes an increase in the effective stress, and consequent permeability reduction. On the other hand, pore pressure reduction leads to desorption, a decrease in effective stress, and matrix shrinkage. Consequently, the permeability increases as the width of cleat increases. Fig. 6a and b indicate in the case of the conventional model, the permeability decreases from its initial value at the reservoir boundary towards the wellbore. It is due to the fact that this model does not consider the matrix shrinkage and the

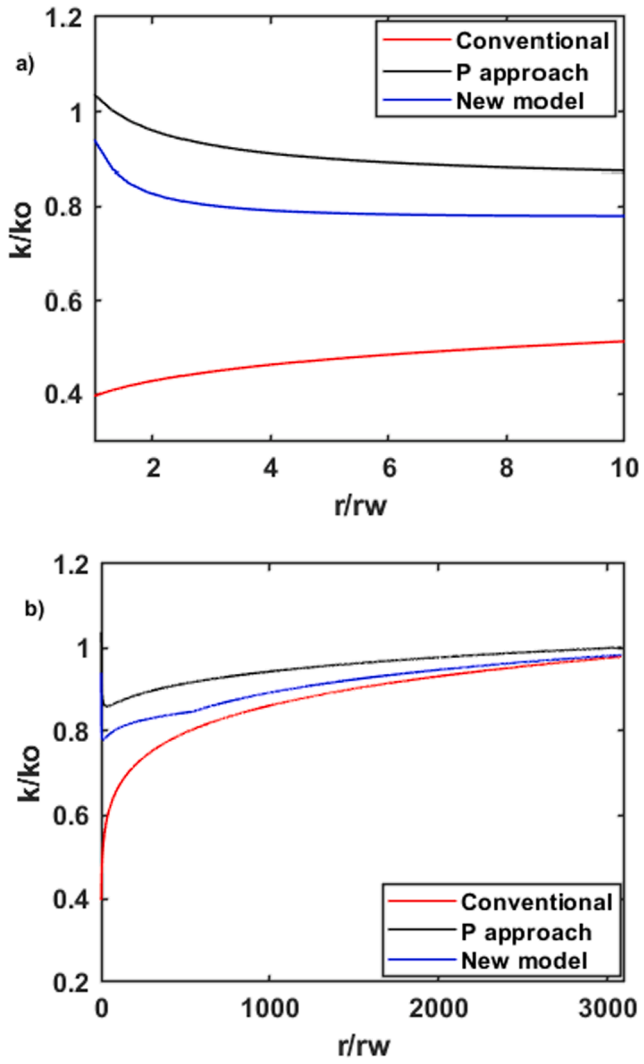

Fig. 6. Permeability distribution, a) near the wellbore, b) in the reservoir.

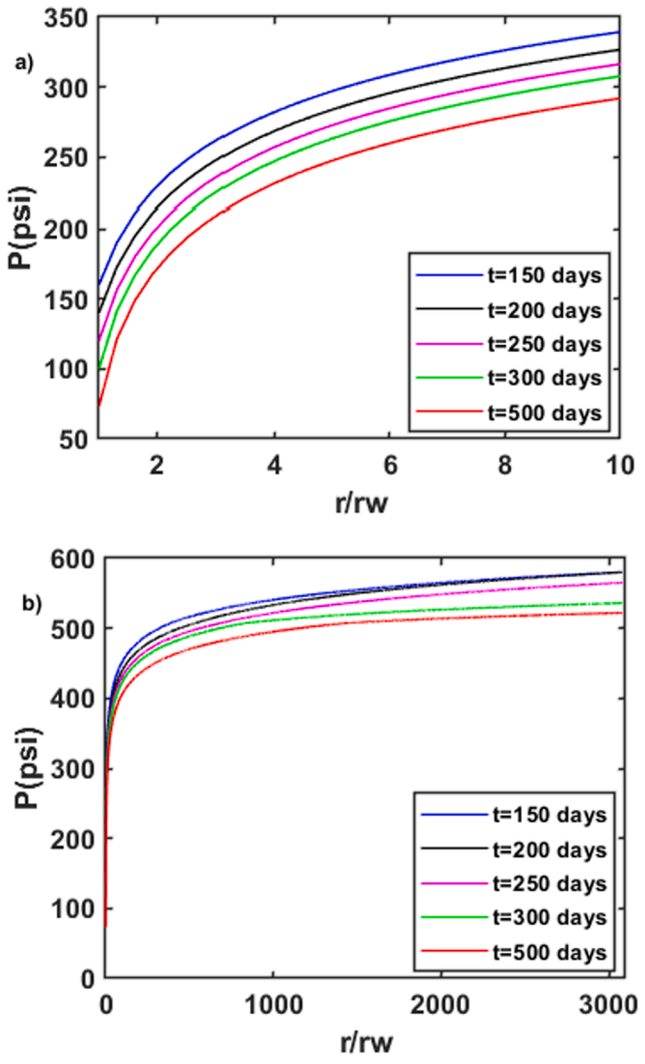

Fig. 7. Pressure distribution profile with time, a) near the wellbore, b) in the reservoir.

poromechanical effect is the only contributing parameter in the stress distribution. However, Fig. 6a shows the permeability increases around the wellbore by considering P approach and new models, as they consider both poromechanical and desorption effects. On the other hand, the P approach results in higher permeability values than the new model as it overestimates the desorption effect by ignoring the non-desorption area. Fig. 6b shows that the permeability distribution curve by the new model in desorption area (r/rw less than 540) is different from the non-desorption area. Comparing the conventional model (red curves) with the new model (blue curve) reveals that the matrix shrinkage effect in the desorption area, slowdowns the decline rate of permeability in the new model. Moreover, the new model results approach to the conventional model beyond the desorption radius as there is no matrix shrinkage effect.

To investigate the effect of production and desorption radius expansion on the stress changes and permeability distribution, the presented data in Table 2 mostly from Sun et al. [24] was used. The data from Table 1 was used for parameters that are constant during production such as initial stress value, elastic parameters, Langmuir parameters, wellbore, and reservoir radius. The value of Bottom Hole Pressure (BHP) is continuously decreasing and desorption radius is expanding.

Fig. 7 shows the pressure profile versus distance from the wellbore during production. The BHP is continuously reducing, and after 250 days of production, the boundary pressure decreases to 565 psi from its initial value of 580 psi. P^2 approach is applied for pressure profile within the desorption area, and P approach is utilized for the non-desorption area.

Fig. 8a and b illustrate the radial stress distribution at the different production times near the wellbore and within the reservoir, respectively. The radial stress decreases by production for both areas around the wellbore and within the reservoir and it approaches the initial horizontal stress at the reservoir boundary as the coal was subjected to the constant radial stress at the outer boundary.

The tangential stress profile during production near the wellbore and within the reservoir has been shown in Fig. 9a and b, respectively. It should be noted that the tangential stress profile versus distance will promptly change in the desorption area and beyond that in the non-desorption area, the change rate is slow. The tangential stress will decrease by production near the wellbore and in the desorption area but, it does not significantly change in the non-desorption area where there is no shrinkage effect. Moreover, the peak of the tangential stress (corresponds to desorption radius) illustrated in Fig. 9b progresses towards the reservoir boundary with production.

Stress-dependant permeability near the wellbore and within the reservoir during production are depicted in the Fig. 10a and b,

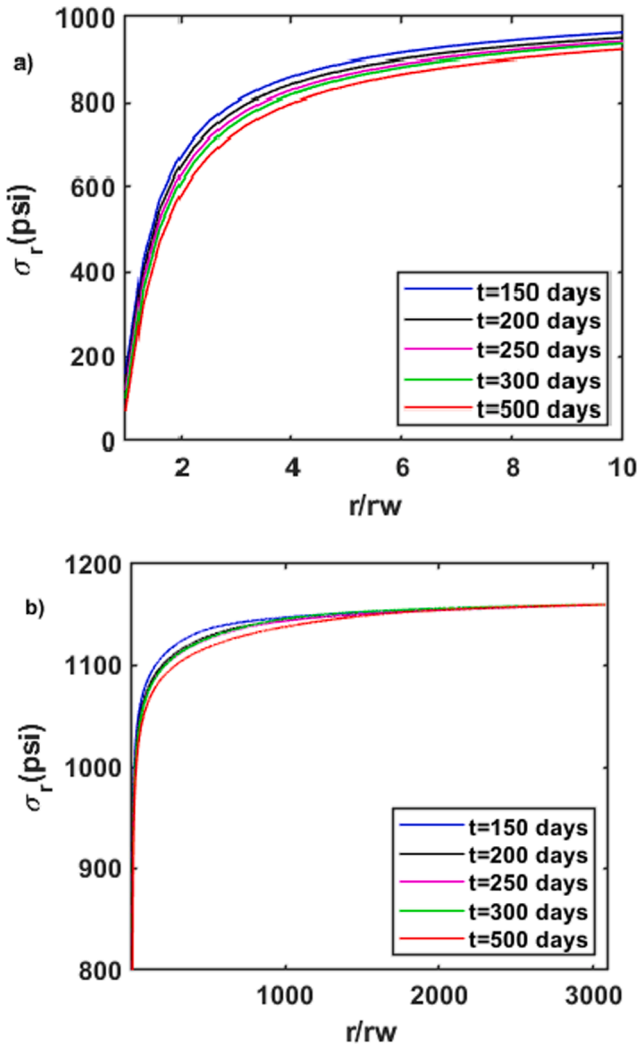

Fig. 8. Radial stress distribution with time, a) near the wellbore, b) in the reservoir.

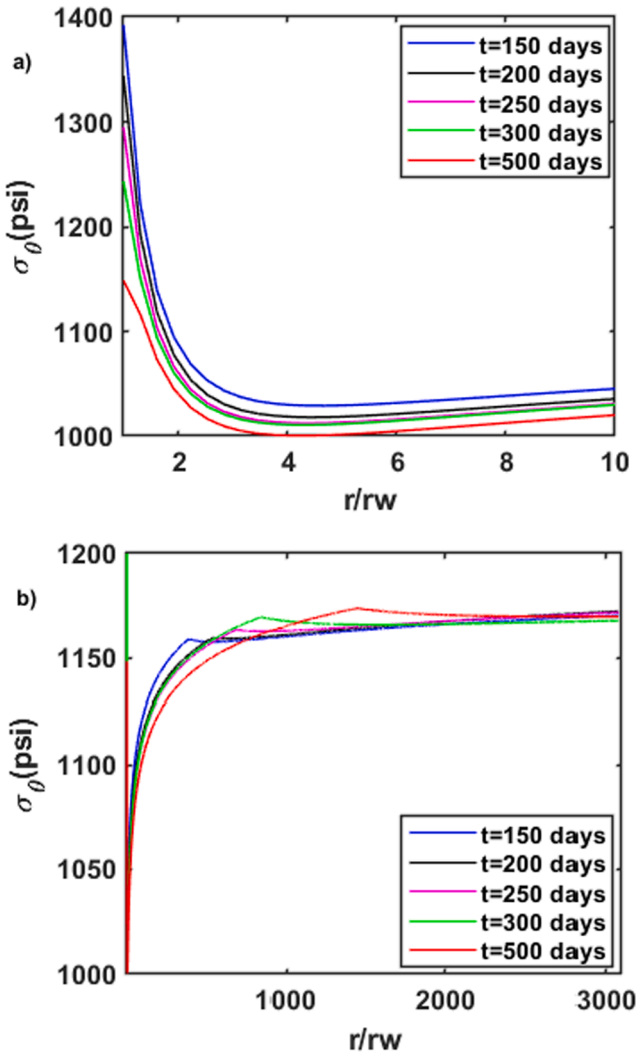

Fig. 9. Tangential stress distribution with time, a) near the wellbore, b) in the reservoir.

respectively. The permeability evolution is a dynamic process and its value depends on the distance from the wellbore and time. Fig. 10a indicates as the production continues, the permeability inside the desorption area and near the wellbore increases because the production results in more matrix shrinkage in the desorption area, and the shrinkage effect overcomes the poromechanical effect. The mean horizontal stress has its minimum value near the wellbore and therefore there is minimum compression in this area, which results in the maximum permeability value. There is no depletion until 250 days of production and the reservoir boundary pressure is equal to its initial pressure (Table 2) and that is why the permeability ratio even near the wellbore is less than one before 250 days of production. However, after 250 days of production, the reservoir boundary pressure declines to 565 psi from its initial value of 580 psi. Fig. 10a indicates after 250 days of production, the desorption effect overcomes the poromechanical effect, and consequently, the permeability ratio in the desorption area reaches more than one. The permeability in the desorption area increases 1.4 times after 500 days of production. On the other hand, Fig. 10b indicates that the permeability ratio in the non-desorption area is less than one even after 500 days of production as there is no desorption effect and the poromechanical effect is the only contributing process. Moreover, the permeability does not significantly change by production before 250 days of production in the non-desorption area and within the reservoir.

5. Limitations, and future work

To the best of authors' knowledge, there is no publically available measured stress value versus distance from the wellbore in CSG to validate the developed model results directly. However, it should be noted the applied concept of two different regions in CSG reservoirs (desorption area and non-desorption area) and desorption radius expansion solution have previously been validated by Sun et al. [24]. Moreover, the analytical solution for stress distribution in this study was derived from the fundamental constitutive equations which have widely applied in the literature.

The developed model does not consider the effect of anisotropy for simplicity and it also assumes the elastic parameters do not change during production. The anisotropy can affect the coal permeability [25], and the presented model can be improved by considering the anisotropy and executing laboratory measurements to develop the correlation for elastic parameters change during production. Besides, there is a possibility of rock failure around the CSG wells [4,23,30]. The effect of that on the stress distribution and permeability is not considered in this study. The boundary condition has a considerable effect on the stress distribution [7], and considering different boundary conditions could be valuable for future research. Moreover, CSG wells are usually stimulated with hydraulic fracturing which is ignored in this study and could be an interesting research area for further development.

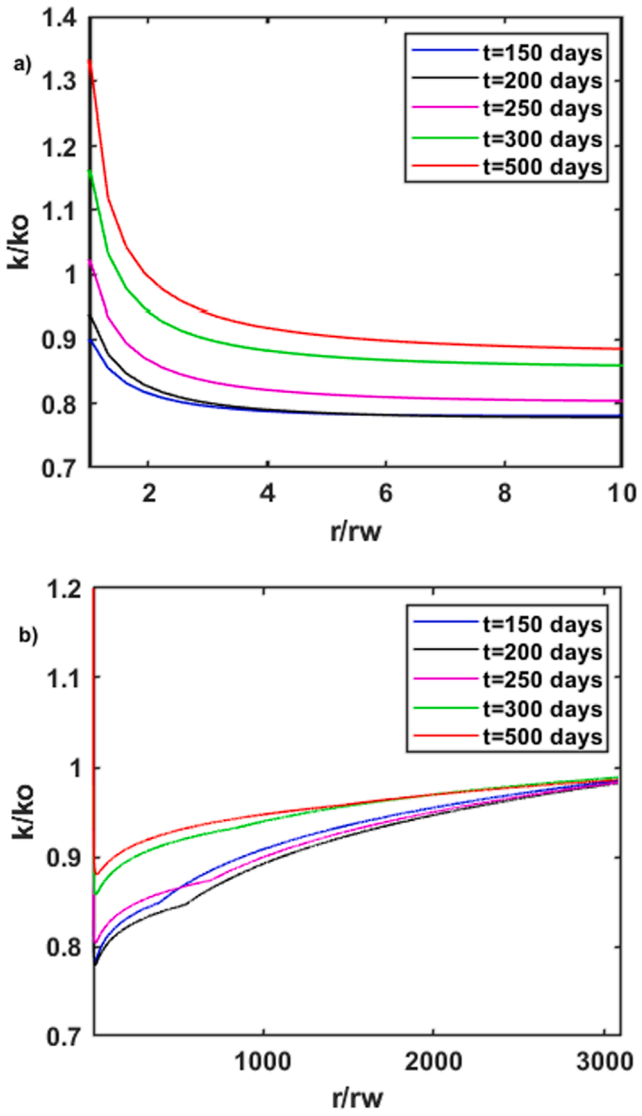

Fig. 10. Permeability distribution with time, a) near the wellbore, b) in the reservoir.

6. Conclusions

An analytical model was developed for stress distribution in CSG reservoirs. The model takes the desorption radius into the account, which divides the reservoir domain into two different regions of desorption area and non-desorption area. The developed model enables dynamic stress distribution during production by considering desorption radius expansion within the reservoirs. Based on results, it is concluded that none of the conventional or P approach models can reflect the correct stress distribution in CSG. The conventional model overestimates tangential and mean horizontal stress in the desorption area, whereas the P approach underestimates these stresses in the desorption area. However, considering the matrix shrinkage effect by the developed model in this study results in a reasonable tangential and mean horizontal stress.

The estimated radial, tangential, and mean horizontal stress distribution from the model were utilized to develop a dynamic permeability distribution model in CSG reservoirs. The proposed model results in a more realistic evaluation of permeability since it considers the effect of matrix shrinkage only in the desorption area. In addition, the proposed model concludes that the permeability has its maximum value near the wellbore where the mean horizontal stress is minimum. The permeability in the desorption area increases with time as the reservoir is depleting by time and desorption radius is expanding towards the reservoir boundary.

Declaration of Competing Interest

The authors declare that they have no known competing financial interests or personal relationships that could have appeared to influence the work reported in this paper.

Appendix A

A1. Conventional stress modelling

The following equations represent the stress modelling for conventional reservoirs where there is no matrix shrinkage effect:

$$\sigma_r = \frac{1-2\nu}{1-\nu}\frac{F_p}{r^2} + \frac{Ec_5}{2(1+\nu)(1-2\nu)} - \frac{Ec_6}{(1+\nu)r^2} \tag{35}$$

$$\sigma_\theta = -\frac{1-2\nu}{1-\nu}\frac{F_p}{r^2} + \frac{(1-2\nu)}{1-\nu}p + \frac{Ec_5}{2(1+\nu)(1-2\nu)} + \frac{Ec_6}{(1+\nu)r^2} \tag{36}$$

The integral constants are as following:

$$c_5 = \frac{2(1+\nu)(1-2\nu)}{E}\left(p_w + \frac{r_o^2}{(r_o^2-r_w^2)}(\sigma_o - p_w) - \frac{(1-2\nu)}{(1-\nu)(r_o^2-r_w^2)}\left(F_p(r_o) - F_p(r_w)\right)\right) \tag{37}$$

$$c_6 = \frac{(1+\nu)r_w^2 r_o^2}{E(r_o^2-r_w^2)}(\sigma_o - p_w) - \frac{(1+\nu)(1-2\nu)r_w^2}{E(1-\nu)(r_o^2-r_w^2)}\left(F_p(r_o) - F_p(r_w)\right) \tag{38}$$

And the P approach is considered as pressure distribution:

$$P = P_o + \frac{P_w - P_o}{ln\left(\frac{r_w}{r_o}\right)} ln\left(\frac{r}{r_o}\right) \tag{39}$$

$$F_p = \int prdr = -\frac{P_w - P_o}{ln\left(\frac{r_w}{r_o}\right)} \frac{r^2}{4} + P\frac{r^2}{2} \tag{40}$$

A2. P approach by Cui et al. [2]

The following equations represents the stress distribution in CSG reservoirs developed by Cui et al. [2] where the matrix shrinkage was considered for entire domain and the pressure distribution were described by P approach:

$$\sigma_r = \frac{(1-2\nu)}{(1-\nu)} \frac{F_p - F_p(r_w)}{r^2} + \frac{E}{3(1-\nu)} \frac{F_s - F_s(r_w)}{r^2} + \frac{Ec_1}{2(1+\nu)(1-2\nu)} - \frac{Ec_2}{(1+\nu)r^2} \tag{41}$$

$$\sigma_\theta = -\frac{1-2\nu}{1-\nu} \frac{F_p}{r^2} - \frac{E}{3(1-\nu)} \frac{F_s}{r^2} + \frac{1-2\nu}{1-\nu} p + \frac{E\varepsilon_v}{3(1-\nu)} + \frac{Ec_7}{2(1+\nu)(1-2\nu)} + \frac{Ec_8}{(1+\nu)r^2} \tag{42}$$

$$c_7 = \frac{2(1+\nu)(1-2\nu)}{E}\sigma_o - \frac{(1+\nu)(1-2\nu)^2}{E(1-\nu)}p_o - \frac{(1+\nu)(1-2\nu)}{3(1-\nu)}\varepsilon_{vo} \tag{43}$$

$$c_8 = \frac{(1+\nu)r_w^2}{E}(\sigma_o - p_w) - \frac{(1+\nu)(1-2\nu)r_w^2}{2E(1-\nu)}p_o - \frac{(1+\nu)r_w^2}{6(1-\nu)}\varepsilon_{vo} \tag{44}$$

$$P = P_o + \frac{P_w - P_o}{ln\left(\frac{r_w}{r_o}\right)} ln\left(\frac{r}{r_o}\right) \tag{45}$$

$$F_p = \int prdr = -\frac{P_w - P_o}{ln\left(\frac{r_w}{r_o}\right)} \frac{r^2}{4} + P\frac{r^2}{2} \tag{46}$$

$$F_s = \int \varepsilon_v rdr \tag{47}$$

$$\varepsilon_v = \frac{\varepsilon_l b_l p}{1 + b_l p} = \frac{\varepsilon_l p}{p + p_\varepsilon} \tag{48}$$

Appendix B. Supplementary data

Supplementary data to this article can be found online at https://doi.org/10.1016/j.fuel.2020.119951.

References

[1] Connell LD, et al. Laboratory characterisation of coal matrix shrinkage, cleat compressibility and the geomechanical properties determining reservoir permeability. Fuel 2016;165:499–512.
[2] Cui X, Bustin RM, Chikatamarla L. Adsorption-induced coal swelling and stress: Implications for methane production and acid gas sequestration into coal seams. J Geophys Res Solid Earth 2007;112(B10).
[3] Day S, Fry R, Sakurovs R. Swelling of Australian coals in supercritical CO2. Int J Coal Geol 2008;74(1):41–52.
[4] Espinoza DN, Pereira JM, Vandamme M, Dangla P, Vidal-Gilbert S. Desorption-induced shear failure of coal bed seams during gas depletion. Int J Coal Geol 2015; 137:142–51.
[5] Fan L, Liu S. Numerical prediction of in situ horizontal stress evolution in coalbed methane reservoirs by considering both poroelastic and sorption induced strain effects. Int J Rock Mech Min Sci 2018;104:156–64.
[6] Fjær E, Holt RM, Horsrud P, Raaen AM, Risnes R. Chapter 4 Stresses around boreholes. Borehole failure criteria. In: Fjær E, Holt RM, Horsrud P, Raaen AM, Risnes R, editors. Petroleum Related Rock Mechanics. Elsevier; 2008. p. 135–74.
[7] Han G, Dusseault MB. Description of fluid flow around a wellbore with stress-dependent porosity and permeability. J Petrol Sci Eng 2003;40(1):1–16.
[8] Huang F, Kang Y, Liu H, You L, Li X. Critical conditions for coal wellbore failure during primary coalbed methane recovery: a case study from the San Juan Basin. Rock Mechanics and Rock Engineering; 2019.
[9] Kaffash A, Zare-Reisabadi MR. Borehole stability evaluation in overbalanced and underbalanced drilling: based on 3D failure criteria. Geosyst Eng 2013;16(2): 175–82.
[10] Li Y, Cao S, Fantuzzi N, Liu Y. Elasto-plastic analysis of a circular borehole in elastic-strain softening coal seams. Int J Rock Mech Mining Sci $V 2015;80: 316–24.
[11] Liu S, Harpalani S. Permeability prediction of coalbed methane reservoirs during primary depletion. Int J Coal Geol 2013;113:1–10.
[12] Liu T, et al. Stress response during in-situ gas depletion and its impact on permeability and stability of CBM reservoir. Fuel 2020;266:117083.
[13] Lv A, Masoumi H, Walsh SDC, Roshan H. Elastic-softening-plasticity around a borehole: an analytical and experimental study. Rock Mechanics and Rock Engineering; 2018.
[14] Masoudian MS, Hashemi MA. Analytical solution of a circular opening in an axisymmetric elastic-brittle-plastic swelling rock. J Nat Gas Sci Eng 2016;35: 483–96.
[15] McKee CR, Bumb AC. Flow-testing coalbed methane production wells in the presence of water and gas. SPE-14447-PA 1987;2(04):599–608.
[16] Mimouna A, Prioul R. Closed-form approximations to borehole stresses for weak transverse isotropic elastic media. Int J Rock Mech Min Sci 2017;98:203–16.
[17] Mitra A, Harpalani S, Liu S. Laboratory measurement and modeling of coal permeability with continued methane production: Part 1 – Laboratory results. Fuel 2012;94:110–6.
[18] Palmer I. Permeability changes in coal: analytical modeling. Int J Coal Geol 2009; 77(1):119–26.

[19] Pan Z, Connell LD. Modelling permeability for coal reservoirs: a review of analytical models and testing data. Int J Coal Geol 2012;92:1–44.
[20] Saurabh S, Harpalani S. Stress path with depletion in coalbed methane reservoirs and stress based permeability modeling. Int J Coal Geol 2018;185:12–22.
[21] Seidle JP, Jeansonne MW, Erickson DJ. Application of matchstick geometry to stress dependent permeability in coals. SPE Rocky Mountain Regional Meeting: Society of Petroleum Engineers, Casper, Wyoming; 1992. p. 12.
[22] Shi JQ, Durucan S. Drawdown induced changes in permeability of coalbeds: a new interpretation of the reservoir response to primary recovery. Transp Porous Media 2004;56(1):1–16.
[23] Shovkun I, Espinoza DN. Coupled fluid flow-geomechanics simulation in stress-sensitive coal and shale reservoirs: Impact of desorption-induced stresses, shear failure, and fines migration. Fuel 2017;195:260–72.
[24] Sun Z, et al. A semi-analytical model for drainage and desorption area expansion during coal-bed methane production. Fuel 2017;204:214–26.
[25] Tan Y, et al. Experimental study of impact of anisotropy and heterogeneity on gas flow in coal. Part II: Permeability. Fuel 2018;230:397–409.
[26] Wu Y, Liu J, Elsworth D, Miao X, Mao X. Development of anisotropic permeability during coalbed methane production. J Nat Gas Sci Eng 2010;2(4):197–210.
[27] Xu B, et al. An analytical model for desorption area in coal-bed methane production wells. Fuel 2013;106:766–72.
[28] Zare-Reisabadi MR, Kaffash A, Shadizadeh SR. Determination of optimal well trajectory during drilling and production based on borehole stability. Int J Rock Mech Min Sci 2012;56:77–87.
[29] Zare Reisabadi M, Haghighi M, Khaksar A. Stress changes and coal failure analysis in coal seam gas wells accounting for matrix shrinkage: an example from Bowen Basin, East Australia. SPE/AAPG/SEG Asia Pacific Unconventional Resources Technology Conference. Unconventional Resources Technology Conference 2019: 11.
[30] Zare Reisabadi M, Haghighi M, Salmachi A, Sayyafzadeh M, Khaksar A. Analytical modelling of coal failure in coal seam gas reservoirs in different stress regimes. Int J Rock Mech Min Sci 2020;128:104259.
[31] Zare Reisabadi M, Haghighi M, Sayyafzadeh M, Khaksar A. Effect of matrix shrinkage on wellbore stresses in coal seam gas: an example from Bowen Basin, east Australia. J Nat Gas Sci Eng 2020;77:103280.
[32] Zhang L, Zhang S, Jiang W, Wang Z, Wang L. An analytical model of wellbore strengthening considering complex distribution of cleat system. J Nat Gas Sci Eng 2018;60:77–91.

6 Conclusions and recommendations

6.1 Conclusions

This thesis presents a comprehensive investigation on stress distribution near the CSG wells, coal failure, stress distribution within the reservoirs, and permeability variation for CSG reservoirs. New analytical models were developed and applied in the real case studies to predict/prevent coal failure and understand the effect of key parameters on permeability evolution. The following conclusions can be drawn from this study:

1. The matrix shrinkage effect in CSG reservoirs causes the greater values of stress path with depletion in comparison to the conventional reservoirs. The stress path values will increase by depletion and make the CSG reservoirs more susceptible to failure.
2. For a vertical well in a normal stress regime, the matrix shrinkage leads to more reduction of radial stress near the wellbore during depletion (compare to a well in the conventional reservoir). Moreover, the matrix shrinkage causes the reduction of tangential stress near the vertical wellbore wall (unlike the conventional reservoirs). Therefore, there will be less stress differential on the vertical wellbore wall for a CSG reservoir than a case without the matrix shrinkage.
3. In a horizontal well, the radial stress decreases during production irrespective of matrix shrinkage; however, the reduction of radial stress is more significant if the matrix shrinkage effect is considered. However, for a horizontal well, the matrix shrinkage will cause an increase of the near-wellbore wall tangential stress. The increase of tangential stress and reduction of radial stress near the CSG's horizontal wellbore wall results in more deviatoric stress compare to the conventional case.

4. In a vertical wellbore in the normal stress regime, the matrix shrinkage helps the stability of the wellbore during depletion. Conversely, for a horizontal wellbore or a highly deviated well, the matrix shrinkage will cause the reduction of MCFDP during depletion, hence a higher risk of coal failure.
5. It has been concluded that the wells in a strike-slip stress regime are more susceptible to failure compared to the normal fault regime. Moreover, horizontal and deviated wells are less prone to coal failure than vertical wells in strike-slip stress regimes. In this case, depletion could change the in situ stress regime from strike-slip to a normal stress regime. This stress change makes coal prone to failure.
6. In a reverse faulting stress regime, horizontal wells in direction of maximum horizontal stress are the most stable and least susceptible to coal failure at the early stage of production. However, with pressure depletion and the change of stress regime to normal fault regime, the optimum production trajectory will change, and deviated wells in minimum horizontal stress direction will be less susceptible to coal failure. In contrary to the normal fault stress regime, in a reverse fault regime, the influence of depletion on MCFDP for vertical wells is more than horizontal and highly deviated wellbores.
7. In terms of stress distribution within the CSG reservoir and permeability evolution, previous models, in which either uniform desorption or no desorption was assumed, cannot reflect the correct stress distribution in coalbed and accordingly overestimate or underestimate permeability, respectively.
8. A new analytical model was developed for stress distribution within the CSG reservoirs and permeability modelling. The model takes the desorption radius into the account, which divides the reservoir domain into two different regions of

desorption area and non-desorption area. The conventional model overestimates tangential and mean horizontal stress in the desorption area, whereas the P approach underestimates these stresses in the desorption area. However, considering the matrix shrinkage effect by the developed model in this study results in a reasonable tangential and mean horizontal stress.

9. The proposed model results in a more realistic evaluation of permeability since it considers the effect of matrix shrinkage only in the desorption area. In addition, the proposed model concludes that the permeability has its maximum value near the wellbore where the mean horizontal stress is minimum.
10. The permeability in the desorption area increases with time as the reservoir is depleting by time and the desorption radius is expanding towards the reservoir boundary.

6.2 Recommendations

Based on the understandings gained through this study, some suggestions are made for future work:

1. The proposed model in this study for stress distribution near the wellbore does not consider the effect of the cleat system on the stress path for simplicity, which is an important research topic for further investigation.
2. The developed model does not consider the effect of anisotropy for simplicity and it also assumes the elastic parameters do not change during production. The anisotropy can affect the coal permeability, and the presented model can be improved by considering the anisotropy and executing laboratory measurements to develop the correlation for elastic parameters change during production.
3. All the available stress path models in the literature assume that the stress changes of both maximum and minimum horizontal stresses are the same. However, as

coal is highly anisotropic, the stress path might be anisotropic as well. Therefore, True-Triaxial loading experiments will be recommended to execute on the cubic coal samples to apply different horizontal stresses which simulate the realistic subsurface conditions.

4. CSG wells are usually stimulated with hydraulic fracturing which is ignored in this study and could be an interesting research area for further development.

Appendix

1D mechanical earth model in a carbonate reservoir: implications for wellbore stability

Mohammadreza Zare Reisabadi, Mojtaba Rajabi, Arian Velayati, Yasser Pourmazaheri, Manouchehr Haghighi., AAPG Asia Pacific Region GTW, Pore Pressure & Geomechanics: From Exploration to Abandonment. Perth, Australia, June 6-7, 2018.

Statement of Authorship

Title of Paper	1D mechanical earth model in a carbonate reservoir: implications for wellbore stability
Publication Status	☑ Published ☐ Accepted for Publication ☐ Submitted for Publication ☐ Unpublished and Unsubmitted w ork w ritten in manuscript style
Publication Details	Mohammadreza Zare Reisabadi, Mojtaba Rajabi, Arian Velayati, Yasser Pourmazaheri, Manouchehr Haghighi., AAPG Asia Pacific Region GTW, Pore Pressure & Geomechanics: From Exploration to Abandonment. Perth, Australia, June 6-7, 2018.

Principal Author

Name of Principal Author (Candidate)	Mohammadreza Zare Reisabadi		
Contribution to the Paper	Literature review, Model construction, Analysis of results, wiring the manuscript.		
Overall percentage (%)	80		
Certification:	This paper reports on original research I conducted during the period of my Higher Degree by Research candidature and is not subject to any obligations or contractual agreements with a third party that would constrain its inclusion in this thesis. I am the primary author of this paper.		
Signature		Date	09/03/2021

Co-Author Contributions

By signing the Statement of Authorship, each author certifies that:

i. the candidate's stated contribution to the publication is accurate (as detailed above);

ii. permission is granted for the candidate in include the publication in the thesis; and

iii. the sum of all co-author contributions is equal to 100% less the candidate's stated contribution.

Name of Co-Author	Mojtaba Rajabi		
Contribution to the Paper	Reviewing the manuscript		
Signature		Date	16/03/2021

Name of Co-Author	Arian Velayati		
Contribution to the Paper	Experimental Lab work		
Signature		Date	17-03-21

Name of Co-Author	Yasser Pourmazaheri		
Contribution to the Paper	Experimental Lab work		
Signature		Date	11/03/21

Name of Co-Author	Manouchehr Haghighi		
Contribution to the Paper	Support in analysis of results		
Signature		Date	9/3/21

1D Mechanical Earth Model in a Carbonate Reservoir of the Abadan Plain, Southwestern Iran: Implications for Wellbore Stability*

Mohammadreza Zare Reisabadi[1], Mojtaba Rajabi[1], Manouchehr Haghighi[1], Arian Velayati[2], and Yasser Pourmazaheri[1]

Search and Discovery Article #42298 (2018)**
Posted October 15, 2018

*Adapted from extended abstract prepared in conjunction with poster presentation given at 2018 AAPG Asia Pacific Region GTW, Pore Pressure & Geomechanics: From Exploration to Abandonment, Perth, Australia, June 6-7, 2018
 DOI:10.1306/42298Reisabadi2018

[1]Australian School of Petroleum, University of Adelaide, Adelaide, Australia (mohammadreza.zarereisabadi@adelaide.edu.au)
[2]Research Institute of Petroleum Industry, Tehran, Iran

Abstract

Knowledge of the rock mechanical properties and stress tensor including orientation and magnitude of *in-situ* stresses has numerous implications in different aspects of petroleum exploration and production. In particular, these geomechanical parameters control fluid flow in naturally-fractured reservoirs, hydraulic fracture stimulation, wellbore stability, and reduce non-productive time in drilling operations. Knowledge of the *in-situ* stress state is particularly important in Iran, which has an extensive and mature petroleum exploration and production industry and is also prone to stress-related geohazards such as earthquakes. Yet, the 2016 release of the World Stress Map project contains very little *in-situ* stress information for Iran.

In this study, we present a comprehensive one-dimensional mechanical earth model in an appraisal well in a carbonate oil-bearing reservoir in southwestern Iran. Different rock mechanical tests including Brazilian, Uniaxial compressive strength, and tri-axial compressive tests are applied on the core samples to determine rock strength and elastic properties such as tensile strength, UCS, cohesion, friction angle, Young's modulus, and Poisson's ratio. These static rock mechanical properties then provide a reference to calibrate the well-log derived or dynamic rock mechanical properties. We use different sets of data such as pressure tests, leak off tests, borehole image log, and wireline data to estimate the continuous profile of vertical and horizontal stresses and pore pressure in different lithological layers of the studied well. Analysis of borehole breakouts and drilling induced tensile fractures suggest a NE-SW orientation for the maximum horizontal stress orientation which is consistent with deep earthquake focal mechanism solutions in the study area, derived from the World Stress Map database. The results also indicate normal (in some intervals strike-slip) tectonic stress regime which is different from deep earthquake focal mechanism solutions. The constructed 1-D MEM was calibrated by wellbore stability analysis of the current drilled well. The results indicated the unstable borehole in some intervals which was consistent with borehole image and caliper logs. Finally, we use the constructed 1D mechanical earth model in this study for sensitivity analysis of different wellbore trajectories and mud weight window for future well planning and safe drilling in this under-development oil field.

Geology and State of Stress in the Abadan Plain Basin

Abadan Plain Basin is located in the western Dezful Embayment, southwestern Iran. The basin is bounded by the Dezful Embayment in the north and the northeast; Persian Gulf–Mesopotamian foreland basin and Saudi Arabia in the southwest and south; and to Iraq in the west (Moallemi and Kermanshah, 2012). In comparison to the Dezful Embayment that mainly show NW–SE trend for anticlines and structural closure, the Abadan Plain contains N-S to NE-SW trend (i.e. Arabian trend based on Ahmadhadi et al. (2008).

To date, the World Stress Map-2016 database only contains three reliable stress orientations from petroleum wells in Iran (Heidbach et al., 2016; Rajabi et al., 2010), despite Iran has an extensive and mature petroleum exploration and production industry (Rajabi et al., 2014). Based on the information from two petroleum wells in the Abadan Plain, Rajabi et al. (2010) revealed that the orientation of maximum horizontal stress (S_{Hmax}) in this region is NE-SW (Figure 1). However, the other parameters of stress tensor, such as stress magnitudes and tectonic stress regime, are poorly understood in this region (Figure 1).

Methodology

Mechanical Earth Model is a quantitative representation of the *in-situ* stresses, pore pressure, rock strength properties, and rock elastic properties which usually constructed for a specific depth, well or field. It contains all required information for analysis of any geomechanics-related applications, such as wellbore stability, sand production prediction, hydraulic fracturing design, reservoir geomechanics modelling, CO_2 storage, compaction, and subsidence (Rajabi et al., 2017). In this study we constructed a one-dimensional Mechanical Earth Model (1-D MEM) based on various types of data in the study well. We first carried out Brazilian test, Tri-axial Compressive Strength Test, and Uniaxial Compressive Strength Test to measure the static rock mechanical properties. We then calculated log-derived or dynamic rock mechanical properties which then calibrated with static results (Figure 2). The calibrated elastic properties then have been used to calculate the magnitude of horizontal stresses based on poroelastic equations. We determined the overburden stress from the wireline log data by integrating formation bulk density. Finally, the analysis of borehole breakouts and drilling induced tensile fractures in image logs of the study well revealed the orientation of S_{Hmax}.

Results and Discussions

Interpretation of eight borehole breakouts and two possible drilling-induced tensile fractures in the studied wells revealed a trend of NE-SW for the S_{Hmax} orientation which is fully consistent with the previous studies in the region (Heidbach et al., 2016; Rajabi et al., 2010). Magnitudes of vertical and horizontal stresses show the presence of normal (strike-slip in some intervals) in the study area. The presence of normal tectonic stress regime in this region is somehow interesting as this area is located in the continental collision zone between the Arabian plate and Central Iran plate. Due to lack of leak-off test data we cannot calibrate the log-derived horizontal stress magnitude. However, a recent study by Haghi et al. (2018) shows the presence of normal tectonic stress regime in the Bangestan reservoir, northern Dezful Embayment in the Zagros Fault and Thrust Belt.

We applied a wellbore stability analysis based on the constructed 1-D MEM and the well trajectory. We calculated the stress concentration around the borehole base on previously developed analytical model (Zare-Reisabadi et al., 2012, Zare et al., 2010). The comparison between the principal stresses around the borehole and the rock failure criteria to determine whether the borehole wall has failed or not (Figure 3). The sensitivity analysis of borehole stability revealed that vertical (in the normal stress regions) or moderately deviated wells (in the strike-slip stress regions) are more stable wells.

References Cited

Ahmadhadi, F., J.-M Daniel, M. Azzizadeh, and O. Lacombe, 2008, Evidence for Pre-folding Vein Development in the Oligo-Miocene Asmari Formation in the Central Zagros Fold Belt, Iran: Tectonics, v. 27/1, TC1016, 22 p. doi:10.1029/2006TC001978

Haghi, A.H., R. Chalaturnyk, and H. Ghobadi, 2018, The State of Stress in SW Iran and Implications for Hydraulic Fracturing of a Naturally Fractured Carbonate Reservoir: International Journal of Rock Mechanics and Mining Sciences, v. 105, p. 28-43.

Heidbach, O., M. Rajabi, K. Reiter, and M. Ziegler, 2016, World Stress Map 2016: GFZ Data Services. doi.org/10.5880/WSM.2016.002.

Moallemi, S.A., and M. Kermanshah, 2012, Significances of Integrated Study of the Abadan Plain Depositional Basin: Exploration and Production (in Persian by National Iranian Oil Company), v. 94, p. 20-22.

Rajabi, M., S. Sherkati, B. Bohloli, and M. Tingay, 2010, Subsurface Fracture Analysis and Determination of In-Situ Stress Direction Using FMI Logs: An Example from the Santonian Carbonates (Ilam Formation) in the Abadan Plain, Iran: Tectonophysics, v. 492/1-4, p. 192-200.

Rajabi, M., M. Tingay, and O. Heidbach, 2014. The Present-Day Stress Pattern in the Middle East and Northern Africa and Their Importance: The World Stress Map Database Contains the Lowest Wellbore Information in These Petroliferous Areas: International Petroleum Technology Conference, Doha, Qatar.

Rajabi, M., M. Tingay, O. Heidbach, R. Hillis, and S. Reynolds, 2017, The Present-Day Stress Field of Australia: Earth-Science Reviews, v. 168, p. 165-189.

Zare-Reisabadi, M.R., A. Kaffash, and S.R. Shadizadeh, 2012, Determination of Optimal Well Trajectory During Drilling and Production Based on Borehole Stability: International Journal of Rock Mechanics and Mining Science, v. 56, p. 77-87.

Zare, M.R., S.R. Shadizadeh, and B. Habibnia, 2010, Mechanical Stability Analysis of Directional Wells: A Case Study in Ahwaz Oilfield: 34rd Annual SPE International Technical Conference and Exhibition, 31 July-7 August, Tinapa-Calabar, Nigeria, SPE 136989-MS, 10 p. doi.org/10.2118/136989-MS

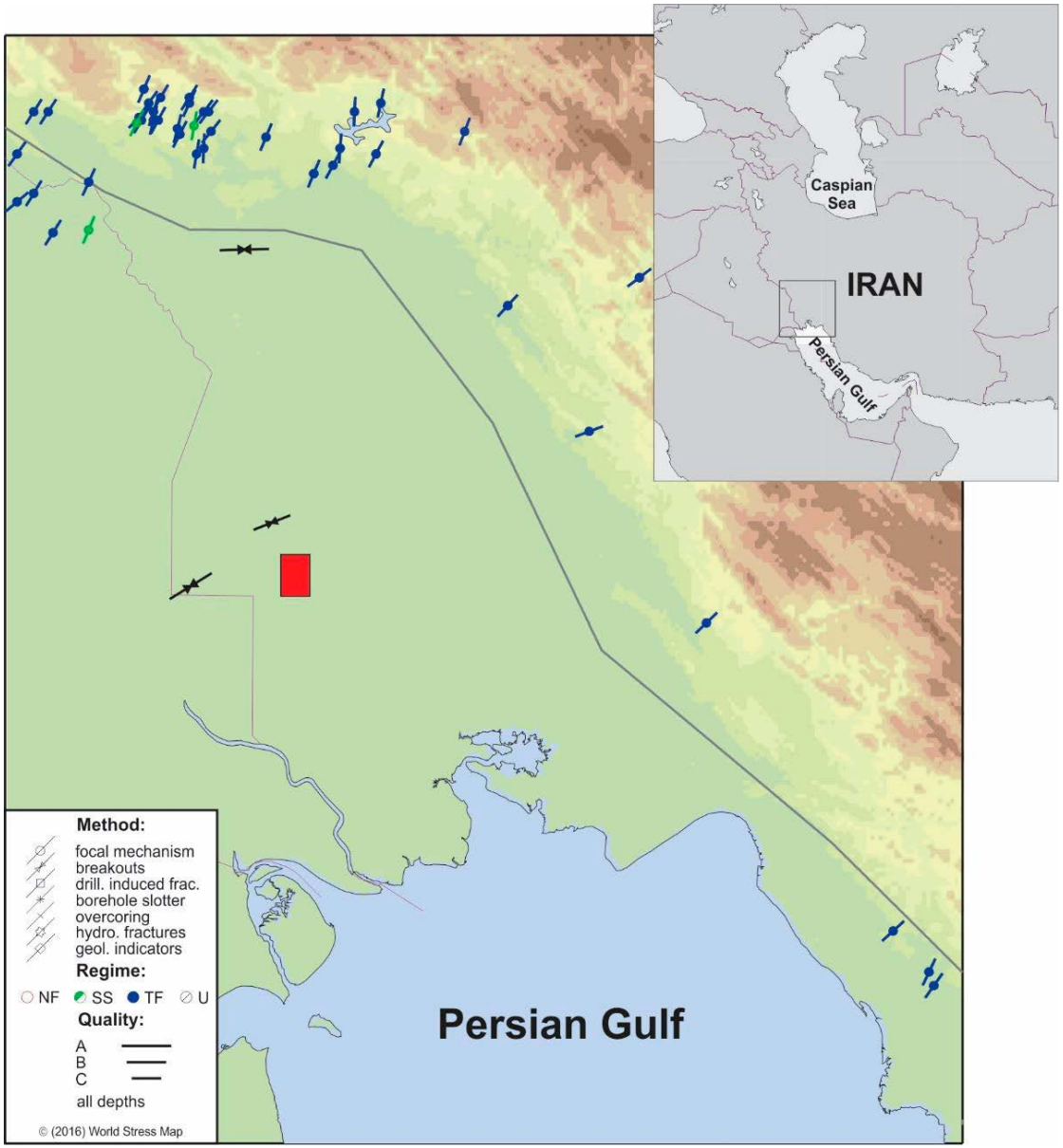

Figure 1. Maximum horizontal stress orientations in the study area from the World Stress Map database (Heidbach et al., 2016). Symbols and different colours indicate the method of measurement (circles are focal mechanism solutions, inward-facing arrows are breakouts) and the stress regime (SS=strike–slip faulting stress regime; TF=thrust faulting stress regime; black=undefined stress regime). Length of the lines indicates quality of data. The study well is located in the red rectangle.

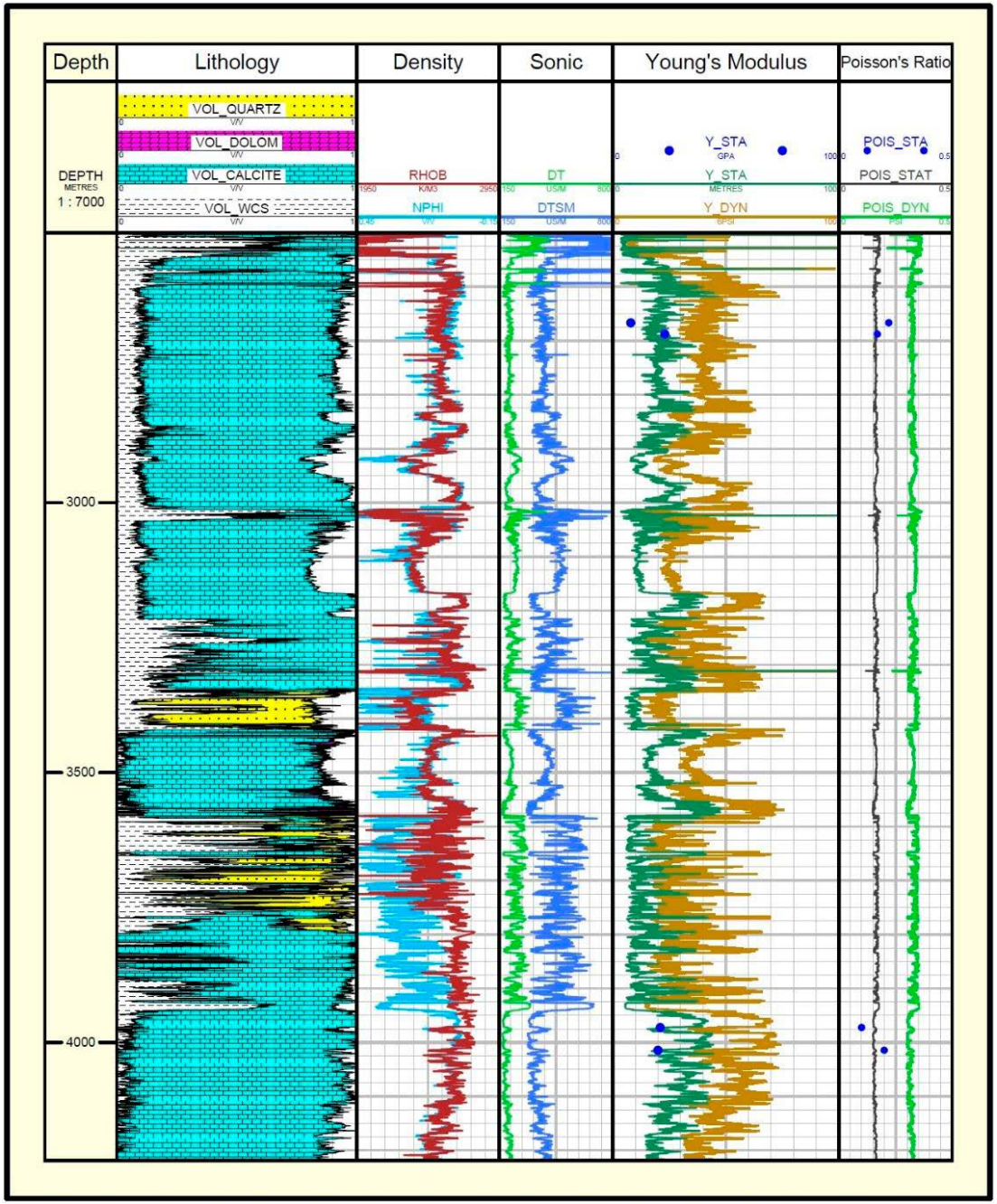

Figure 2. Dynamic and static elastic properties of studied well.

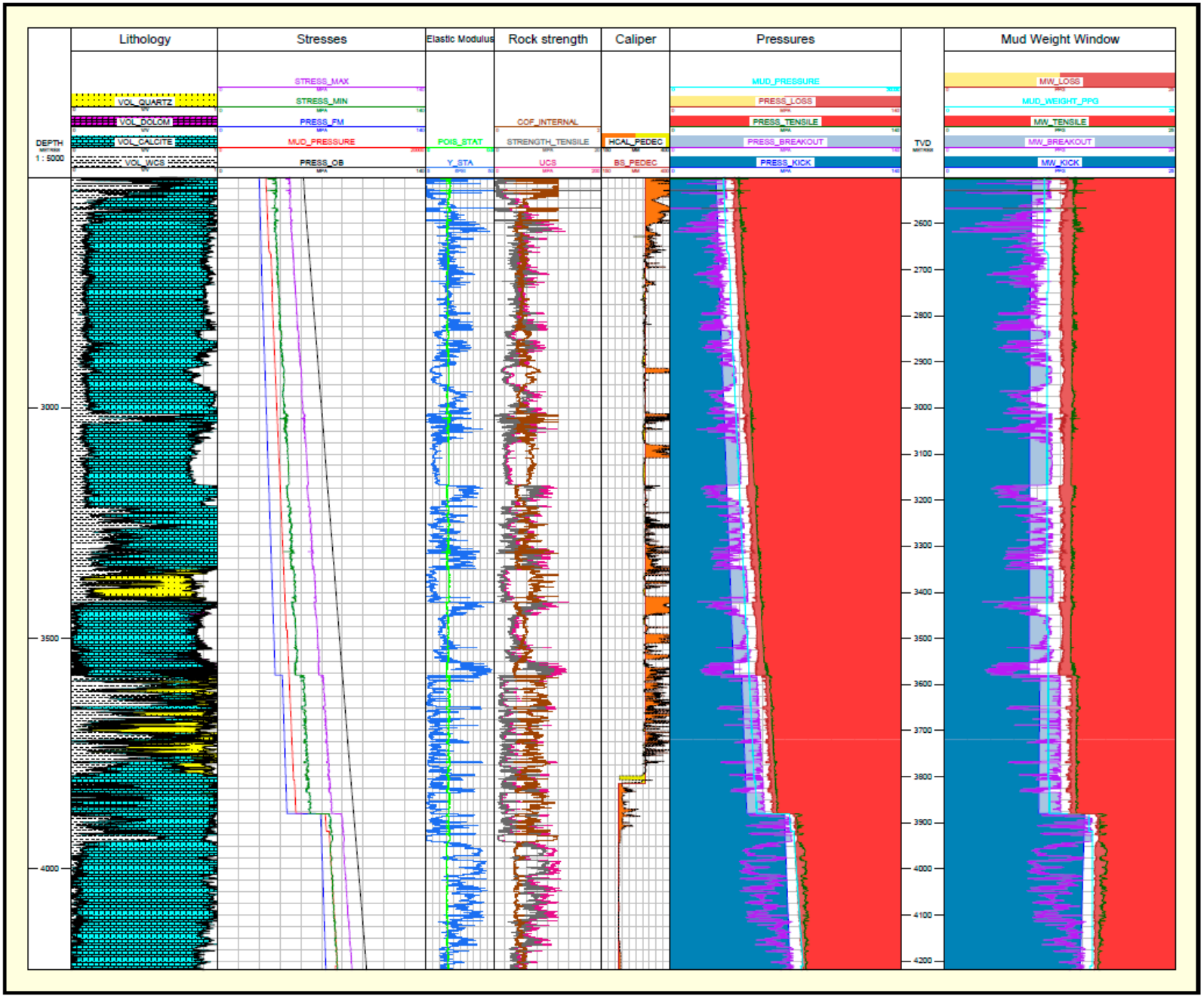

Figure 3. 1-D MEM and Wellbore stability analysis results.